

Washington University in St. Louis
Washington University Open Scholarship

Engineering and Applied Science Theses &
Dissertations

McKelvey School of Engineering


Summer 8-15-2017

Composition-Dependent Mechanisms of Multiscale Tendon Mechanics

Fei Fang

Washington University in St. Louis

Follow this and additional works at: https://openscholarship.wustl.edu/eng_etds

 Part of the [Biomedical Engineering and Bioengineering Commons](#), and the [Mechanical Engineering Commons](#)

Recommended Citation

Fang, Fei, "Composition-Dependent Mechanisms of Multiscale Tendon Mechanics" (2017). *Engineering and Applied Science Theses & Dissertations*. 319.

https://openscholarship.wustl.edu/eng_etds/319

This Dissertation is brought to you for free and open access by the McKelvey School of Engineering at Washington University Open Scholarship. It has been accepted for inclusion in Engineering and Applied Science Theses & Dissertations by an authorized administrator of Washington University Open Scholarship. For more information, please contact digital@wumail.wustl.edu.

WASHINGTON UNIVERSITY IN ST. LOUIS

Department of Mechanical Engineering & Materials Science

Dissertation Examination Committee:

Dr. Spencer P. Lake, Chair

Dr. Philip V. Bayly

Dr. Jin-Yu Shao

Dr. Simon Y. Tang

Dr. Jessica E. Wagenseil

Composition-Dependent Mechanisms of Multiscale Tendon Mechanics

by

Fei Fang

A dissertation presented to
The Graduate School
of Washington University in
partial fulfillment of the
requirements for the degree
of Doctor of Philosophy

August 2017
St. Louis, Missouri

© 2017, Fei Fang

Table of Contents

List of Figures	iv
List of Tables	xi
Acknowledgments.....	xii
Abstract.....	xiv
Chapter 1: Introduction.....	1
1.1 Motivation and research aims	1
1.2 Summary of chapters.....	3
Chapter 2: Background	6
2.1 Tendon function, degeneration/injury, and treatment	6
2.2 Tendon structure and composition	7
2.3 Tendon behavior under mechanical loading by experimental approaches	8
2.4 The contribution of different components to tendon mechanics.....	15
2.5 References	22
Chapter 3: Multiscale Biomechanical Analysis of Bovine Flexor Tendons under Shear and Compression Loading	35
3.1 Introduction	35
3.2 Materials and methods	39
3.3 Results	48
3.4 Discussion	59
3.5 Conclusion.....	66
3.6 References	67
Chapter 4: Multiscale Mechanical Integrity of Human Supraspinatus Tendon in Shear after Elastin Depletion.....	71
4.1 Introduction	71
4.2 Materials and methods	73
4.3 Results	81
4.4 Discussion	90
4.5 Conclusion.....	95
4.6 References	95

Chapter 5: Multiscale Mechanical Evaluation of Human Supraspinatus Tendon in Shear after Glycosaminoglycan Reduction	99
5.1 Introduction	99
5.2 Materials and methods	102
5.3 Results	108
5.4 Discussion	113
5.5 References	117
Chapter 6: The Role of Collagen Crosslinks in Multiscale Mechanics of Rat Supraspinatus Tendon in Tension	121
6.1 Introduction	121
6.2 Materials and methods	123
6.3 Results	131
6.4 Discussion	138
6.5 References	140
Chapter 7: Summary and Future Directions	144
7.1 Summary of findings	144
7.2 Future directions	148
7.3 References	157

List of Figures

Fig. 2.1 (A) Schematic of the multiscale hierarchical structure of tendons [14]. (B) Image of atomic force microscopy shows D-period (red line) in collagen fibrils from mouse supraspinatus tendon [15]. (C) Transmission electron microscopy shows stained collagen fibrils and GAGs in native tendon [13]. (D) Multi-photon microscopy shows stained collagen fibrils and nuclei from bovine deep digital flexor tendon with photobleached lines created..... 7

Fig. 2.2 Multiscale evaluation of tendon behavior/deformation as the response to tensile or shear loading. (A) D-period change of mouse SST during static tensile loading and AFM-acquired images measuring fibril D-period with line highlighted [15]. (B) A measure of microscale fiber sliding, termed between rows rotation, increased with increasing applied shear strain, while images taken via multi-photon microscopy showed fiber sliding during shear stress relaxation testing (white arrows denote photobleached lines broken due to fiber sliding). (C) Crimp frequency of tendon in tensile loading decreased from the toe to linear regions of the stress-strain curve and representative images of polarized light showing the change of crimp pattern [61]. (D) Circular variance values demonstrating increased fiber alignment during ramp to failure tensile testing, and fiber alignment maps and histograms calculated from polarized-light images [59]. 11

Fig. 2.3 Images demonstrating that some of the minor constituents, suggested to have mechanical roles, are found in tendon. Immunohistochemistry for decorin (stained purple) from equine CDET [154], elastin (stained cyan) from human SST (ellipses denoting nuclei), collagen II (stained brown) from mouse Achilles tendon [159], collagen III (marked by arrows, also stained purple), lubricin (stained purple) from equine SDFT [154], and COMP (stained brown) from equine SDFT [156]. 20

Fig. 3.1 Dissection scheme for preparation of test samples from proximal and distal regions of DDFT. Cylindrical samples obtained from each region were cut in half to allow for both histological analysis and mechanical tests (black dotted line = location of DDFT bifurcation; arrows showed loading direction)..... 39

Fig. 3.2 Schematic diagram of custom-made mechanical test system. The inset shows the top view of position of clamps (gray blocks) and tendon samples (orange blocks). Blue arrows indicate which clamps were moved and in which directions, while the other clamps were attached to the load cell and held stationary. 40

Fig. 3.3 Mechanical response in compression tests. Typical load-time curve during three-step incremental stress-relaxation tests shows larger forces for distal than proximal samples (compression forces are shown in absolute values, although actual forces are negative). 41

Fig. 3.4 Camera pictures of samples under (A) pre-load and (B) 0.24 shear clamp strain. Camera pictures under (D) pre-load and (E) 0.24 compression clamp strain. (C) and (F) show coordinates and strains for shear and compression testing (white arrows show loading direction; red lines denote primary direction of collagen alignment)..... 43

Fig. 3.5 Composite images of samples under (A) pre-load and (B) 0.24 shear clamp strain. Composite images of samples under (C) pre-load and (D) 0.24 compression clamp strain (white arrows show loading direction)..... 43

Fig. 3.6 (A) and (B) show methods of computing strain and rotations based on nuclei centroids (asterisks (*) show the location of the origin); (C) and (D) show two-photon microscopy images of a sample loaded in shear; nuclei outlined by rectangles and by circles illustrate rotation between fibers (indicative of sliding) and rotation within fiber (indicative of uncrimping/realignment), respectively. 47

Fig. 3.7 Maximum and minimum stresses are significantly larger for distal samples compared to proximal samples (n=9/group)..... 49

Fig. 3.8 (A) Normalized stress relaxation was evaluated for each strain step of distal and proximal samples in compression tests (curves were averaged by group, error bars not shown for clarity). (B) Relaxation ratios for compression tests increased slightly with increasing strain, but were not different between regions (n=9/group; average +/- standard deviation)..... 49

Fig. 3.9 Fitting results of the two-relaxation-time solid linear model for compression tests. (A) Typical model fit to experimental data (shown data is for a distal sample; proximal samples also show good model fits); inset shows schematic of the solid linear model. (B) Elastic moduli of different model components are significantly larger for distal samples at each of three steps (corresponding to compressive clamp strains of 0.08, 0.16, 0.24). (C) Relaxation time constants are very similar for distal and proximal samples at each strain step. (Plots show average +/- standard deviation; n=9/group; horizontal bars indicate significant differences between regions). 50

Fig. 3.10 Mechanical response in shear tests. (A) Typical load-time curve during three-step incremental stress-relaxation tests show larger forces for distal than proximal samples. (B) Maximum and minimum stresses are significantly larger for distal samples compared to proximal samples, except minimum stresses at 0.08 strain are not different between regions (n=14/group; average +/- standard deviation)..... 51

Fig. 3.11 (A) Normalized stress relaxation was evaluated for each strain step of distal and proximal samples in shear tests (curves were averaged by group, error bars not shown for clarity). (B) Relaxation ratios for shear tests decreased slightly with increasing strain, but were not different between regions (n=14/group; average +/- standard deviation)..... 52

Fig. 3.12 Fitting results of the two-relaxation-time solid linear model for shear tests. (A) Elastic moduli of different model components are significantly larger for distal samples at the second and third strain steps (corresponding to shear strains of 0.16 and 0.24). (B) Relaxation time constants are similar for distal and proximal samples, with differences only at the last strain step. (Plots show average +/- standard deviation; n=14/group; horizontal bars indicate significant differences between regions). 53

Fig. 3.13 Multiscale strain values of distal and proximal DDFT samples in (A) shear and (B) compression show strain attenuation at smaller length scales (dashed horizontal lines indicate magnitude of applied clamp strains; data are shown as mean ± 95% confidence intervals; * for $p < 0.05$). 54

Fig. 3.14 (A) Rotation under shear and (B) compression for distal and proximal samples vs. clamp strain within row and between rows (rotation is computed as shown in Fig. 3.13; data are shown as mean ± 95% confidence intervals; * for $p < 0.05$). 55

Fig. 3.15 (A) Nuclear aspect ratio of distal and proximal samples before loading; change of nuclear aspect ratio normalized by undefomed NAR under shear (B) and compression (C) for distal and proximal samples after strain applied (data are shown as mean ± 95% confidence intervals; * for $p < 0.05$). 56

Fig. 3.16 Two-photon microscopy images show lines photobleached on two subfascicles under (A) shear pre-load, (B) 0.24 shear strain, (C) compressive pre-load, and (D) 0.24 compressive strain; images in which photobleached lines are on single subfascicle under (E) shear pre-load, (F) 0.24 shear strain, (G) compressive pre-load, and (H) 0.24 compressive strain (white arrows indicate sliding between subfascicles). 57

Fig. 3.17 Individual symbols shows strain values for distal and proximal samples grouped according to whether photobleached lines are on two subfascicles or single subfascicles for (A) shear and (B) compressive loading (lines and error bars are mean ± 95% confidence intervals; * for $p < 0.05$; # for $0.05 \leq p \leq 0.1$). 57

Figure 3.18 Representative picosirious red stained sections of distal (A) and proximal (C) samples by 4X objective of polarized light microscope. Images of distal (B) and proximal (D) samples at 40X, taken at the locations denoted by * in (A) and (B). The distal region shows non-uniform staining through the thickness and less collagen crimping compared to the proximal region. Anterior surface is towards the top of each image. 58

Fig. 3.19 Averaged intensity plots along tendon thickness (shown by arrows) for distal (A) and proximal (D) regions. Representative alcian blue stained sections of distal (B) and proximal (E) samples by 4X objective of white light microscope. Images of distal (C) and proximal (F) samples by 40X objective, taken at the locations denoted by * in (B) and (E). The distal region

shows non-uniform staining through the thickness and staining in distal region is greater overall compared to the proximal region. Anterior surface is towards the top of each image. 59

Fig. 4.1 The experimental design. (A) Samples (black, blue, and red blocks, lines inside showing alignment of collagen fibers), obtained from medial (M), anterior (A), and posterior (P) regions of SST used for biomechanical testing and compositional analysis. (B) Representative supraspinatus tendon (SST) specimen showing anatomical orientation. (C) Bursal and joint surfaces of SST sample mounted to clamps. Solid black blocks indicate three locations for photobleaching during multiphoton imaging; blue arrow shows shear loading direction and the black arrow shows the z-axis of the sample (through thickness)..... 75

Fig. 4.2 Typical microscopy images from three locations in the same SST sample (from medial region) under pre-load and 0.24 shear strain, demonstrating that organization and deformation of local matrix differ within one sample from a single region. The white arrows show shear loading direction. Location 1 is from the bursal side, location 2 from the central zone, location 3 from the joint side. Scale bar =100 μm 77

Fig. 4.3 Typical microscopy images from three locations in the same SST sample (from medial region) under pre-load and 0.24 shear strain, demonstrating that organization and deformation of local matrix differ within one sample from a single region. The white arrows show shear loading direction. Location 1 is from the bursal side, location 2 from the central zone, location 3 from the joint side. Scale bar =100 μm 79

Fig. 4.4 The quantity of elastin in samples treated with different concentrations of elastase for six hours (A) or with 5 units/ml elastase for different times (B). (C) Remaining elastin content along the sample depth; inset shows a sample (red block) attached to clamps (green blocks) incubated in elastase solution. The normalized depth is defined as 0 (top) to 1 (bottom). 81

Fig. 4.5 Peak and equilibrium stresses of samples from SST anterior (A), posterior (P), and medial (M) regions for elastase treatment (A&C) and PBS incubation (B&D). Data are shown as mean \pm SD; * for $p < 0.05$; # for $0.05 \leq p \leq 0.1$ 83

Fig. 4.6 Peak (A) and equilibrium (B) stresses of each region before treatment/incubation by grouping PBS-incubated and elastase-treated samples together. Peak (C) and equilibrium (D) reduced ratio, calculated using the equation above, demonstrated stress decrease more after elastase treatment than PBS incubation. 84

Fig. 4.7 Averaged stress-time curves of elastase-treated and PBS-incubated samples from anterior (A), posterior (P), and medial (M) regions, normalized by corresponding control stresses. The short dash and solid lines show normalized peak stresses for each group. 85

Fig. 4.8 Local matrix-based strain values of samples from SST anterior (A), posterior (P), and medial (M) regions before and after (A) elastase treatment or (B) PBS incubation. Data are

shown as mean \pm SD; no statistical differences were found between elastase- and PBS-treated samples..... 86

Fig. 4.9 Rotation calculated using deformed photobleached grids of samples from SST anterior (A), posterior (P), and medial (M) regions before and after (A) elastase treatment or (B) PBS incubation. Data are shown as mean \pm SD; no statistical differences were found between elastase- and PBS-treated samples..... 86

Fig. 4.10 Between-rows rotations (indicative of fiber sliding) and within-row rotations (indicative of fiber uncrimping/reorganization) vs. clamp strain for control and elastase-treated samples. Data are shown as mean \pm SD; * for $p < 0.05$; # for $0.05 \leq p \leq 0.1$ 87

Fig. 4.11 Representative H&E and alcian blue histological sections show different collagen organization even inside the same cadaveric tendon. (A&D) Highly organized collagen fibers and low cellularity were apparent in some microscale locations. (B&E) Less organized collagen fibers (highlighted by red lines) were situated between bundles of organized collagen fibers, with increased proteoglycans between organized fibers. (C&F) Disorganized collagen fibers (highlighted by red circles) were also found with increased cellularity and PGs. Images acquired with 20X objective; scale bar = 100 μ m. 89

Fig. 4.12 Distribution of elastic fibers shown by fluorescent SRB stain (top row) and histological VVG stain (bottom row). Relatively long elastic fibers (highlighted by white arrows) localized along well-organized collagen fibers (A&D). In locations of somewhat less organized collagen fibers, both short disorganized and long organized elastic fibers were observed (B&E). In locations of several disorganized collagen fibers, elastic fibers were short and disorganized (C&F). To differentiate elastic fibers from nuclei in fluorescent SRB images, nuclei are circled with dotted ellipses. Images acquired with 40 \times objective for SRB and 20 \times and 40 \times objectives for VVG stain; scale bars = 100 μ m. 89

Fig. 5.1 Normalized GAG amounts in SST samples treated for 6 hours with different concentrations of ChABC buffer (A) or with 0.2 units/ml ChABC buffer for different durations of incubation (B). (C) GAG amount within DDFT after ChABC treatment exhibited a gradient distribution along the sample width; inset displays how clamps (gray blocks) and attached sample (pink block) are secured for incubation and the subsequent mechanical test, where the normalized width is shown as 0 (top) to 1 (bottom) and is indicated as the x axis in the plot. .. 103

Fig. 5.2 Microscopy images from three locations of the same sample before and after application of 0.24 shear strain. Different locations within one sample from a single SST region showed heterogeneous organization of collagen fibers and different modes of deformation: no obvious deformation at Location 1; fiber sliding at Location 2; fiber reorganization at Location 3. Rotation angle, θ , was calculated as the angle between the horizontal axis of images and deformed photobleached grids. Grid intersection points (red dots added for visualization purpose

only) were used to calculate local matrix-based strain, while white arrows show shear loading direction.	105
Fig. 5. 3 Typical histological images of paired control and treated SST samples, which were stained by H&E and Alcian blue to show collagenous extracellular matrix (pink, A-C) and GAGs (blue, D-I), respectively. After ChABC treatment, the ECM was not visibly disrupted. GAG amount decreased differentially by location within each sample (demonstrated by varying intensity of staining in E and F compared to D), and GAG-rich pericellular matrix was observed to have been particularly degraded. Images A-F were acquired by 10× objective and images G-I by 40× objective. Treated-top and treated-middle are sections from the top and middle of treated samples, respectively. Arrows in images G-I denote cell nuclei.	110
Fig. 5.4 Peak (A) and equilibrium (B) stresses for control (untreated) samples increased at larger strain steps, but were not significantly different across three SST regions; inset shows three regions (M = medial; A = anterior; P = posterior) in SSTs.	110
Fig. 5.5 Averaged stress–time curves of SST samples from anterior (A), posterior (P), and medial (M) regions after PBS incubation and ChABC treatment, normalized by corresponding peak stresses from the 0.24 strain step of mechanical test conducted before incubation or treatment. Samples subjected to ChABC treatment showed larger decreases in stress than samples following PBS incubation. Short solid and dashed lines show normalized peak stresses for each group. .	111
Fig. 5.6 Group peak stresses (A), equilibrium stresses (B), and stress relaxation percent (C) showed moderate changes at increasing strain steps, but were similar before and after ChABC treatment.	112
Fig. 5. 7 Larger absolute values of peak (A) and equilibrium (B) reduced ratios after ChABC treatment compared to values following PBS incubation indicate that stresses decreased more after ChABC treatment.	112
Fig. 5.8 Samples before and after ChABC treatment exhibit similar measures of microscale deformation, namely local matrix-based strain (A) and rotation (B).....	113
Fig. 6.1 The relative gene expression of LOX and different LOX isoforms in mice Achilles tendon and SST.	125
Fig. 6.2 Bone-tendon-muscle assembly cultured in the custom-built device. (A) Constant tension was applied by the weight to the tendon. (B) Culture medium was covered to prevent contamination.....	127
Fig. 6.3 HP and LP contents normalized by collagen amount in tendons of rats which started at eight-weeks old to be injected with no (C), low dose (L), and high dose (H) BAPN for four weeks. HP and LP did not decrease with treatment.....	128

Fig. 6.4 Tensile mechanical testing device. The inset, denoted by the white rectangle, shows rat SST glued to sandpaper tabs, which are then connected to the micro-stage by suture.....	130
Fig. 6.5 Tensile mechanical testing device mounted on the two-photon microscopy stage.	130
Fig. 6.6 HP (A) and LP (B) amounts in different types of tendons (porcine Achilles tendon, bovine patellar tendon, rat SST, mouse Achilles tendon, and mouse SST) quantified by our technique described in Section 6.2 (left side of the dash line) and further compared with HP (A) and LP (B) densities in tissues from literature (right side of the dash line, T: tendon, C: cartilage, L: ligament, M: meniscus, B: bone, CT: cervical tissue).....	132
Fig. 6.7 Cell viability of tendons after two-week culture. (A) Live cells were stained green. (B) Dead cells were stained red. (C) Composite channels showed both live and dead cells.....	132
Fig. 6.8 Peak stress (N=2 for control, N=4 for other groups), linear, and toe modulus (N=1 for control, N=4 for other groups) of <i>in vivo</i> cultured tendons. C, L, and H are SST groups cultured with no, low, or high LOXL2 concentration, respectively.	133
Fig. 6.9 Rat weight during four weeks of injection normalized by day 0 body weight.....	133
Fig. 6.10 Peak (A) and equilibrium stresses (B) of <i>in vivo</i> treated tendons from control (C), low dose (L), and high dose (H) groups. 0.06, 0.12, and 0.18 are applied step strains during mechanical testing.....	134
Fig. 6.11 Difference of peak (A) and equilibrium stresses (B) between left and right SSTs from control (C), low dose (L), and high dose (H) groups. 0.06, 0.12, and 0.18 are applied step strain; * for $p < 0.05$; # for $0.05 \leq p \leq 0.1$	135
Fig. 6.12 Correlation plots between tissue strain and peak stresses of control, low dose, and high dose BAPN treated groups. Solid lines show best linear fit, with corresponding slope and R^2 values.	136
Fig. 6.13 Correlation plots between tissue strain and equilibrium stresses of control, low dose, and high dose BAPN treated groups. Solid lines show best linear fit, with corresponding slope and R^2 values.....	136
Fig. 6.14 Microscale tensile strain (A) and shear strain (B) of control, low dose, and high dose BAPN treated groups, calculated using microscopic images.	137
Fig. 6.15 Crosslink densities HP (A) and LP (B) of control, low dose, and high dose BAPN treated groups. * for $p < 0.05$	137

List of Tables

Table 3.1 Results for samples from the distal region compared to the proximal region for shear and compression testing (↑ , ↔, and ↓ represent larger, equivalent, and smaller values in the distal region compared to proximal, respectively; D = distal; P = proximal).....	60
Table 6.1 Optimized MRM conditions and quantification limit.....	125

Acknowledgments

First and foremost, I want to especially thank my thesis advisor Dr. Spencer P. Lake for his invaluable support and guidance over the last five years. For the research perspective, I am always encouraged and motivated by his passion to devote to research and his commitment to teaching. His rigorous research attitude deeply influences me. His patience and generous help have not only made me learn different experimental skills, but also revolutionized the way I think to resolve scientific problems. For the personal perspective, I am very grateful for his exhaustive tutoring for my career development and also his warmth and kindness of being both wonderful mentor and good friend. I am so lucky to join his lab and mostly inspired by him to enjoy research.

I would also like to thank all my dissertation committee members, Dr. Philip V. Bayly, Dr. Jin-Yu Shao, Dr. Simon Y. Tang, and Dr. Jessica E. Wagenseil for giving me wonderful insight, suggestions, and comments. I am also grateful for the support and help from all those, past and present, in Lake lab, especially Ryan M. Castile, Chelsey L. Dunham, Alex J. Reiter, Jeremy Eekhoff. They have always been wonderful friends and lab mates to help me prepare for experiment, share research ideas, have great times during conference, and pass along extremely important critiques to improve my papers and presentations. Thank you to all of them for making me enjoy every moment working in the lab.

I want to end with thanking my parents, Hongxia Xu and Jinhui Fang, for giving me endless love and providing me with independence to study aboard and follow my interest. I am so grateful for having so amazing sister, Qi Fang, and brother-in-law, Yanchun Jiang, with continuous love, unconditional support, and understanding. They are the inspiration of my life

and I cannot be here without them. Finally, I want to express my gratitude to all my lovely friends and relatives who are indispensable in my life.

Fei Fang

Washington University in St. Louis

August 2017

ABSTRACT OF THE DISSERTATION

Composition-Dependent Mechanisms of Multiscale Tendon Mechanics

by

Fei Fang

Doctor of Philosophy in Mechanical Engineering

Washington University in St. Louis, 2017

Research Advisor: Professor Spencer P. Lake

Tendons serve as an integral part of the musculoskeletal system by transferring loads from muscle to bone and providing joint mobility and stability. From the physiologically-loading perspective, while progress has been made in evaluating mechanical behavior of different types of tendons in tension, further work is needed to relate tendon mechanics to compositional and microstructural properties, particularly under non-tensile loading modalities (i.e., shear, compression). This information is vital to explore mechanisms of how mechanical signals lead to changes in tendon structure and composition to enable these tissues to function properly, including in in vivo multiaxial loading conditions. From the structural perspective, tendon exhibits a hierarchical organization as collagen is bundled into fibrils, fibers, fascicles, and finally full tissue. Within this hierarchy, linking components are believed to act as connections to maintain mechanical integrity. Three linking components have been proposed, namely elastic fibers, proteoglycans, and collagen crosslinks, however conclusions about their specific mechanical roles, assessed using experimental and computational approaches, are inconsistent. In addition, it remains unknown whether/how these linking components regulate tendon microscale behavior (i.e., at the level of cells) and mechanical signal transfer across length scales.

Therefore, this study aimed to (1) develop a protocol that combined a biomechanical test device with two-photon microscopy to measure tendon mechanical strength and multiscale deformation; (2) apply this experimental approach to evaluate region-dependent biomechanics of tendons and related physical mechanisms governing their microscale behavior; (3) determine the role of proteoglycans and elastic fibers in tendon multiscale mechanical behavior using enzyme-treated tendons; and (4) elucidate the contribution of collagen crosslinks to tendon mechanics using *in vivo* treatment and *in vitro* culture. We found that different regions of bovine flexor tendon exhibited distinct elasticity, but not viscosity, when subjected to shear and compression, and that fiber sliding and reorganization were the primary modes of microscale deformation. Elastic fibers contributed to supraspinatus tendon (SST) mechanical strength in shear, while proteoglycans appeared to not contribute to SST multiscale biomechanics. Rat SST with decreased collagen crosslink density showed inferior mechanical properties, demonstrating the role of collagen crosslinks on tendon mechanical behavior. Taken together, these results have illustrated tendon composition-mechanics relationships by evaluating mechanical contribution of specific linking components at different length scales. In addition, this work provides insight into mechanical consequences that may accompany extracellular matrix changes during tissue injury/degeneration, and as well provides useful data to aid the design of biomimetic engineered tissues with appropriate structure and composition.

Chapter 1: Introduction

1.1 Motivation and research aims

As an essential element in the musculoskeletal system, tendon achieves joint movement by assisting the transfer of muscle force to bone and also helps maintain joint stability. Tendon injury or degeneration, often attributed to overloading or aging, is common throughout the world and causes significant pain and disability. Unfortunately, tendon has very poor self-healing ability due to its relatively acellular and avascular features. Even after conservative treatment or surgical repair, injured tendons are often compromised. Common functional problems such as joint stiffness, repeated tissue ruptures, and limited movement often persist even after therapeutic intervention. Therefore, a comprehensive depiction of tendon structure-composition-function relationships is crucial to understand how these tissues function in healthy conditions and to evaluate changes that occur during tendon injury and healing. For regenerative machine, this information could also provide insight to design optimized biomaterials with matched mechanical and structural properties, which can provide appropriate functions and maintain a supportive friendly environment for fibroblasts/tenocytes.

Generally, tendon has been reported to have anisotropic, inhomogeneous, and viscoelastic mechanical properties under tensile loading. When subjected to tensile loading to failure, tendon exhibits a characteristic stress vs. strain curve, which can be divided into toe, linear, and failure regions. In the toe region, wavy collagen fibers on the microscale become uncrimped as load increases. When tendon reaches the linear region, both collagen fiber stretching and sliding would occur as microstructural changes. As a consequence of this deformation pattern, strains transferred from tissue to nuclei scales are always attenuated. This physical feature shields cells

from relatively high tissue strain, regulates mechanotransduction, and modifies synthesis of extracellular matrix, in response to altered loading. Additionally, tendons (i.e., supraspinatus, Achilles, flexor) interact with other tissues (i.e., bone) in the physiological loading environment, which can induce multiaxial loading, such as shear, compression, and rotation, in addition to tensile loads. Although enormous studies have focused on evaluating tendon mechanical properties in tension, the knowledge of structural changes to non-tensile loading, its related mechanical signal transfer, and corresponding mechanotransduction responses are lacking.

Structurally, tendon is composed of hierarchically organized matrix, with collagen molecules staggered together into fibrils, which in turn bundles into fibers, fascicles, and finally whole tendon. Linking components are proposed to bridge this stratified structure to preserve mechanical integrity. Tendon is mainly composed of collagen type I, with small quantities of proteoglycans, elastic fibers, other collagens (e.g., types II, III, etc.), and glycoproteins. Enzymatic collagen crosslinks, elastic fibers, and proteoglycans are the three candidates which have been proposed to connect collagen, collagen fibrils, or collagen fibers, to assist mechanical signal transfer at different length scales. However, the contribution of these components to tendon multiscale mechanics and the related physical mechanisms regulating tendon microscale deformation has not been well described. To resolve these questions, this study aimed to: (1) determine region-specific mechanical strength and microscale deformation of bovine flexor tendons in compression and shear; (2) evaluate the physical mechanisms regulating mechanical behavior of human supraspinatus tendons (SSTs) under shear and determine specific roles of elastic fibers and proteoglycans in SST mechanics; (3) examine the contribution of enzymatic collagen crosslinks to multiscale mechanics of rat SSTs. Micromechanical testing with simultaneous imaging using a multi-photon microscopy system was performed to quantify

tendon multiscale stress and strain response under shear, compression, or tensile loading. Tendon morphology and distribution of constituents (i.e., total collagen, proteoglycans, elastic fibers) were examined by histology and immunohistochemistry. Elastic fibers and enzymatic crosslinks were quantified by competitive ELISA and high-performance liquid chromatography, respectively. By addressing the contribution of different tissue constituents to tendon mechanics and evaluating tendon behavior under non-tensile loading, this study greatly enhances understanding of tendon structure-function relationships, provides data that can aid efforts to prevent tendon degeneration or injury, and helps improve therapeutic methods by informing rational design of engineered tissues.

1.2 Summary of chapters

Chapter 2 reviews current understanding about tendon structure, composition, function, degeneration, and treatment. To better characterize tendon multiscale mechanical properties, various advanced experimental approaches at fibril, fiber, and fascicle/tissue scales are summarized. In addition, a summary of current understanding at mechanical and biological contributions of tendon primary components (i.e., collagen crosslinks, elastic fibers, proteoglycans) and other constituents with small amounts (i.e., tenascin-C, lubricin, other collagens) are also presented.

In Chapter 3, a custom built biomechanical testing device combined with two-photon microscopy was designed to measure both tissue and microscale deformation of bovine flexor tendon under shear loading. Region-specific mechanical behavior of bovine flexor tendon is presented and further correlated with various measures of tendon structure and composition. This chapter demonstrates the testing protocol and workflow of multiphoton image acquisition, which establishes techniques used in later chapters.

Based on the findings that intact bovine flexor tendon has region-dependent multiscale mechanical properties in Chapter 3, Chapter 4 applies similar experimental approaches to determine whether elastic fibers contribute to SST mechanics in shear loading on the tissue and micron scales. SST was selected due to its clinically high injury incidence and complex physiological loading environment. Elastic fibers were partially depleted from SSTs, and mechanical strength and multiscale deformation under shear stress relaxation loading were compared before and after depletion. Similarly, Chapter 5 describes how enzyme treatment and biomechanical testing with two-photon microscopy were performed to determine whether proteoglycans play a role in SST multiscale mechanical behavior in shear loading.

Chapter 6 focuses on another linking component, enzymatic collagen crosslinks, and evaluates whether collagen crosslinks can be taken as a marker of tendon tensile mechanical strength and whether they influence mechanical signal transfer across different length scales. Different from previous experiments, *in vivo* treatment and *in vitro* tissue culture were adopted here to decrease and increase collagen crosslinks in SSTs, respectively. The density of SST collagen crosslinks were quantified by liquid chromatography-tandem mass spectrometry and correlated with SST mechanical parameters.

Finally, Chapter 7 summarizes the major conclusions of this dissertation and describes the significance of this work to comprehensive understanding of tendon structure-function relationships. Building upon these conclusions, this chapter also discusses several future directions to further address tendon multiscale mechanics and related mechanotransduction.

Chapter 2: Background¹

2.1 Tendon function, degeneration/injury, and treatment

Tendons are stiff fibrous connective tissues that stabilize movable and flexible joints, facilitate the transmission of muscular forces to bone, and resist high tensile forces [1, 2]. This unique function requires specific tendon constituents and a complicated hierarchical structure [3-6]. Tendon degeneration or injury caused by aging, overuse, laceration, or interactions with neighboring anatomy is common clinical problem. Damage can lead to altered structural and/or compositional properties, such as rupture/tear on the mesoscale, disorganized collagen fibers on the microscale, changes in the relative proportions of collagen types (i.e., more collagen type III and II, less collagen I), increased synthesis of proteoglycans, which can lead contribute to impaired mechanical properties and decreased mobility and stability [7-9]. Traditional treatment strategies for tendon injury include conservative approaches and surgical repair/replacement, but constrained movement, increased joint stiffness, and tissue re-ruptures often occur after repair [8]. Fortunately, new treatment strategies such as the application of engineered biomaterials seeded with stem cells have been explored to meet the challenges of tendon repair [8]. A comprehensive understanding of tendon mechanical properties in physiological loading environments and correlation of mechanics with structural/compositional properties will help prevent tendon injury, detect early-stage degeneration, aid in development of appropriate therapies, and guide the design of customized tissue replacements.

¹Reprinted from (1) Fang, F., and Lake, SP., 2016, "Experimental evaluation of multiscale tendon mechanics," J Ortho Res; (2) Fang, F., and Lake, SP., 2016, "modelling approaches for evaluating multiscale tendon mechanics." Interface focus, 6, 20150044.

2.2 Tendon structure and composition

Tendons have a complex hierarchical structure that spans several length scales: tropocollagen (~300 nm long) formed helically by three intracellular peptide alpha chains that are assembled into fibrils; fibrils (~1 μm long) that are crosslinked to form fibers; fibers (ranging 1 to 300 μm) are bundled together to build fascicles, with spindle-shaped cells (i.e., tenocytes) sparsely situated in rows between fibers; and fascicles (on centimeter scale) are enclosed by a connective layer called the epitenon to compose the full tendon tissue (Fig. 2.1) [10-15]. This unique structural organization of tendon provides characteristics that enable proper functional properties. For example, waviness (or crimp) of fibers along the long axis of tendon is proposed

to contribute to the distinct toe region of the non-linear stress-strain curve observed in tensile testing [12, 16]. The crimp pattern is also superposed by a 3D helical superstructure of collagen fibers, detected by polarized light microscopy and interference microscopy with 3D modeling [17, 18]. This helical pattern was demonstrated to contribute to greater recovery and less hysteresis loss of energy-

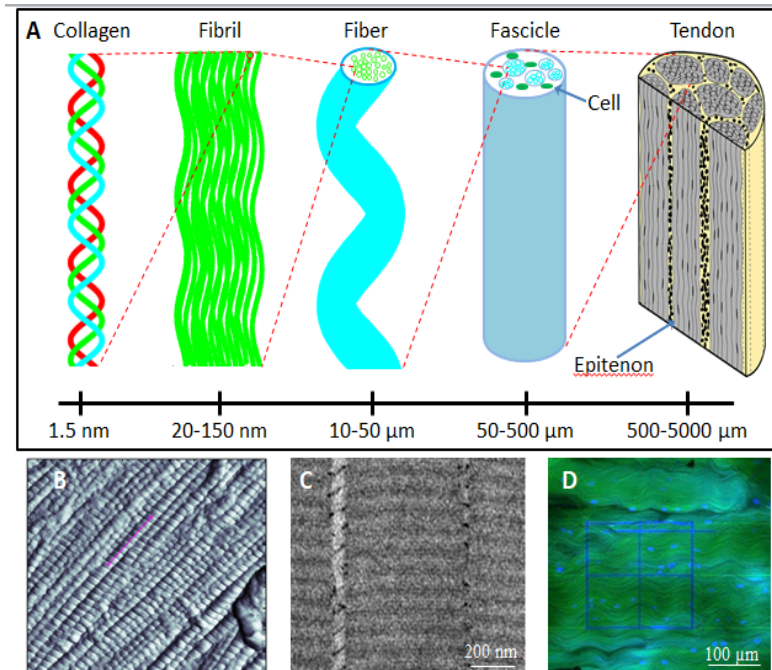


Fig. 2.1 (A) Schematic of the multiscale hierarchical structure of tendons [14]. (B) Image of atomic force microscopy shows D-period (red line) in collagen fibrils from mouse supraspinatus tendon [15]. (C) Transmission electron microscopy shows stained collagen fibrils and GAGs in native tendon [13]. (D) Multiphoton microscopy shows stained collagen fibrils and nuclei from bovine deep digital flexor tendon with photobleached lines created.

storing tendons compared to positional tendons [19]. Besides these unique sub-structural features, tendon mechanical behavior is also dependent on the relative quantities and locations of various compositional components [10].

Tendon is composed of ~55-70% water and predominantly consists of 60-85% collagen of dry weight [20, 21]. Type I collagen comprises ~95% of total collagen, but tendon also has small amounts of types II, III, V, XII, and XIV [22]. Tendons also contain proteoglycans (i.e., decorin, fibromodulin, biglycan, lumican, aggrecan) in relatively small quantities, with types and amounts varying according to different species, ages, and anatomical locations. In tendon, proteoglycans have been found to play an important role in facilitating fibrillogenesis, regulating extracellular matrix assembly, and modulating cell-matrix interaction [23-26]. Properties of, and interactions between, structural components at different length scales of the hierarchical tendon organization are significant for providing adequate mechanical function in a variety of *in vivo* loading environments. Elucidation and characterization of these multiscale properties and relationships are necessary to understand tendon in healthy conditions as well as in degeneration, damage, and injury.

2.3 Tendon behavior under mechanical loading by experimental approaches

Since tendon has a highly ordered multiscale fibrillar structure, spanning from molecular to tissue scales, evaluation of tendon mechanics should be conducted at each hierarchical scale, at the links among different length scales, and also across adjacent length scales (Fig. 1) [10, 12]. Both modeling and experimental approaches have been employed to determine and predict tendon anisotropic, inhomogeneous, and viscoelastic properties under different loading scenarios at a single scale [11]. Mathematical approaches utilize a mathematical formulation that can

closely match the mechanical response of tendon and describes gross tendon mechanical behavior by combining or generalizing the mechanical behavior of different components in tendon (e.g., collagen fiber distribution) [27-34]. This approach is based on a continuum assumption, wherein the mathematical formulation used to represent tendon behavior assumes a continuum assumption on the tissue scale. In addition, several other different mathematical modeling schemes have also been developed to evaluate mechanical properties of individual tendon constituents, or their interactions, on the molecular level. To address more complex aspects (e.g., multiaxial physiological loading, varying compositional and structural properties), many studies have also utilized computational modeling to analyze tendon behavior and explore structure-function relationships [35-39]. Tendon modeling offers a method that can provide insight into tendon relationships that are impossible to measure *in vivo* and can be beneficial in handling large amounts of data and complicated loading situations. Appropriately defined models can be formulated for a specific tendon with its unique properties (e.g., multiaxial mechanical properties, location-specific microstructural organization, inhomogeneous distribution of non-fibrillar matrix, site-specific geometry, etc.) and, using a multiscale approach, could be constructed to enable mechanical evaluation across the full range of length scales relevant to the hierarchical organization of tendon. Importantly, well-validated models enable predictions of tissue behavior under different loading conditions, including those that are difficult to explore experimentally, and can be utilized to study the effects of disease, degeneration, and/or injury on functional mechanical properties.

In this section, we focus on experimental approaches and summarize previous work starting at smaller length scales of tendon hierarchy and working up to full tissue. The smallest levels of structural organization of connective tissues are relevant to overall mechanical function; for

example, on the molecular scale, the staggered array of collagen has been shown to contribute to viscoelastic properties. However, most analysis has focused on the fibril scale and larger for considering tendon mechanics [40-42].

2.3.1 Fibril scale

Collagen fibrils (diameter ranging from 20-500 nm) (Fig.1), which are assembled by microfibrils (~3.5 nm diameter), have been shown to contribute significantly to tendon mechanics [5, 6, 43-45]. A combination of transmission/scanning electron microscopy (TEM/SEM), atomic force microscopy (AFM), polarized Raman spectroscopy, and X-ray diffractometry have been employed to directly visualize fibril structure, address the linking/interaction of fibrils with surrounding fibrils, and/or calculate fibril strain under loading [46-49]. SEM/TEM shows D-period as alternative gap and overlap regions in images; D-period is often taken to calculate microscale deformation (Fig. 2A) [50-53]. Besides visualizing deformation, AFM has the high-throughput capabilities to dynamically generate maps of fibril mechanical properties such as elastic modulus and dissipated energy with high spatial resolution [40, 41, 54]. A technique called polarized Raman spectroscopy was used to measure the orientation of molecular structure and fibril reorganization within tendon fascicles loaded in tension [47, 55]. X-ray diffractometry, as well, was utilized to show that intra-fibril shearing during both creep and stress relaxation testing is a structural contributor to tendon multi-level behavior [46, 48, 49, 56]. These imaging techniques have succeeded in monitoring tendon nanoscale deformation caused by several different loading scenarios. One limitation of these techniques is that the required testing environments cannot mimic relevant *in vivo* physiological loading environments, especially with respect to hydration state and temperature. Furthermore, it is necessary to strengthen the crosstalk between different techniques by comparing reported

measurements of similar parameters so that results/conclusions of various studies derived from these techniques can be combined and integrated.

2.3.2 Fiber scale

On the fiber level, tendon structural characteristics, such as helical twist and crimp, have been visualized using imaging techniques, including polarized light, interference, and phase

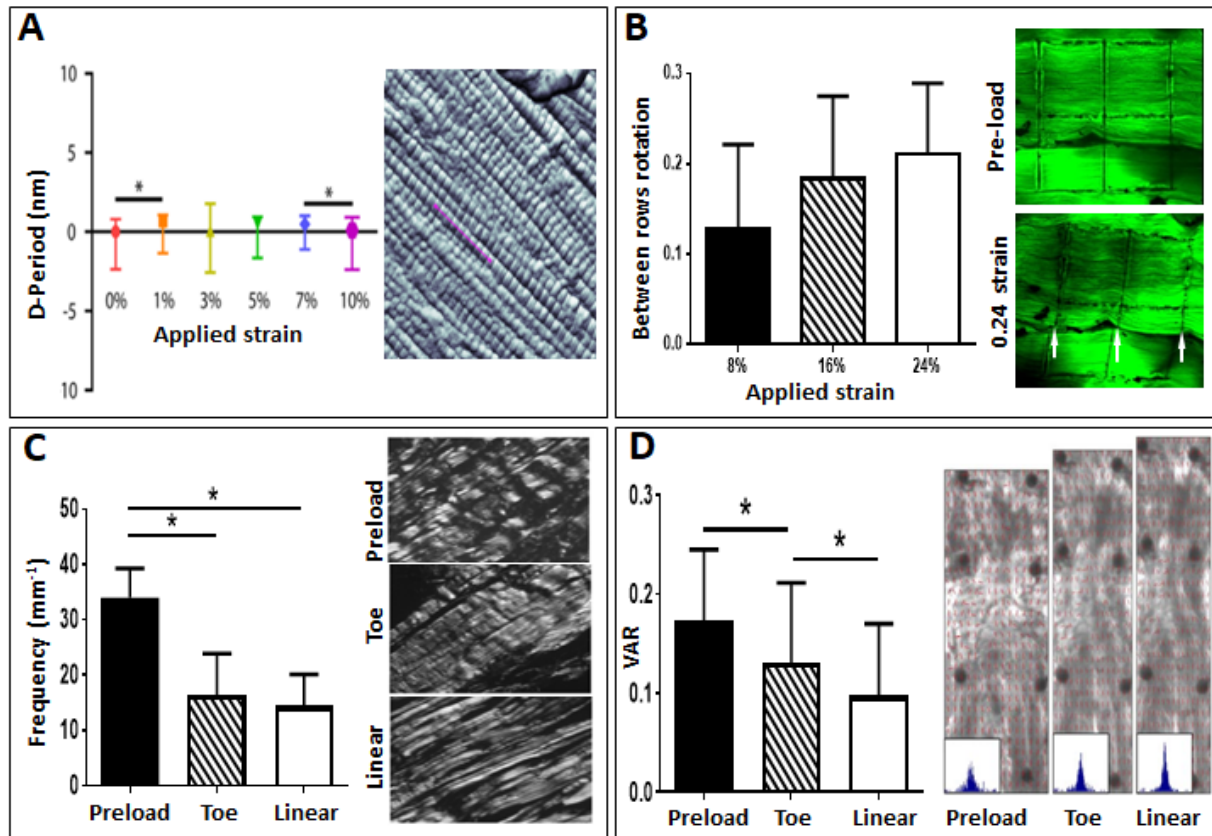


Fig. 2.2 Multiscale evaluation of tendon behavior/deformation as the response to tensile or shear loading. (A) D-period change of mouse SST during static tensile loading and AFM-acquired images measuring fibril D-period with line highlighted [15]. (B) A measure of microscale fiber sliding, termed between rows rotation, increased with increasing applied shear strain, while images taken via multiphoton microscopy showed fiber sliding during shear stress relaxation testing (white arrows denote photobleached lines broken due to fiber sliding). (C) Crimp frequency of tendon in tensile loading decreased from the toe to linear regions of the stress-strain curve and representative images of polarized light showing the change of crimp pattern [61]. (D) Circular variance values demonstrating increased fiber alignment during ramp to failure tensile testing, and fiber alignment maps and histograms calculated from polarized-light images [59].

contrast microscopy [53, 57]. The proposed biomechanical implications of these specific structural features have been examined in a number of studies, utilizing confocal/multi-photon/second harmonic generation (SHG) microscopy and quantitative polarized light imaging (QPLI) [19, 40-42, 57-65].

Confocal microscopy has been adopted to identify how unique helical feature of tendons from different anatomical locations govern specific mechanical properties. Superficial digital flexor tendon (SDFT), which functions in limb positioning and energy storing, was found to exhibit greater rotation and less sliding of collagen fibers during stress relaxation, compared to positional common digital extensor tendon (CDET) [19]. Different mechanical responses between these two tendons in tension may be due to greater helical pitch angle in SDFT than CDET [19]. Supporting these experimental results, micromechanical computational models incorporating fibril helical patterns were able to characterize stress-strain behavior under static loading and predicted that smaller helical angles contributed to less stiffness and smaller Poisson's ratio [66, 67]. However, it is still unknown how the helical structure would be altered, such as the decrease or disappearance of helical twist, under different loading scenarios [68]. Crimp of collagen fibers has been reported to resemble smooth sine waves or triangles with different lengths and widths in SEM and histological images, while also exhibiting the appearance of alternative dark and light transverse bands in images of linear/circular QPLI and optical coherence tomography (Fig. 2C&D) [60]. Collagen crimp has been proposed to contribute to strain-stress non-linearity by stretching as a result of small tensile forces at low strains, and function as something of a shock absorber [60, 69]. Another hypothesis is that the recoil or crimp of collagen fibers is potentially maintained by elastic fibers, which have been observed within the hierarchical tendon structure [70-72].

Sliding, another deformation mechanism that contributes to strain attenuation from tissue to micron scales, is distinctly observed in microscopic images of tendon after the application of stain (Fig. 2B) [19, 40, 41, 54, 64, 65, 68, 73]. From a structural perspective, organizational maps demonstrated that tendon was composed of discontinuous collagen fibrils, making possible rigid displacement such as fibril realignment and sliding [74]. From a functional perspective, sliding could act as a force damper to prevent overloading, help endow tendons with viscoelasticity, and/or modulate force/strain transfer to maintain a homeostatic environment for compositional remodeling and mechanotransduction [4, 75]. Fiber reorganization has also been suggested to contribute to tendon nonlinear mechanical properties (Fig. 2D) [58, 59]. Although fiber alignment in tendon did not significantly change during stress relaxation testing [63], fiber realignment along the loading direction increased dramatically in the toe region of a stress-strain curve to failure [58, 59] and linear region modulus was shown to positively correlate with the degree of fiber alignment [58]. Other factors, such as tendon age, loading protocol, disease, and injury, which alter fiber alignment on the microscale, collectively influence mechanical behavior in tension [62, 76-79].

Due to the development and availability of various techniques to evaluate tendon mechanics at the fiber level, previous studies have thoroughly examined tendon features at the microscale, their contributions to tendon response under different loading conditions, and the physical mechanisms governing tendon response under tensile loading. This information is fundamental for interpreting how tendon stress/loading is passed down from tissue to fiber scales.

2.3.3 Fascicle/tissue scale

Fascicles, assembled by multiple collagen fibers and encompassed by a soft connective layer called the interfascicular matrix (IFM)/endotenon, are then grouped together to comprise full

tendon tissue (Fig. 1). Using laser-capture microdissection and mass spectrometry, the IFM was shown to have greater variety and amounts of protein fragments compared to the fascicles themselves [80]. Different constituents between matrix phases, indicative of tendon heterogeneity, could lead to different mechanical properties when comparing measurements at the fascicle and tendon levels due to shear stress transfer and altered stress distribution to decrease failure [75, 80-82]. Furthermore, recent comparison between mechanical behaviors of fascicles from different tendon types suggested that the IFM potentially played a key role in tendon mechanics on the fascicular/tissue level by facilitating sliding between collagen fibers, and protecting cells inside IFM from overload [81-84]. Several questions, such as a full understanding of the IFM composition/structure of tendon from different anatomical locations, its contribution to more nuanced tendon mechanics (e.g., viscoelasticity), and its specific contribution to force/strain transfer among multiple length scales, need to be addressed further.

On the tissue level, tendons have been tested *in vitro* under multiaxial loading conditions (i.e., tension, compression, shear) and their mechanical properties have been shown to vary between individuals, across different anatomical locations, and even within specific regions [39, 85-88]. Although tendons are composed of relatively highly-organized collagen fibers, they often possess microscale heterogeneity and anisotropy, indicated by varying values of mechanical parameters in different loading locations and directions [89].

While beneficial for evaluating tendon mechanics, *in vitro* measurements of mechanical behavior cannot fully replicate the *in vivo* physiological loading environment [73]. To overcome such limitations, ultrasound elastography and magnetic resonance imaging (MRI) have been used to evaluate *in vivo* tendon mechanics. Combined with digital image correlation and/or acoustic markers, these imaging techniques have been used to quantify mechanical strength, viscoelastic

properties, and deformation at different joint positions for monitoring injury or rehabilitation after surgical reconstruction [90-101]. These *in vivo* measurement techniques also enable examination of the effect of age, loading pattern, and loading rate on region-specific responses [93-97, 100, 102]. However, some challenges remain that limit the ability to extract information of tendon strength via MRI and correlate quantitative values with measures of tendon structure. In the future, comparison and correlation of data from advanced techniques using ultrasound elastography and MRI could complement understanding of tendon tissue-scale mechanics.

Taken together, a variety of techniques have enabled evaluation of mechanics at the fibril, fiber, and fascicle/tendon scales, which have elucidated a number of structurally-relevant mechanisms that contribute to tendon mechanical responses. Features (i.e. crimp pattern, helical structure) and modes of microscale deformation (i.e., sliding, reorganization) contribute to typical stress responses under static and cyclic loading. Additional work should be undertaken to combine experimental studies at different length scales, especially including experiments that extend down to (and incorporate) the level of cells, and build appropriate setups to track microscale tendon responses under *in vivo* loading conditions.

2.4 The contribution of different components to tendon mechanics

Collagen I, the primary structural protein of tendon, is acknowledged as the fundamental element responsible for force transmission in connective tissues [4]. At the nanoscale, collagen crosslinks bridge adjacent collagen fibrils [103, 104]. However, several other tissue constituents, such as proteoglycans, elastin, and tenascin-C, have also been localized in tendon using a variety of biological techniques including histology, immunohistochemistry, and biochemical assays, and their mechanical roles have attracted more attention recently [70, 105-109]. This section will

summarize what is currently known regarding the contributions of these tissue constituents to tendon mechanics.

2.4.1 Tendon primary components

Collagen crosslinks. Collagen crosslinks have been shown to quarterly stagger collagen end by end, thus helping to stabilize tendon structure and contribute to nanoscale mechanical strength [103, 104, 110]. These collagen crosslinks have been localized inside, as well as between, collagen microfibrils [111]. Previous studies indicate that types and amounts of collagen crosslinks depend on the degree of hydroxylation and maturation [112, 113].

To evaluate the contribution of enzymatic collagen crosslinks to mechanical properties at different length scales, a few studies have performed *in vivo* or *in vitro* biomechanical testing on tendons with altered amounts of crosslinks and evaluated crosslink amount by high performance liquid chromatography (HPLC) [46, 73, 104]. On both the fibril and tissue levels, crosslink-deficient tendon fibrils and whole tendons showed dramatically reduced fracture stresses or elastic modulus, compared to normal ones [46, 103, 110, 114, 115]. However, conflicting findings from other studies, which showed that tendons with higher concentration of mature collagen crosslinks had similar or deteriorated mechanics than those with lower concentration, make it difficult to clearly determine the mechanical function of enzymatic collagen crosslinks [116, 117]. Additionally, the content and distribution of enzymatic crosslinks in tissues vary and are altered by locations and health conditions [118-120], which further complicates the determination of the role of specific crosslinks in multilevel tendon mechanics. Non-enzymatic collagen crosslinks, in the form of advanced glycation end products such as pentosidine, are often created by glycation related to aging and diabetes [121-123]. The influence of non-enzymatic collagen crosslinks in tendon mechanical behavior was evaluated in sugar-treated and

diabetic tendons [121-123]. On the tissue scale, tendons with increased pentosidine consistently exhibited higher mechanical parameters (i.e., maximum load, toughness, failure modulus, and yield energy), and less stress relaxation compared to native tendons [124-126]. Interestingly, non-enzymatic crosslinks did not continue to influence tendon mechanics on the microscale [127].

These studies illustrate that both enzymatic and non-enzymatic collagen crosslinks may play a role in tendon mechanics. However, more carefully designed and controlled studies, especially at different length scales, need to be performed to address contradictory results, and explore how the alternation of crosslink amounts on the nanoscale can change mechanical properties on the tissue level.

Proteoglycans. Proteoglycans (PGs, e.g., decorin, biglycan, fibromodulin, lumican, aggrecan, versican), composed of a core protein and covalently attached glycosaminoglycan side chains (GAGs), are dispersed throughout the tendon hierarchy, including in intra- and inter-fascicle locations (Fig. 3) [128, 129]. The distribution and density of PGs differ between tendon types and maturity level [130, 131]. PGs serve several functions including to constitute extracellular matrix, modulate collagen fibril diameter during fibrillogenesis, and cooperate with growth factors to regulate cell proliferation [106]. Although tendons typically only contain PGs at about 1-5% dry weight, PGs are thought to contribute to tendon physiology and biomechanical function [106].

An early hypothesis suggested that the core protein of PGs bound to collagen fibrils to form inter-fibrillar bridges and aid in strain transfer between discontinuous collagen fibrils [26, 132]. In support of this, mature tendons exhibited higher failure stresses than immature tendons with less PGs [129, 133]. Additionally, a multi-fibril model, which incorporated a chondroitin-6-

sulphate side chain to mimic discontinuous fibril assembly in mature tendons, showed consistent failure stresses and elastic modulus with experimental data [134]. However, other theoretical models and experiment results question this hypothesis. One molecular model composed of type I collagen molecules and decorin core proteins illustrated that the attained binding force was too weak to facilitate force support [135]. Experimental data have also shown that enzymatic depletion of GAGs from tendon fascicles did not significantly change tendon modulus, relative energy dissipation, peak stresses or peak strains, thereby demonstrating no influence of GAGs on tendon mechanical behavior under tensile loading [136-139]. To address these conflicting modeling and experimental results, a modified shear lag model identified a characteristic length scale relative to GAG spacing and geometry [26]. Using this model, tendon mechanical properties were suggested not to change after GAG deletion if fibril length was significantly larger than the characteristic length scale [26]. As another method to evaluate the mechanical role of PGs, Achilles tendons from decorin-null, biglycan-null, and heterozygote mice showed inferior mechanical properties in tension compared to tendons from wildtype mice [23]. However, patellar tendons from biglycan-heterozygote and biglycan-null mice exhibited increased viscoelasticity, but similar elastic and compressive properties compared to wild type [140]. These inconsistent reports imply that the role of PGs likely depends on tendon location, loading types, and even ages [141]. Furthermore, recent reports showed that tendons with specific PGs knocked-out (i.e., decorin, biglycan) exhibited altered collagen content and fibril diameters [140]. Interestingly, the lack of specific PGs in the knock-out model could be substituted by increased expression of other types of PGs so that tendon mechanical properties remain unchanged [106, 140]. Therefore, it should be taken into consideration whether/how enzymatic depletion or genetic alteration of PGs influences the structure and concentration of

collagen fibers or even modulates the amount of water or other tissue components present in tendon.

Elastin. Elastin is formed by multiple monomeric soluble precursor tropoelastins through lysyl oxidase catalyzed crosslinks and occupies ~1-3% dry mass in tendon (Fig. 2.3) [70, 142]. Elastic fibers are formed by elastin deposited within and around assembled microfibrils, which are comprised of several proteins including fibrillin [70, 143, 144]. Using immunochemistry, previous studies illustrated that elastic fibers in tendon were dispersed between fascicles and around tenocytes, travelling longitudinally along collagen fibers [25, 70, 145]. Elastic fibers not only regulate cell adhesion, cell migration, and even cell signaling, but also may endow soft tissues (i.e., ligament, aorta, skin) with elastic recoil and resilience [106, 146].

To illustrate the mechanical role of elastin in ligaments and intervertebral discs, tensile, transverse tensile, and shear tests of elastin-depleted tissues showed decreased peak stresses and modulus, suggesting that elastin helps maintain multiaxial tissue integrity [70, 72, 147, 148]. Similar to PG studies, potential side effects of elastase treatment and elastin-related genetic modification should be examined carefully. Further research is needed to understand the specific mechanisms governing how elastic fibers regulate tendon force support and transfer among different hierarchical levels of tendon.

2.4.2 Tendon other components with small amounts

In addition to these tissue constituents, tendons also contain varying amounts of other proteins, such as other collagens (e.g., types II, III, V, etc.), lubricin, tenascin-C, and collagen oligomeric matrix protein (COMP), which may contribute mechanically (Fig. 2.3) [4, 149-154]. Interestingly, previous studies showed that fibrils formed by collagen type II and III, related with

tendon healing, were smaller than these of collagen type I [108, 150, 155, 156]. Collagen type II content was higher near the insertion of human SST, which experiences more compressive loading compared to the midsubstance, and collagen type III content was inversely correlated with tendon tensile modulus and collagen alignment [150, 157, 158]. Mutations of collagen type V causes joint hypermobility in classic Ehlers-Danols syndrome, which

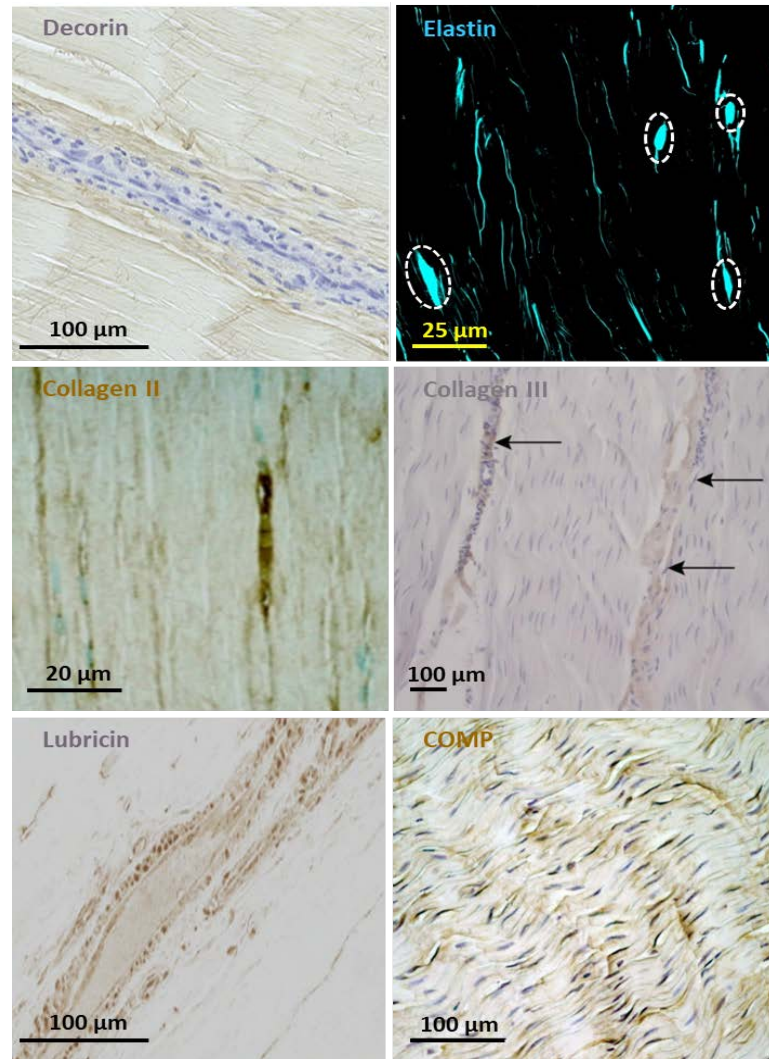


Fig. 2.3 Images demonstrating that some of the minor constituents, suggested to have mechanical roles, are found in tendon. Immunohistochemistry for decorin (stained purple) from equine CDET [154], elastin (stained cyan) from human SST (ellipses denoting nuclei), collagen II (stained brown) from mouse Achilles tendon [159], collagen III (marked by arrows, also stained purple), lubricin (stained purple) from equine SDFT [154], and COMP (stained brown) from equine SDFT [156].

motivates the evaluation of the contribution of collagen type V to tendon mechanics [159]. Tendons from conditional collagen V-null

mice exhibited decreased linear stiffness and modulus values in static tensile loading [160], which corresponded to fibrils with increased diameters, decreased fibril density and less obvious crimp morphology, and abnormal fiber organization [151, 161]. A unique mucin-glycoprotein known as lubricin or proteoglycan 4, is also localized in soft connective tissues, such as cartilage,

ligaments, menisci, intervertebral discs, and tendons [162]. Lubricin has been identified to be essential for cartilage lubrication and cytoprotection, including preventing synovial fluid proteins from depositing onto cartilage and reducing chondrocyte apoptosis [152, 162-165]. Particularly for tendons at anatomical locations where inter-or intra-tendinous shear forces occur (i.e., flexor tendon, Achilles tendon), lubricin has been suggested to facilitate tendon gliding against surrounding tissues on the tissue scale and assist the relative movement between tendon fascicles on the microscale [162, 166]. Flexor tendons treated with lubricin showed lower gliding resistance and decreased adhesions than untreated tendons [167-169]. Both flexor tendons and tail tendon fascicles from lubricin-deficient mice exhibited similar Young's modulus, but decreased viscoelasticity and gliding resistance, compared to tissues from wild-type mice [152, 166, 170].

Tenascin-C, an anti-adhesive protein, was shown to be primarily expressed in the distal (compressed) region of flexor tendons and also expressed more in normal than unloaded tendons, suggesting that it could help tendon maintain fibrocartilaginous regions and provide support for loading [107, 171, 172]. Tenascin-C has also been associated with regulation of cell-matrix interactions and, subsequently, mediation of inflammatory and fibrotic processes to affect tissue during development, degeneration, and pathological processes [143, 171, 173]. COMP, a pentameric protein which binds to fibrillar collagen, has a limited distribution in tendon [174]. Besides the hypothesis that COMP regulates collagen fibrillogenesis, COMP content in horse tendons was positively correlated with tensile stress and stiffness in a skeletal maturity-dependent way [174, 175]. Thus far, evidence seems to suggest that tenascin-C and COMP are important for tendon function, but more work should evaluate whether they modify tendon properties directly or through altering collagen expression and modification.

In summary, different constituents that are present in small quantities in tendon have been examined to address their mechanical roles using approaches such as *in vivo* drug administration, *in vitro* enzyme treatment, and the use of genetically-modified animal models. Although these approaches have some potential limitations, studies have shown that many of these constituents play a role in tendon formation, development, remodeling, and thereby affect tendon mechanical behavior. Because most of previous studies have evaluated their contribution on the tissue scale under tensile loading, additional studies should be conducted to comprehensively explore their roles across multiple scales under different loading conditions.

2.5 References

1. Wang, J.H., *Mechanobiology of tendon*. J Biomech, 2006. 39(9): p. 1563-1582.
2. Lavagnino, M., et al., *Tendon mechanobiology: Current knowledge and future research opportunities*. J Orthop Res, 2015. 33(6): p. 813-822.
3. Nourissat, G., F. Berenbaum, and D. Duprez, *Tendon injury: from biology to tendon repair*. Nature Reviews Rheumatology, 2015. 11(4): p. 223-233.
4. Screen, H.R., et al., *Tendon functional extracellular matrix*. Journal of Orthopaedic Research, 2015. 33(6): p. 793-799.
5. Thompson, M.S., *Tendon mechanobiology: experimental models require mathematical underpinning*. Bulletin of mathematical biology, 2013. 75(8): p. 1238-1254.
6. Handsfield, G.G., L.C. Slane, and H.R. Screen, *Nomenclature of the Tendon Hierarchy: An Overview of Inconsistent Terminology and a Proposed Size-Based Naming Scheme with Terminology for Multi-Muscle Tendons*. Journal of Biomechanics, 2016. 49(13): p. 3122-3124.
7. Shepherd, J.H., et al., *Functionally distinct tendon fascicles exhibit different creep and stress relaxation behaviour*. Proceedings of the Institution of Mechanical Engineers, Part H: Journal of Engineering in Medicine, 2013. 228(1): p. 49-59.
8. Lui, P., *Stem cell technology for tendon regeneration: current status, challenges, and future research directions*. Stem Cells Cloning, 2015. 7: p. 163-174.
9. Riley, G., et al., *Tendon degeneration and chronic shoulder pain: changes in the collagen composition of the human rotator cuff tendons in rotator cuff tendinitis*. Annals of the rheumatic diseases, 1994. 53(6): p. 359-366.
10. Connizzo, B.K., S.M. Yannascoli, and L.J. Soslowsky, *Structure–function relationships of postnatal tendon development: A parallel to healing*. Matrix Biology, 2013. 32(2): p. 106-116.

11. Mouw, J.K., G. Ou, and V.M. Weaver, *Extracellular matrix assembly: a multiscale deconstruction*. Nature Reviews Molecular Cell Biology, 2014. 15(12): p. 771-785.
12. Wang, J.H.-C., *Mechanobiology of tendon*. Journal of biomechanics, 2006. 39(9): p. 1563-1582.
13. Fessel, G. and J.G. Snedeker, *Evidence against proteoglycan mediated collagen fibril load transmission and dynamic viscoelasticity in tendon*. Matrix Biol, 2009. 28(8): p. 503-510.
14. Spiesz, E.M., et al., *Tendon extracellular matrix damage, degradation and inflammation in response to in vitro overload exercise*. Journal of Orthopaedic Research, 2015. 33(6): p. 889-897.
15. Connizzo, B.K., et al., *In situ fibril stretch and sliding is location-dependent in mouse supraspinatus tendons*. Journal of biomechanics, 2014. 47(16): p. 3794-3798.
16. Kastelic, J., I. Palley, and E. Baer, *A structural mechanical model for tendon crimping*. J Biomech, 1980. 13(10): p. 887-893.
17. de Campos Vidal, B., *Image analysis of tendon helical superstructure using interference and polarized light microscopy*. Micron, 2003. 34(8): p. 423-432.
18. Kalson, N.S., et al., *Fibre bundles in the human extensor carpi ulnaris tendon are arranged in a spiral*. J Hand Surg Eur Vol, 2012. 37(6): p. 550-554.
19. Thorpe, C.T., et al., *Helical sub-structures in energy-storing tendons provide a possible mechanism for efficient energy storage and return*. Acta biomaterialia, 2013. 9(8): p. 7948-7956.
20. Thorpe, C.T., et al., *The role of the non-collagenous matrix in tendon function*. Int J Exp Pathol, 2013. 94(4): p. 248-259.
21. Kjøer, M., *Role of extracellular matrix in adaptation of tendon and skeletal muscle to mechanical loading*. Physiological reviews, 2004. 84(2): p. 649-698.
22. Riley, G., *The pathogenesis of tendinopathy. A molecular perspective*. Rheumatology, 2004. 43(2): p. 131-142.
23. Gordon, J.A., et al., *Achilles tendons from decorin- and biglycan-null mouse models have inferior mechanical and structural properties predicted by an image-based empirical damage model*. Journal of biomechanics, 2015. 48(10): p. 2110-2115.
24. Matuszewski, P.E., et al., *Regional variation in human supraspinatus tendon proteoglycans: decorin, biglycan, and aggrecan*. Connective tissue research, 2012. 53(5): p. 343-348.
25. Thakkar, D., et al., *Distribution and expression of type VI collagen and elastic fibers in human rotator cuff tendon tears*. Connective tissue research, 2014. 55(5-6): p. 397-402.
26. Ahmadzadeh, H., et al., *Determining the contribution of glycosaminoglycans to tendon mechanical properties with a modified shear-lag model*. J Biomech, 2013. 46(14): p. 2497-2503.
27. Pioletti, D.P., et al., *Viscoelastic constitutive law in large deformations: application to human knee ligaments and tendons*. J Biomech, 1998. 31(8): p. 753-757.

28. Johnson, G., et al., *A single integral finite strain viscoelastic model of ligaments and tendons*. Journal of biomechanical engineering, 1996. 118(2): p. 221-226.
29. Duenwald, S.E., R. Vanderby Jr, and R.S. Lakes, *Constitutive equations for ligament and other soft tissue: evaluation by experiment*. Acta mechanica, 2009. 205(1-4): p. 23-33.
30. Troyer, K.L., S.S. Shetye, and C.M. Puttlitz, *Experimental characterization and finite element implementation of soft tissue nonlinear viscoelasticity*. Journal of biomechanical engineering, 2012. 134(11): p. 114501.
31. Vena, P., D. Gastaldi, and R. Contro, *A constituent-based model for the nonlinear viscoelastic behavior of ligaments*. Journal of biomechanical engineering, 2006. 128(3): p. 449-457.
32. Cribb, A.M. and J.E. Scott, *Tendon response to tensile stress: an ultrastructural investigation of collagen:proteoglycan interactions in stressed tendon*. J Anat, 1995. 187(2): p. 423-8.
33. Kondratko, J., et al., *Mechanical compromise of partially lacerated flexor tendons*. J Biomech Eng, 2013. 135(1): p. 011001.
34. Ault, H. and A. Hoffman, *A composite micromechanical model for connective tissues: Part I—theory*. Journal of biomechanical engineering, 1992. 114(1): p. 137-141.
35. Sano, H., I. Wakabayashi, and E. Itoi, *Stress distribution in the supraspinatus tendon with partial-thickness tears: an analysis using two-dimensional finite element model*. Journal of shoulder and elbow surgery, 2006. 15(1): p. 100-105.
36. Tang, C., et al., *Parameter optimization for the visco-hyperelastic constitutive model of tendon using FEM*. Bio-medical materials and engineering, 2011. 21(1): p. 9-24.
37. Reese, S.P., S.A. Maas, and J.A. Weiss, *Micromechanical models of helical superstructures in ligament and tendon fibers predict large Poisson's ratios*. J Biomech, 2010. 43(7): p. 1394-1400.
38. Herchenhan, A., et al., *Tenocyte contraction induces crimp formation in tendon-like tissue*. Biomech Model Mechanobiol, 2012. 11(3-4): p. 449-459.
39. Zobitz, M.E., Z.-P. Luo, and K.-N. An, *Determination of the compressive material properties of the supraspinatus tendon*. Journal of biomechanical engineering, 2001. 123(1): p. 47-51.
40. Han, W.M., et al., *Macro- to microscale strain transfer in fibrous tissues is heterogeneous and tissue-specific*. Biophys J, 2013. 105(3): p. 807-817.
41. Han, W.M., et al., *Microstructural heterogeneity directs micromechanics and mechanobiology in native and engineered fibrocartilage*. Nature materials, 2016. 15(4): p. 477-484.
42. Chen, X., et al., *Second harmonic generation microscopy for quantitative analysis of collagen fibrillar structure*. Nature protocols, 2012. 7(4): p. 654-669.
43. Gautieri, A., et al., *Hierarchical structure and nanomechanics of collagen microfibrils from the atomistic scale up*. Nano letters, 2011. 11(2): p. 757-766.

44. Galloway, M.T., A.L. Lalley, and J.T. Shearn, *The role of mechanical loading in tendon development, maintenance, injury, and repair*. J Bone Joint Surg Am, 2013. 95(17): p. 1620-1628.
45. Harvey, A., et al., *Functional imaging of tendon*. Ann. Brit. Machine Vision Assoc, 2009. 2009: p. 1-11.
46. Puxkandl, R., et al., *Viscoelastic properties of collagen: synchrotron radiation investigations and structural model*. Philosophical Transactions of the Royal Society of London B: Biological Sciences, 2002. 357(1418): p. 191-197.
47. Galvis, L., et al., *Polarized Raman anisotropic response of collagen in tendon: towards 3D orientation mapping of collagen in tissues*. PloS one, 2013. 8(5): p. e63518.
48. Gupta, H., et al., *In situ multi-level analysis of viscoelastic deformation mechanisms in tendon collagen*. Journal of structural biology, 2010. 169(2): p. 183-191.
49. Sasaki, N., et al., *Time-resolved X-ray diffraction from tendon collagen during creep using synchrotron radiation*. Journal of biomechanics, 1999. 32(3): p. 285-292.
50. Veres, S.P., J.M. Harrison, and J.M. Lee, *Repeated subrupture overload causes progression of nanoscaled discrete plasticity damage in tendon collagen fibrils*. Journal of Orthopaedic Research, 2013. 31(5): p. 731-737.
51. Frisch, K.E., et al., *Quantification of collagen organization using fractal dimensions and Fourier transforms*. Acta histochemica, 2012. 114(2): p. 140-144.
52. Veres, S.P., J.M. Harrison, and J.M. Lee, *Cross-link stabilization does not affect the response of collagen molecules, fibrils, or tendons to tensile overload*. Journal of Orthopaedic Research, 2013. 31(12): p. 1907-1913.
53. Kalson, N., et al., *Fibre bundles in the human extensor carpi ulnaris tendon are arranged in a spiral*. Journal of Hand Surgery (European Volume), 2012. 37(6): p. 550-554.
54. Screen, H.R., Bader, D. L., Lee, D. A., Shelton, J. C., *Local Strain Measurement within Tendon Strain*, 2004. 40(4): p. 157-163.
55. Masic, A., et al., *Observations of multiscale, stress-induced changes of collagen orientation in tendon by polarized Raman spectroscopy*. Biomacromolecules, 2011. 12(11): p. 3989-3996.
56. Fratzl, P., et al., *Fibrillar structure and mechanical properties of collagen*. Journal of structural biology, 1998. 122(1): p. 119-122.
57. de Campos Vidal, B., *Image analysis of tendon helical superstructure using interference and polarized light microscopy*. Micron, 2003. 34(8): p. 423-432.
58. Lake, S.P., et al., *Tensile properties and fiber alignment of human supraspinatus tendon in the transverse direction demonstrate inhomogeneity, nonlinearity, and regional isotropy*. Journal of biomechanics, 2010. 43(4): p. 727-732.
59. Lake, S.P., et al., *Effect of fiber distribution and realignment on the nonlinear and inhomogeneous mechanical properties of human supraspinatus tendon under longitudinal tensile loading*. Journal of orthopaedic research: official publication of the Orthopaedic Research Society, 2009. 27(12): p. 1596.

60. Franchi, M., et al., *Crimp morphology in relaxed and stretched rat Achilles tendon*. Journal of anatomy, 2007. 210(1): p. 1-7.
61. Miller, K.S., et al., *Examining differences in local collagen fiber crimp frequency throughout mechanical testing in a developmental mouse supraspinatus tendon model*. Journal of biomechanical engineering, 2012. 134(4): p. 041004.
62. Miller, K.S., B.K. Connizzo, and L.J. Soslowsky, *Collagen fiber re-alignment in a neonatal developmental mouse supraspinatus tendon model*. Annals of biomedical engineering, 2012. 40(5): p. 1102-1110.
63. Miller, K.S., et al., *Effect of preconditioning and stress relaxation on local collagen fiber re-alignment: inhomogeneous properties of rat supraspinatus tendon*. Journal of biomechanical engineering, 2012. 134(3): p. 031007.
64. Reese, S.P., S.A. Maas, and J.A. Weiss, *Micromechanical models of helical superstructures in ligament and tendon fibers predict large Poisson's ratios*. Journal of biomechanics, 2010. 43(7): p. 1394-1400.
65. Szczesny, S.E., R.S. Edelman, and D.M. Elliott, *DTAF dye concentrations commonly used to measure microscale deformations in biological tissues alter tissue mechanics*. PLoS One, 2014. 9(6): p. e99588.
66. Bajuri, M., et al., *A hyperelastic fibre-reinforced continuum model of healing tendons with distributed collagen fibre orientations*. Biomechanics and modeling in mechanobiology, 2016: p. 1-10.
67. Shearer, T., *A new strain energy function for modelling ligaments and tendons whose fascicles have a helical arrangement of fibrils*. Journal of biomechanics, 2015. 48(12): p. 3017-3025.
68. Birch, H.L., C.T. Thorpe, and A.P. Rumian, *Specialisation of extracellular matrix for function in tendons and ligaments*. Muscles, ligaments and tendons journal, 2013. 3(1): p. 12-22.
69. Herchenhan, A., et al., *Tenocyte contraction induces crimp formation in tendon-like tissue*. Biomechanics and modeling in mechanobiology, 2012. 11(3-4): p. 449-459.
70. Grant, T.M., et al., *Elastic fibres are broadly distributed in tendon and highly localized around tenocytes*. Journal of anatomy, 2013. 222(6): p. 573-579.
71. Grant, T.M., et al., *The Mechanical, Structural, and Compositional Changes of Tendon Exposed to Elastase*. Annals of biomedical engineering, 2015. 43(10): p. 2477-2486.
72. Henninger, H.B., et al., *Elastin governs the mechanical response of medial collateral ligament under shear and transverse tensile loading*. Acta biomaterialia, 2015. 25: p. 304-312.
73. Svensson, R.B., et al., *Mechanical properties of human patellar tendon at the hierarchical levels of tendon and fibril*. Journal of Applied Physiology, 2012. 112(3): p. 419-426.
74. Provenzano, P.P. and R. Vanderby, *Collagen fibril morphology and organization: implications for force transmission in ligament and tendon*. Matrix Biology, 2006. 25(2): p. 71-84.

75. Szczesny, S.E., et al., *Quantification of Interfibrillar Shear Stress in Aligned Soft Collagenous Tissues via Notch Tension Testing*. Scientific reports, 2015. 5.
76. Miller, K.S., et al., *Characterizing local collagen fiber re-alignment and crimp behavior throughout mechanical testing in a mature mouse supraspinatus tendon model*. Journal of biomechanics, 2012. 45(12): p. 2061-2065.
77. Freedman, B.R., et al., *Biomechanical and structural response of healing Achilles tendon to fatigue loading following acute injury*. Journal of biomechanics, 2014. 47(9): p. 2028-2034.
78. Connizzo, B.K., et al., *Diabetes alters mechanical properties and collagen fiber re-alignment in multiple mouse tendons*. Annals of biomedical engineering, 2014. 42(9): p. 1880-1888.
79. Bagnaninchi, P., et al., *In-depth imaging and quantification of degenerative changes associated with Achilles ruptured tendons by polarization-sensitive optical coherence tomography*. Physics in medicine and biology, 2010. 55(13): p. 3777.
80. Thorpe, C.T., et al., *Anatomical heterogeneity of tendon: Fascicular and interfascicular tendon compartments have distinct proteomic composition*. Scientific reports, 2016. 6.
81. Komolafe, O.A. and T.C. Doehring, *Fascicle-scale loading and failure behavior of the Achilles tendon*. Journal of biomechanical engineering, 2010. 132(2): p. 021004.
82. Kondratko-Mittnacht, J., et al., *Shear load transfer in high and low stress tendons*. Journal of the mechanical behavior of biomedical materials, 2015. 45: p. 109-120.
83. Thorpe, C.T., et al., *Capacity for sliding between tendon fascicles decreases with ageing in injury prone equine tendons: a possible mechanism for age-related tendinopathy*. Eur. Cells Mater, 2013. 25: p. 48-60.
84. Thorpe, C.T., et al., *Specialization of tendon mechanical properties results from interfascicular differences*. Journal of The Royal Society Interface, 2012: p. rsif20120362.
85. Reyes, A., et al., *Prediction of the elastic strain limit of tendons*. journal of the mechanical behavior of biomedical materials, 2014. 30: p. 324-338.
86. Kolz, C.W., T. Suter, and H.B. Henninger, *Regional mechanical properties of the long head of the biceps tendon*. Clinical Biomechanics, 2015. 30(9): p. 940-945.
87. Thomas, S.J., K.S. Miller, and L.J. Soslowky, *The upper band of the subscapularis tendon in the rat has altered mechanical and histologic properties*. Journal of Shoulder and Elbow Surgery, 2012. 21(12): p. 1687-1693.
88. Lee, S.-B., et al., *The bursal and articular sides of the supraspinatus tendon have a different compressive stiffness*. Clinical Biomechanics, 2000. 15(4): p. 241-247.
89. Böl, M., et al., *Tissue-scale anisotropy and compressibility of tendon in semi-confined compression tests*. Journal of biomechanics, 2015. 48(6): p. 1092-1098.
90. Riggins, C.N., et al., *Analysis of collagen organization in mouse achilles tendon using high-frequency ultrasound imaging*. Journal of biomechanical engineering, 2014. 136(2): p. 021029.

91. Okotie, G., et al., *Tendon strain measurements with dynamic ultrasound images: evaluation of digital image correlation*. Journal of biomechanical engineering, 2012. 134(2): p. 024504.
92. Slane, L.C. and D.G. Thelen, *The use of 2D ultrasound elastography for measuring tendon motion and strain*. Journal of biomechanics, 2014. 47(3): p. 750-754.
93. Slane, L.C. and D.G. Thelen, *Achilles tendon displacement patterns during passive stretch and eccentric loading are altered in middle-aged adults*. Medical engineering & physics, 2015. 37(7): p. 712-716.
94. Hsiao, M.-Y., et al., *Reduced Patellar Tendon Elasticity with Aging: In Vivo Assessment by Shear Wave Elastography*. Ultrasound in medicine & biology, 2015. 41(11): p. 2899-2905.
95. Franz, J.R., et al., *Non-uniform in vivo deformations of the human Achilles tendon during walking*. Gait & posture, 2015. 41(1): p. 192-197.
96. Slane, L.C., et al., *Middle-aged adults exhibit altered spatial variations in Achilles tendon wave speed*. Physiological measurement, 2015. 36(7): p. 1485-1496.
97. Kösters, A., et al., *Influence of loading rate on patellar tendon mechanical properties in vivo*. Clinical Biomechanics, 2014. 29(3): p. 323-329.
98. Cortes, D.H., et al., *Continuous Shear Wave Elastography: A New Method to Measure Viscoelastic Properties of Tendons in Vivo*. Ultrasound in medicine & biology, 2015. 41(6): p. 1518-1529.
99. Suydam, S.M., et al., *Viscoelastic properties of healthy achilles tendon are independent of isometric plantar flexion strength and cross-sectional area*. Journal of Orthopaedic Research, 2015. 33(6): p. 926-931.
100. Chimenti, R.L., et al., *Insertional Achilles tendinopathy associated with altered transverse compressive and axial tensile strain during ankle dorsiflexion*. Journal of Orthopaedic Research, 2017. 35(4): p. 910-915.
101. Chen, X.-M., et al., *Shear wave elastographic characterization of normal and torn achilles tendons a pilot study*. Journal of ultrasound in Medicine, 2013. 32(3): p. 449-455.
102. Chimenti, R.L., et al., *Ultrasound strain mapping of Achilles tendon compressive strain patterns during dorsiflexion*. Journal of biomechanics, 2016. 49(1): p. 39-44.
103. Marturano, J.E., et al., *Lysyl oxidase-mediated collagen crosslinks may be assessed as markers of functional properties of tendon tissue formation*. Acta biomaterialia, 2014. 10(3): p. 1370-1379.
104. Makris, E.A., et al., *Developing functional musculoskeletal tissues through hypoxia and lysyl oxidase-induced collagen crosslinking*. Proceedings of the National Academy of Sciences, 2014. 111(45): p. 4832-4841.
105. Koob, T. and K.G. Vogel, *Proteoglycan synthesis in organ cultures from regions of bovine tendon subjected to different mechanical forces*. Biochemical Journal, 1987. 246(3): p. 589-598.
106. Halper, J., *Proteoglycans and diseases of soft tissues*, in *Progress in Heritable Soft Connective Tissue Diseases*. 2014, Springer. p. 49-58.

107. Martin, J., et al., *The role of tenascin-C in adaptation of tendons to compressive loading*. Biorheology, 2003. 40(1, 2, 3): p. 321-329.
108. Pajala, A., et al., *TenascinC and type I and III collagen expression in total Achilles tendon rupture. An immunohistochemical study*. 2009. 24(10): p. 1207-1211.
109. Smith, L.J., et al., *Tunability of collagen matrix mechanical properties via multiple modes of mineralization*. Interface Focus, 2016. 6(1): p. 20150070.
110. Marturano, J.E., et al., *Characterization of mechanical and biochemical properties of developing embryonic tendon*. Proceedings of the National Academy of Sciences, 2013. 110(16): p. 6370-6375.
111. Sung, H.W., et al., *Crosslinking of biological tissues using genipin and/or carbodiimide*. Journal of Biomedical Materials Research Part A, 2003. 64(3): p. 427-438.
112. Eyre, D.R., M.A. Paz, and P.M. Gallop, *Crosslinking in collagen and elastin*. Annual review of biochemistry, 1984. 53(1): p. 717-748.
113. Eyre, D.R., M.A. Weis, and J.-J. Wu, *Advances in collagen crosslink analysis*. Methods, 2008. 45(1): p. 65-74.
114. Svensson, R.B., et al., *Fracture mechanics of collagen fibrils: influence of natural crosslinks*. Biophysical journal, 2013. 104(11): p. 2476-2484.
115. Haut, R., *The effect of a lathyritic diet on the sensitivity of tendon to strain rate*. Journal of biomechanical engineering, 1985. 107(2): p. 166-174.
116. Coupe, C., et al., *Mechanical properties and collagen crosslinking of the patellar tendon in old and young men*. Journal of applied physiology, 2009. 107(3): p. 880-886.
117. Hansen, P., et al., *Lower strength of the human posterior patellar tendon seems unrelated to mature collagen crosslinking and fibril morphology*. Journal of applied physiology, 2010. 108(1): p. 47-52.
118. Bank, R.A., et al., *Lysylhydroxylation and non-reducible crosslinking of human supraspinatus tendon collagen: changes with age and in chronic rotator cuff tendinitis*. Annals of the Rheumatic Diseases, 1999. 58(1): p. 35-41.
119. Suzuki, D., et al., *Biochemical study of collagen and its crosslinks in the anterior cruciate ligament and the tissues used as a graft for reconstruction of the anterior cruciate ligament*. Connective tissue research, 2008. 49(1): p. 42-47.
120. Willett, T.L., et al., *Changes in collagen with aging maintain molecular stability after overload: evidence from an in vitro tendon model*. Journal of biomechanical engineering, 2010. 132(3): p. 031002.
121. Reddy, G.K., *Glucose-mediated in vitro glycation modulates biomechanical integrity of the soft tissues but not hard tissues*. Journal of orthopaedic research, 2003. 21(4): p. 738-743.
122. Sajithlal, G., P. Chithra, and G. Chandrakasan, *Advanced glycation end products induce crosslinking of collagen in vitro*. Biochimica et Biophysica Acta (BBA)-Molecular Basis of Disease, 1998. 1407(3): p. 215-224.

123. Andreassen, T.T., H. Oxlund, and C.C. Danielsen, *The influence of non-enzymatic glycosylation and formation of fluorescent reaction products on the mechanical properties of rat tail tendons*. *Connective tissue research*, 1988. 17(1): p. 1-9.
124. Reddy, G.K., L. Stehno-Bittel, and C.S. Enwemeka, *Glycation-induced matrix stability in the rabbit achilles tendon*. *Archives of Biochemistry and Biophysics*, 2002. 399(2): p. 174-180.
125. Galeski, A., et al., *Mechanical and structural changes in rat tail tendon induced by alloxan diabetes and aging*. *Journal of biomechanics*, 1977. 10(11): p. 775-782.
126. Iqbal, M., et al., *Relationship between mechanical properties and pentosidine in tendon: effects of age, diet restriction, and aminoguanidine in broiler breeder hens*. *Poultry science*, 2000. 79(9): p. 1338-1344.
127. Gonzalez, A.D., et al., *Multiscale analysis of morphology and mechanics in tail tendon from the ZDSD rat model of type 2 diabetes*. *Journal of biomechanics*, 2014. 47(3): p. 681-686.
128. Thorpe, C.T., et al., *Distribution of proteins within different compartments of tendon varies according to tendon type*. *Journal of anatomy*, 2016. 229(3): 450-458.
129. Cribb, A. and J. Scott, *Tendon response to tensile stress: an ultrastructural investigation of collagen: proteoglycan interactions in stressed tendon*. *Journal of anatomy*, 1995. 187(2): p. 423-428.
130. Thorpe, C.T., et al., *The role of the non-collagenous matrix in tendon function*. *International journal of experimental pathology*, 2013. 94(4): p. 248-259.
131. Ramakrishnan, N., Y. Xia, and A. Bidthanapally, *Fourier-transform infrared anisotropy in cross and parallel sections of tendon and articular cartilage*. *Journal of orthopaedic surgery and research*, 2008. 3(1): p. 1-12.
132. Attia, M., et al., *Greater glycosaminoglycan content in human patellar tendon biopsies is associated with more pain and a lower VISA score*. *British journal of sports medicine*, 2013: p. bjsports-2013-092633.
133. Pins, G.D., et al., *Self-assembly of collagen fibers. Influence of fibrillar alignment and decorin on mechanical properties*. *Biophysical journal*, 1997. 73(4): p. 2164-2172.
134. Redaelli, A., et al., *Possible role of decorin glycosaminoglycans in fibril to fibril force transfer in relative mature tendons—a computational study from molecular to microstructural level*. *Journal of biomechanics*, 2003. 36(10): p. 1555-1569.
135. Vesentini, S., A. Redaelli, and F.M. Montevecchi, *Estimation of the binding force of the collagen molecule-decorin core protein complex in collagen fibril*. *Journal of biomechanics*, 2005. 38(3): p. 433-443.
136. Fessel, G. and J.G. Snedeker, *Evidence against proteoglycan mediated collagen fibril load transmission and dynamic viscoelasticity in tendon*. *Matrix Biology*, 2009. 28(8): p. 503-510.

137. Rigozzi, S., et al., *Tendon glycosaminoglycan proteoglycan sidechains promote collagen fibril sliding—AFM observations at the nanoscale*. Journal of biomechanics, 2013. 46(4): p. 813-818.
138. Fessel, G. and J.G. Snedeker, *Equivalent stiffness after glycosaminoglycan depletion in tendon—an ultra-structural finite element model and corresponding experiments*. Journal of theoretical biology, 2011. 268(1): p. 77-83.
139. Lujan, T.J., et al., *Effect of dermatan sulfate glycosaminoglycans on the quasi-static material properties of the human medial collateral ligament*. Journal of orthopaedic research, 2007. 25(7): p. 894-903.
140. Dourte, L.M., et al., *Influence of decorin on the mechanical, compositional, and structural properties of the mouse patellar tendon*. Journal of biomechanical engineering, 2012. 134(3): p. 031005.
141. Dunkman, A.A., et al., *The injury response of aged tendons in the absence of biglycan and decorin*. Matrix Biology, 2014. 35: p. 232-238.
142. WATANABE, T., et al., *An enzyme-linked immunosorbent assay (ELISA) for the quantitation of urinary desmosine*. Tokai journal of experimental and clinical medicine, 1989. 14(4): p. 347-356.
143. Halper, J. and M. Kjaer, *Basic components of connective tissues and extracellular matrix: elastin, fibrillin, fibulins, fibrinogen, fibronectin, laminin, tenascins and thrombospondins*, in *Progress in Heritable Soft Connective Tissue Diseases*. 2014, Springer. p. 31-47.
144. Wagenseil, J.E. and R.P. Mecham, *New insights into elastic fiber assembly*. Birth Defects Research Part C: Embryo Today: Reviews, 2007. 81(4): p. 229-240.
145. Ritty, T.M., K. Ditsios, and B.C. Starcher, *Distribution of the elastic fiber and associated proteins in flexor tendon reflects function*. The Anatomical Record, 2002. 268(4): p. 430-440.
146. Kielty, C.M., *Elastic fibres in health and disease*. Expert reviews in molecular medicine, 2006. 8(19): p. 1-23.
147. Barbir, A., et al., *Effects of enzymatic digestion on compressive properties of rat intervertebral discs*. Journal of biomechanics, 2010. 43(6): p. 1067-1073.
148. Henninger, H.B., et al., *Effect of elastin digestion on the quasi-static tensile response of medial collateral ligament*. Journal of Orthopaedic Research, 2013. 31(8): p. 1226-1233.
149. Lavagnino, M., et al., *Tendon mechanobiology: Current knowledge and future research opportunities*. Journal of Orthopaedic Research, 2015. 33(6): p. 813-822.
150. Buckley, M.R., et al., *Distributions of types I, II and III collagen by region in the human supraspinatus tendon*. Connective tissue research, 2013. 54(6): p. 374-379.
151. Connizzo, B.K., et al., *Collagen V expression is crucial in regional development of the supraspinatus tendon*. Journal of Orthopaedic Research, 2016. 34(12) : p. 2154-2161.
152. Juneja, S.C. and C. Veillette, *Defects in tendon, ligament, and enthesis in response to genetic alterations in key proteoglycans and glycoproteins: a review*. Arthritis, 2013. 2013.

153. Birch, H.L., et al., *Age-related changes to the molecular and cellular components of equine flexor tendons*. Equine veterinary journal, 1999. 31(5): p. 391-396.
154. Thorpe, C.T., et al., *Distribution of proteins within different compartments of tendon varies according to tendon type*. Journal of anatomy, 2016. 229(3): p. 450-458.
155. Buckley, M.R., et al., *The dynamics of collagen uncrimping and lateral contraction in tendon and the effect of ionic concentration*. Journal of biomechanics, 2013. 46(13): p. 2242-2249.
156. Adamczyk, C., et al., *An immunohistochemical study of the extracellular matrix of entheses associated with the human pisiform bone*. Journal of anatomy, 2008. 212(5): p. 645-653.
157. Södersten, F., et al., *Immunolocalization of collagens (I and III) and cartilage oligomeric matrix protein in the normal and injured equine superficial digital flexor tendon*. Connective tissue research, 2013. 54(1): p. 62-69.
158. Bell, R., et al., *ADAMTS5 is required for biomechanically-stimulated healing of murine tendinopathy*. Journal of Orthopaedic Research, 2013. 31(10): p. 1540-1548.
159. Wenstrup, R.J., et al., *Regulation of collagen fibril nucleation and initial fibril assembly involves coordinate interactions with collagens V and XI in developing tendon*. Journal of Biological Chemistry, 2011. 286(23): p. 20455-20465.
160. Butler, M., et al., *Nonoperative and Operative Treatments for Rotator Cuff Tears: Future Research Needs: Identification of Future Research Needs From Comparative Effectiveness Review No. 22*. 2013: Rockville (MD).
161. Connizzo, B.K., et al., *Collagen V-heterozygous and-null supraspinatus tendons exhibit altered dynamic mechanical behaviour at multiple hierarchical scales*. Interface Focus, 2016. 6(1): p. 20150043.
162. Sun, Y.L., et al., *Lubricin in human achilles tendon: The evidence of intratendinous sliding motion and shear force in achilles tendon*. Journal of Orthopaedic Research, 2015. 33(6): p. 932-937.
163. Jay, G.D. and K.A. Waller, *The biology of lubricin: near frictionless joint motion*. Matrix Biology, 2014. 39: p. 17-24.
164. Waller, K.A., et al., *Role of lubricin and boundary lubrication in the prevention of chondrocyte apoptosis*. Proceedings of the National Academy of Sciences, 2013. 110(15): p. 5852-5857.
165. Rhee, D.K., et al., *Consequences of disease-causing mutations on lubricin protein synthesis, secretion, and post-translational processing*. Journal of Biological Chemistry, 2005. 280(35): p. 31325-31332.
166. Reuvers, J., et al., *The mechanical properties of tail tendon fascicles from lubricin knockout, wild type and heterozygous mice*. Journal of structural biology, 2011. 176(1): p. 41-45.
167. Zhao, C., et al., *The Effects of Bio-Lubricating Molecules on Flexor Tendon Reconstruction in A Canine Allograft Model In Vivo*. Plastic and reconstructive surgery, 2014. 133(5): p. 628-637.

168. Zhao, C., et al., *Surface modification counteracts adverse effects associated with immobilization after flexor tendon repair*. Journal of Orthopaedic Research, 2012. 30(12): p. 1940-1944.
169. Zhao, C., et al., *CORR® ORS Richard A. Brand Award for Outstanding Orthopaedic Research: Engineering flexor tendon repair with lubricant, cells, and cytokines in a canine model*. Clinical Orthopaedics and Related Research®, 2014. 472(9): p. 2569-2578.
170. Hayashi, M., et al., *The effect of lubricin on the gliding resistance of mouse intrasynovial tendon*. PloS one, 2013. 8(12): p. e83836.
171. Mokone, G.G., et al., *The guanine-thymine dinucleotide repeat polymorphism within the tenascin-C gene is associated with Achilles tendon injuries*. The American Journal of Sports Medicine, 2005. 33(7): p. 1016-1021.
172. Järvinen, T.A., et al., *Mechanical loading regulates the expression of tenascin-C in the myotendinous junction and tendon but does not induce de novo synthesis in the skeletal muscle*. Journal of Cell Science, 2003. 116(5): p. 857-866.
173. Riley, G.P., et al., *Tenascin-C and human tendon degeneration*. The American journal of pathology, 1996. 149(3): p. 933-943.
174. Smith, R., et al., *Correlation of cartilage oligomeric matrix protein (COMP) levels in equine tendon with mechanical properties: A proposed role for COMP in determining function-specific mechanical characteristics of locomotor tendons*. Equine Veterinary Journal, 2002. 34(S34): p. 241-244.
175. Piróg, K.A., et al., *A mouse model offers novel insights into the myopathy and tendinopathy often associated with pseudoachondroplasia and multiple epiphyseal dysplasia*. Human molecular genetics, 2010. 19(1): p. 52-64.

Chapter 3: Multiscale Biomechanical Analysis of Bovine Flexor Tendons under Shear and Compression Loading²

3.1 Introduction

Tendons predominantly support uniaxial forces along the principal direction of collagen fiber alignment and exhibit mechanical nonlinearity, viscoelasticity, and anisotropy [1, 2]. In addition, some tendons also experience varying levels of compressive, shear, and/or frictional forces as they wrap around bones or interact with neighboring anatomical structures [3-5]. For example, the supraspinatus tendon (SST), one of four musculotendinous units in the rotator cuff of the shoulder, experiences shear and compressive forces as a result of the wide range of motion of the shoulder joint and complex interactions with neighboring anatomy [6-9]. As a result, specific locations of the human SST exhibit significantly different fiber alignment and tensile modulus during tensile loading [5, 10], as well as compositional differences (i.e., collagens, proteoglycans) by location [8, 11]. Even different locations within the same tendon can function in unique, and at times complex, *in vivo* loading environments.

Another tendon subjected to complex physiological loading is the bovine deep digital flexor tendon (DDFT); while the proximal region of this tendon is loaded predominantly in tension, the anterior side of the distal region contacts the sesamoid bone of the lower leg and experiences compression and (likely) shear [4]. This unique loading environment greatly influences tissue

²Reprinted from (1) Fang, F., Sawhney, AS., and Lake, SP., 2014, "Different regions of bovine deep digital flexor tendon exhibit distinct elastic, but not viscous, mechanical properties under both compression and shear loading." *J Biomech*, 47, 2869-2877; (2) Fang, F., and Lake, SP., 2015, "Multiscale strain analysis of tendon subjected to shear and compression demonstrates strain attenuation, fiber sliding, and reorganization." *J Orthop Res*, 33, 1704-1712.

composition and organization as cells remodel the ECM in response to a multiaxial, non-uniform mechanical stimulus. Thus, while the proximal region exhibits properties typical for tendon (i.e., highly organized and aligned collagen fibers, relatively low levels of large proteoglycans), the distal region contains a fibrocartilage-rich zone with characteristics common to multiaxially-loaded tissues (e.g., less aligned collagen, increased glycosaminoglycans).

Many studies have investigated how tendon behaves under tensile loading, namely the mechanical response and the way in which strain transfers across multiple hierarchical levels (e.g., fibrils, fascicles, etc.) [12]. The viscoelastic properties of tendon loaded in tension have been demonstrated via stress-relaxation [13] and cyclic loading tests [14]. Mechanical behavior under such loading regimes has been explained through correlations of mechanical properties with specific organization changes, such as collagen fiber realignment [14] and uncrimping [15], as well as sliding between collagen fibers [13]. Unfortunately, there have been few studies evaluating how tendon responds when loaded in compression and shear, which is particularly relevant for understanding regions of tendons that experience such non-tensile loading during normal physiologic function. One study performed location-specific indentation tests on human supraspinatus tendon and reported significant mechanical inhomogeneity [16]. Another study used supersonic shear imaging to correlate shear elastic modulus of patellar tendons with tangent traction modulus [17]. These studies have provided some insights, however no study has evaluated the non-linearity and viscoelasticity of tendon under non-tensile loading, nor characterized how tendon regions of varying composition and organization respond differently to compression and shear loading. Studying tendon behavior under multiaxial loading would deepen understanding of structure-function relationships, including correlating functional

mechanics to location-specific properties and elucidating time-dependent behavior, and provide insight into tissue changes that may occur under altered loading conditions.

Additionally, how strains transfer between different hierarchical levels of tendon (i.e., from tissue to local extracellular matrix (ECM) to nuclei) and what mechanisms regulate behavior under uniaxial tension have been explored. Local strains along fibers under tension were found to be significantly smaller than applied strains by tracking photobleached grids on rat tail tendon fascicles with confocal microscopy, and the deflection of grids indicated sliding between collagen fibers [18]. Superficial digital flexor tendons experienced greater rotation, faster recovery, and less hysteresis loss than common digital extensor tendons during tensile loading, motivating the hypothesis that helix recoil facilitates better energy storage and recovery in energy-storing than in the positional tendons [19]. Nuclei centroids have also been used to track local matrix strain and cell nucleus strain [20]. However, to the best of our knowledge, no studies have examined the strain response of tendon under compression or shear loading, nor the physical mechanisms regulating tendon behavior under such loading regimes. It is also unknown whether tendons in different locations exhibit different shear or compressive strains, and if this behavior correlates with structural and compositional properties. A deeper understanding of the multiscale response of tendons to loading would provide insight into how specific ECM components (e.g., collagen network, non-fibrillar matrix) are distributed and how they function to support and transfer multiaxial forces. This knowledge will be of great value by (1) defining structure-function relationships under physiologically-relevant non-tensile loading conditions, (2) quantifying the microscale deformations that cells experience to drive location-specific changes of ECM composition/organization, (3) providing insight into altered multiscale strain behavior that may occur following ECM changes, accompanying tendon injury/degeneration, and (4)

establishing criteria for rationally designed tendon replacements to meet requirements for proper function in complex *in vivo* loading environments.

Therefore, the objectives of this study were to: (1) evaluate the mechanical response of tendons of varying properties (in this case, distal and proximal regions from bovine deep digital flexor tendon) under compressive and shear loading, then correlate structural characteristics to functional mechanical properties; and (2) investigate multiscale strain transfer within the distal and proximal regions of bovine DDFTs in order to explore mechanisms governing tendon deformation under non-tensile loading. Under shear and compression loading, stresses were recorded by a load cell device and strains were quantified at the tissue, local matrix, and nuclear levels by tracking bead markers, photobleached lines, nuclei centroids, and nuclear aspect ratios (NAR) via multi-photon microscopy. For tendon mechanical strength, we hypothesized that the mechanical responses (e.g., stress magnitudes, moduli, relaxation rates and ratios) would differ in distal and proximal regions during both shear and compression loading, and that different mechanical responses would be caused by specific variations of organization and composition. Specifically, we hypothesized that compared with the proximal region, the distal region would have higher compressive and shear modulus and slower rates of relaxation, due to increased quantities of proteoglycan (and water) and less organized collagen fibers. Concerning strain transfer, we hypothesized that the mechanical responses (e.g., stress magnitudes, moduli, relaxation rates and ratios) would differ in distal and proximal regions during both shear and compression loading, and that different mechanical responses would be caused by specific variations of organization and composition. Specifically, we hypothesized that compared with the proximal region, the distal region would have higher compressive and shear modulus and slower rates of relaxation, due to increased quantities of proteoglycan (and water) and less

organized collagen fibers.

3.2 Materials and methods

Sample preparation. Bovine DDFTs (age 14-30 months, n=10) were obtained from Animal Technologies, Inc. (Tyler,

Texas). Thawed blocks of 2-cm length were harvested from locations 4-cm and 2-cm away from the natural bifurcation in order to

obtain samples from the proximal and distal regions, respectively (Fig.

3.1) [21]. The medial and lateral surfaces of each sample (~6-8 mm thick)

were leveled on a freezing stage (BFS-30MP, Physitemp, Clifton, NJ) sledge microtome (Leica 1400, Buffalo Grove, IL) to ensure smooth surfaces for microscopy imaging. The anterior surface, which articulates with the paratendinous sheath and sesamoid, and the posterior surface were not modified. From these segments, two 8-mm diameter cylindrical samples were removed using a biopsy punch, and each sample was cut in half along the predominant fiber direction [22]. One hemicylindrical sample was evaluated for mechanical testing and the other was examined for histological analysis. The anterior-to-posterior thickness and cross-sectional area were measured using a non-contact laser scanning system (Keyence, Elmwood Park, NJ).

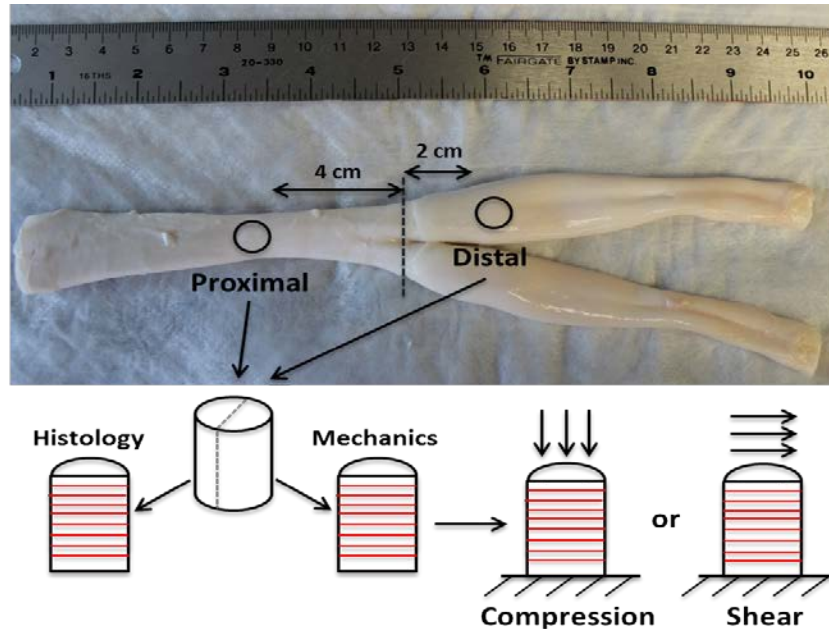


Fig. 3.1 Dissection scheme for preparation of test samples from proximal and distal regions of DDFT. Cylindrical samples obtained from each region were cut in half to allow for both histological analysis and mechanical tests (black dotted line = location of DDFT bifurcation; arrows showed loading direction).

Compression testing. Hemicylindrical samples (n=10 each for distal and proximal) were placed flat-side down in a glass bottom dish filled with phosphate buffered saline (PBS), and secured in a custom-made mechanical test system (Fig. 3.2) consisting of custom clamps, a miniature platform load cell (Strain Measurement Devices, Wallingford, CT), XYZ-axis linear positioning stage (Newport, Santa Clara, CA), and precision micro-translation stage (Physik Instrument, Auburn, MA).

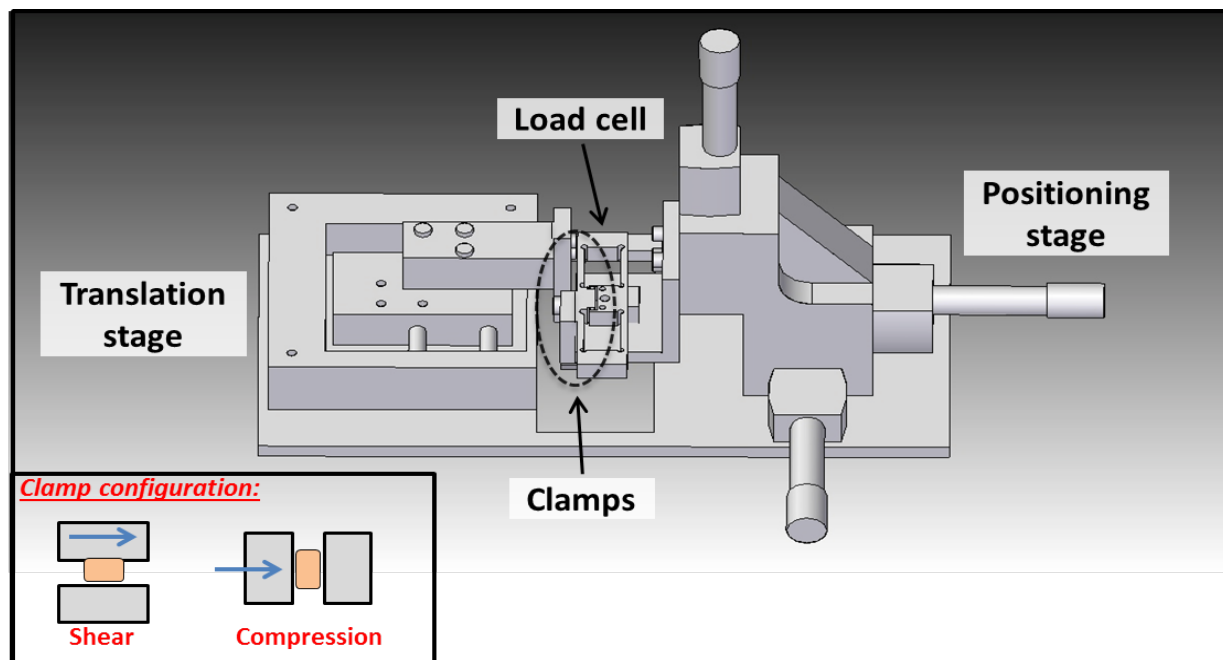


Fig. 3.2 Schematic diagram of custom-made mechanical test system. The inset shows the top view of position of clamps (gray blocks) and tendon samples (orange blocks). Blue arrows indicate which clamps were moved and in which directions, while the other clamps were attached to the load cell and held stationary.

The output of the load cell (20-N capacity; 0.02 N resolution) was calibrated by comparing preliminary tests of materials of known stiffness with similar tests on a planar biaxial electromechanical test machine (TestResources, Shakopee, MN). The positions of the tissue clamps were adjusted with the triple axis positioning stage during mounting to avoid off-axis loading and friction between the glass dish and clamps. A 0.01 N compressive pre-load was

applied and the zero-strain sample length was measured using digital calipers (0.01 mm resolution). For the loading protocol, each sample was compressed in three incremental steps of 0.08 strain at a rate of 20 mm/s, with 12 minutes relaxation time between each step [23] (Fig. 3.3). An incremental stress-relaxation protocol was utilized in order to evaluate the viscoelastic response as a function of strain level. Compressive strain (ϵ) was defined as:

$$\epsilon = d/T \quad (3.1)$$

where d is the displacement applied by the clamps and T is the sample thickness.

Shear testing. An additional set of bovine deep flexor tendons (n=16 each for distal and proximal) were prepared to obtain hemicylindrical distal and proximal samples. The same custom test system (described above) was utilized, where compression clamps were replaced with shear clamps. One shear clamp was rotated 90° relative to the compression clamp's position, such that actuator motion in the same direction was able to apply both compression and shear displacements for

the two different test protocols (Figure 2). After lightly gluing the top and bottom hemicylindrical surfaces to the shear clamps with cyanoacrylate and immersing in PBS with the flat-surface down,

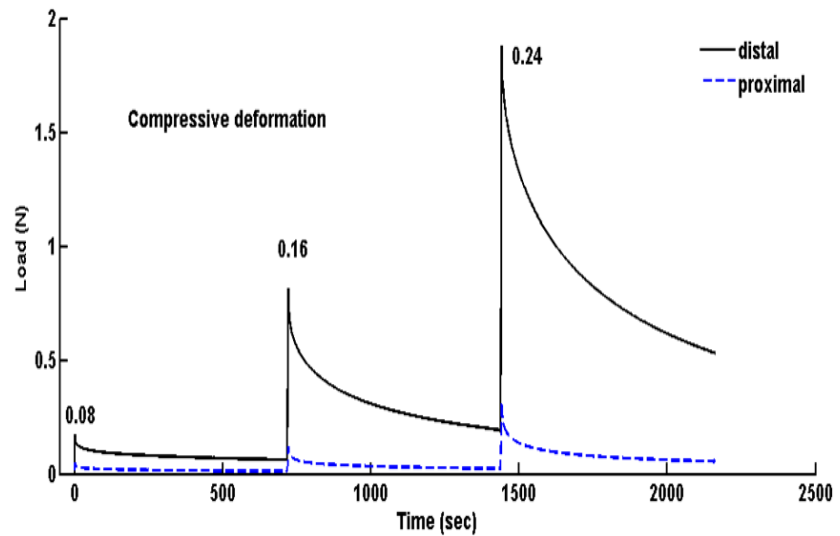


Fig. 3.3 Mechanical response in compression tests. Typical load-time curve during three-step incremental stress-relaxation tests shows larger forces for distal than proximal samples (compression forces are shown in absolute values, although actual forces are negative).

samples were then mounted in our system with the clamps positioned to match the measured sample-specific thickness. These fixtures applied shear to tendon samples through the thickness by holding the right clamp fixed and horizontally displacing the left clamp with the micro-translation stage. A 0.01N horizontal pre-load was applied to define the zero-strain point. Both distal and proximal samples were tested in three incremental steps of 0.08 shear strain at a rate of 20 mm/s, with 12 minutes relaxation time between each step. Shear strain (γ) was defined as:

$$\gamma = \arctan(d/T) \quad (3.2)$$

where d is the displacement applied by the clamps and T is the sample thickness.

Macro-level imaging. Four stainless steel balls (diameter = 1/32'') were glued onto the lateral surface of each sample (n=10 each for distal and proximal). For shear testing, samples were first glued to shear clamps and mounted in a custom micromechanical test device configured with a digital camera (Nikon, Melville, NY) to track 2D tissue strains [21]. Images were acquired after applying the pre-load and after 8 minutes of relaxation for each strain step (Fig. 3.3A and B). For compression testing, Images were taken in the same way as described for shear testing (Fig. 3.4 D and E).

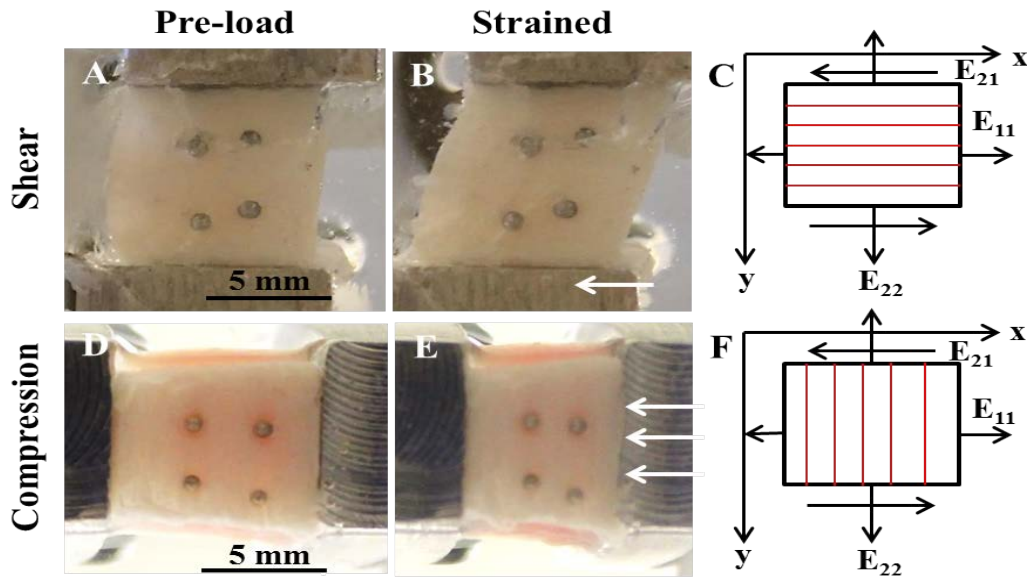


Fig. 3.4 Camera pictures of samples under (A) pre-load and (B) 0.24 shear clamp strain. Camera pictures under (D) pre-load and (E) 0.24 compression clamp strain. (C) and (F) show coordinates and strains for shear and compression testing (white arrows show loading direction; red lines denote primary direction of collagen alignment).

Micro-level imaging. An additional set of bovine DDFTs (n=10 each for distal and proximal)

was prepared for micro-level imaging. Samples were incubated for 25 minutes in 10 $\mu\text{g/ml}$ 5-(4,6-dichlorotriazinyl) aminofluorescein (5-DTAF) solution (Life Technologies, Carlsbad, CA) in 0.1 M sodium bicarbonate buffer to stain collagen, and were rinsed three times with PBS [24]. Next, a 1 $\mu\text{g/ml}$ 4',6-diamidino-2-

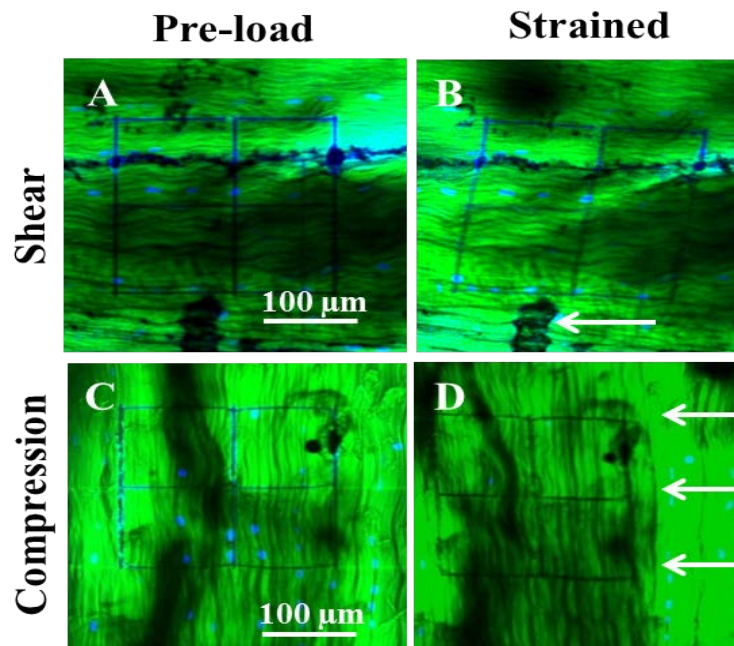


Fig. 3.5 Composite images of samples under (A) pre-load and (B) 0.24 shear clamp strain. Composite images of samples under (C) pre-load and (D) 0.24 compression clamp strain (white arrows show loading direction).

phenylindole (DAPI) (Thermo Fisher Scientific, West Palm Beach, FL) solution was used to stain samples for 20 minutes to visualize cell nuclei. Following staining, samples were mounted in the same loading device and secured to the stage of a Zeiss multichannel inverted/upright multiphoton-confocal microscope system (LSM510-meta; Carl Zeiss, Jena, Germany). After application of a 0.05N pre-load, four adjacent squares (100 μ m x 100 μ m) were photobleached at a depth of approximately 50 μ m at three locations along the anterior-to-posterior (thickness) axis: one at the center and two additional at \pm 2.5-3.0 mm away from the center. Photobleached lines were created by setting the Mai Tai broadband infrared multiphoton laser to 750 nm with 100% of total power, 500 iterations, pixel dwell of 25.6 μ sec, and two cycles. The sample was loaded using the same stress-relaxation shear or compression protocol as above. Multichannel two-photon z-stack images of photobleached lines and nuclei at three locations were collected through the stained depth by a 20X objective (field of view: 224.8 \times 224.8 μ m²; DAPI: 750 nm/BP 450-490 nm; 5-DTAF: 750 nm/LP 516 nm) before the loading and after 8 minutes relaxation for each step (Fig. 3.5), since it was demonstrated in previous work that no microscopic movements were observed after 4 minutes [12, 25].

Histology. Distal and proximal samples were fixed in 10% neutral buffered formalin for 48 hours and dehydrated in 30%, 50%, and 70% alcohol for 15 minutes each. Standard histology protocols were followed to process, embed in paraffin wax, and cut 10- μ m-thick slices. Sections cut near the flat surface of half-cylinder were stained with alcian blue and picosirius red using standard protocols to visualize proteoglycans and collagen, respectively. Images of alcian blue sections were obtained using a bright-field microscope (Olympus, Sun Valley, PA) and polarized light images of picosirius red sections were collected using crossed linear polarizers. For each sample, staggered 4X images were collected and stitched to view the whole section, and zoomed

images in specific locations were acquired with a 40X objective. The average intensity of 4X images for distal and proximal regions along sample thickness was calculated by Image J.

Data analysis. For both compression and shear testing, maximum (F_{max}) and minimum (F_{min}) loads of distal and proximal samples were recorded as the peak and equilibrium forces for each strain step, and maximum and minimum stresses were computed using measured cross-sectional areas. The relaxation ratio (f) was evaluated as follows:

$$f = 100 \times \frac{\sigma_{max} - \sigma_{min}}{\sigma_{max}} \quad (3.3)$$

Stress values during relaxation were normalized (by σ_{max}) and averaged by group. To characterize the viscoelasticity of DDFT in different regions for compressive and shear tests, a two-relaxation-time solid linear model, formed by two Maxwell elements and one spring in parallel (Figure 5A), was utilized to quantify the viscous and elastic components separately [26]. Modulus values were computed by dividing stress values by applied clamp strains. The relaxation response was evaluated as:

$$E_S(t) = E_1 + E_2 e^{-t/\tau_2} + E_3 e^{-t/\tau_3} \quad (3.4)$$

where E_i are moduli of different components in the solid linear model: E_s is the overall sample response and E_1 is the equilibrium modulus, while E_2 and E_3 represent the short and long-term elastic behavior, respectively. Similarly, τ_1 and τ_2 are time constants describing early and late relaxation rates, respectively. Experimental data were fit to the model by the method of least squares in a custom Matlab (Mathworks, Natick, MA) code. Separate model fits were performed for the relaxation response at each of the three strain steps, from the peak force through the end of the relaxation period.

In order to reduce effects from out-of-plane fiber motion and consistently visualize clearly defined photobleached lines, two-photon z-stacks were collapsed to form single, summed 2D multichannel images using Image J (1.47, National Institute of Health, USA). These images were separated to the collagen channel (i.e., DTAF stain) for local matrix calculation and the nuclei channel (i.e., DAPI stain) for nuclei-based calculation. A custom Matlab program was used to compute 2D Lagrangian tissue and local matrix strains using digital photos of surface markers and two-photo microscopy images of photobleached lines, respectively. Coordinates were computed for each point (4 and 9 tracked points/sample for tissue strain and local matrix strain, respectively) at the pre-load (X_1^i, X_2^i , i represented the i^{th} point) and after each step (x_1^i, x_2^i). Assuming a homogeneous deformation, the deformation gradient (\mathbf{F}) and translation vector (\mathbf{p}) were then determined using a least squares solution of the following equation [27, 28]:

$$\begin{pmatrix} x_1^1 & x_1^2 & \dots & x_1^n \\ x_2^1 & x_2^2 & \dots & x_2^n \end{pmatrix} = \begin{pmatrix} F_{11} & F_{12} & p_1 \\ F_{21} & F_{22} & p_2 \end{pmatrix} \begin{pmatrix} X_1^1 & X_1^2 & \dots & X_1^n \\ X_2^1 & X_2^2 & \dots & X_2^n \\ 1 & 1 & \dots & 1 \end{pmatrix} \quad (3.5)$$

Lagrangian strains (\mathbf{E}) were then calculated as:

$$\begin{pmatrix} E_{11} & E_{12} \\ E_{12} & E_{22} \end{pmatrix} = \frac{1}{2} \left\{ \begin{pmatrix} F_{11} & F_{12} \\ F_{12} & F_{22} \end{pmatrix} - \begin{pmatrix} 1 & 0 \\ 0 & 1 \end{pmatrix} \right\} \quad (3.6)$$

where E_{11} , E_{22} are normal strains, and E_{12} is shear strain. Based on how clamp-to-clamp displacements were applied, shear strain was defined as $2 * E_{12}$ in order to compare strains at the tissue or local matrix level with applied clamp strains [29].

Collapsed 2D images for the nuclei channel were thresholded to sharpen nuclear edges. Coordinates of nuclear centroids and the lengths of nuclear short and long axes were measured using ImageJ for analysis of nuclei-based strains and nuclear deformation. Nuclei centroids were tracked to measure (Fig. 3.6): (1) strain along individual fibers (ϵ) using Equation 3.7, (2) angle

change or “rotation” within row of fibers as θ_1 (i.e., relative motion perpendicular to fiber alignment, indicative of uncrimping or realignment) using Equation 3.8, (3) angle change or “rotation” between rows of fibers as θ_2 (i.e., a measure of fiber sliding) using Equation 3.9, and (4) compression between rows of fibers (for compression loading only) as δ using Equation 3.10.

$$\varepsilon = \frac{l-L}{L} \quad (3.7)$$

$$\theta_1 = \frac{y_2 - Y_2}{L} \quad (3.8)$$

$$\theta_2 = \frac{x_1 - X_1}{Y_1} \quad (3.9)$$

$$\delta = \frac{y_1 - Y_1}{Y_1} \quad (3.10)$$

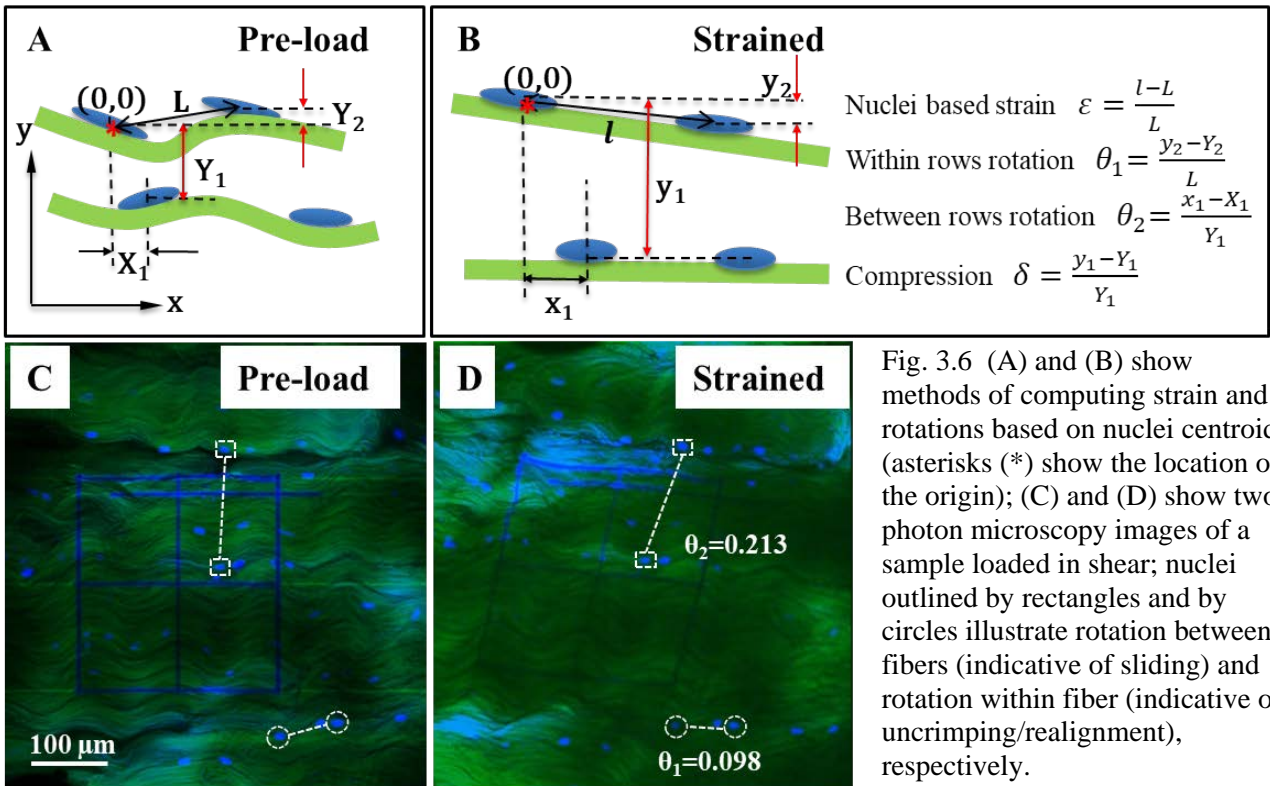


Fig. 3.6 (A) and (B) show methods of computing strain and rotations based on nuclei centroids (asterisks (*) show the location of the origin); (C) and (D) show two-photon microscopy images of a sample loaded in shear; nuclei outlined by rectangles and by circles illustrate rotation between fibers (indicative of sliding) and rotation within fiber (indicative of uncrimping/realignment), respectively.

In these equations, L and l are the lengths between two nuclei before and after tendon

deformation; X_1 , Y_1 , and Y_2 are the measured coordinates of the nuclei before tendon deformation; and x_1 , y_1 , and y_2 are the measured coordinates of the nuclei after tendon deformation. The nuclear aspect ratio (NAR) was calculated for each cell nucleus as the ratio of the long to short axes. Change of NAR values at each strain step, normalized by undeformed NAR, was also quantified under shear and compression loading (Δ NAR).

Statistical analysis. All data are reported as mean \pm 95% confidence intervals. For compressive and shear tests at each of the three steps, significant differences of parameters (i.e., e.g., stresses, relaxation ratios, model constants, tissue strain, local matrix strain) were determined by student paired t -tests between distal and proximal regions using Prism6 (GraphPad Software, La Jolla, CA). Since unequal numbers of tracked nuclei precluded paired statistical comparisons, unpaired t -tests were used to evaluate whether there were significant differences in nuclei-based strains, between-row rotations, within-row rotations, NAR, and Δ NAR values between distal and proximal samples. A one-way analysis of variance with Bonferroni post-hoc tests was also applied for tissue, local matrix, and nuclei-based strains of samples under compression; statistical results for the paired and unpaired tests are reported, with significance set at $p < 0.05$.

3.3 Results

Compression testing. Different regions of bovine flexor tendons presented very different mechanical responses during compressive loading. As demonstrated by a typical force-time curve (Figure 3.3), maximum and minimum loads for both distal and proximal samples increased at each successive compressive step, but distal samples experienced maximum and minimum loads 5-6X larger than proximal samples ($p \leq 0.02$). In addition, maximum and minimum stresses

for distal samples were 4-5X and 3X larger than proximal samples, respectively ($p \leq 0.017$, Figure 3.7A). During hold periods after each strain step, loads relaxed for both groups (Figure 3.7).

Relaxation curves were quite consistent for both distal and proximal samples at all strain steps ($\epsilon = 0.08, 0.16, \text{ and } 0.24$; Figure 3.8A). Average relaxation ratios for all samples in three steps were approximately 60%-80%, demonstrating obvious stress relaxation over time (Figure 3.8B). Relaxation ratios increased slightly with increased clamp strain but were not different between different tendon regions ($p > 0.05$).

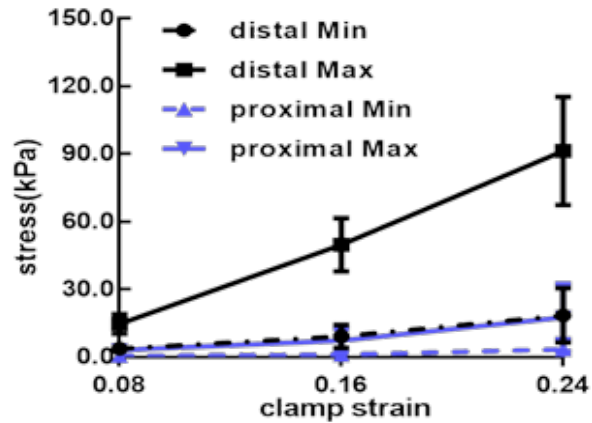


Fig. 3.7 Maximum and minimum stresses are significantly larger for distal samples compared to proximal samples ($n=9/\text{group}$).

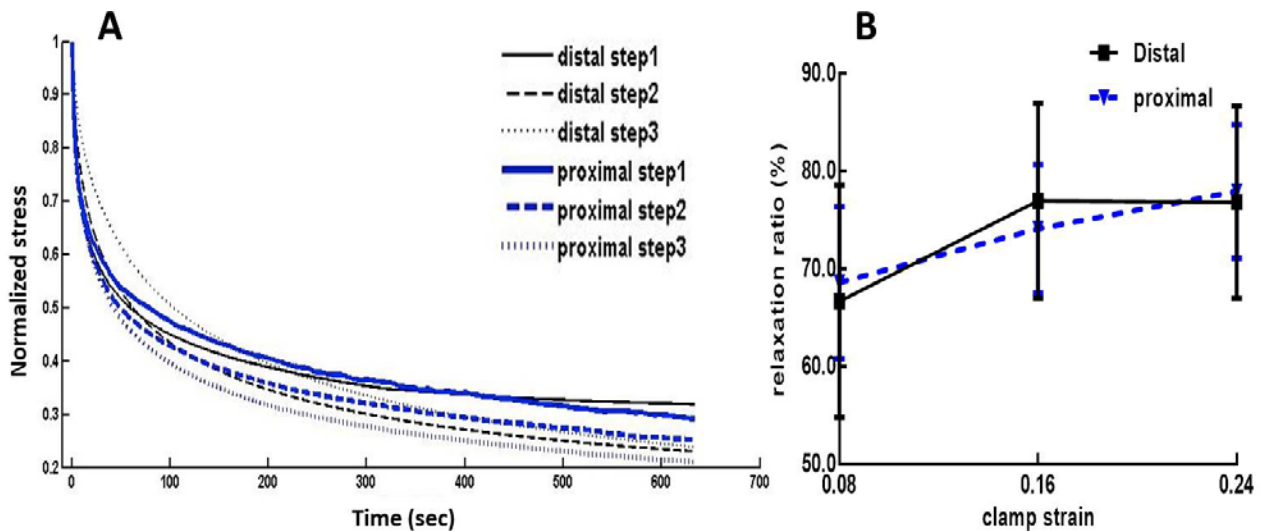


Fig. 3.8 (A) Normalized stress relaxation was evaluated for each strain step of distal and proximal samples in compression tests (curves were averaged by group, error bars not shown for clarity). (B) Relaxation ratios for compression tests increased slightly with increasing strain, but were not different between regions ($n=9/\text{group}$; average \pm standard deviation).

Experimental compressive modulus values for distal and proximal samples excellently fit to the two-relaxation-time solid linear model ($R^2 \geq 0.97$; Fig. 3.9A). In this model, the constants

describe specific aspects of tendon's relaxation properties. Specifically, E_1 represents the equilibrium compressive modulus (at the end of relaxation), E_2 and τ_2 describe the early behavior (~10-15 sec), and E_3 and τ_3 describe the late response (~120-140 sec). Modulus values for distal samples were significantly larger (~5-6X) than for proximal samples at each step ($p \leq 0.001$) (Fig. 3.9B). Interestingly, distal modulus values at the second strain step (i.e., $\epsilon = 0.16$) were smaller than values at either the first or third strain step, however this was not apparent for proximal samples. In contrast to modulus constants, both relaxation time constants were similar

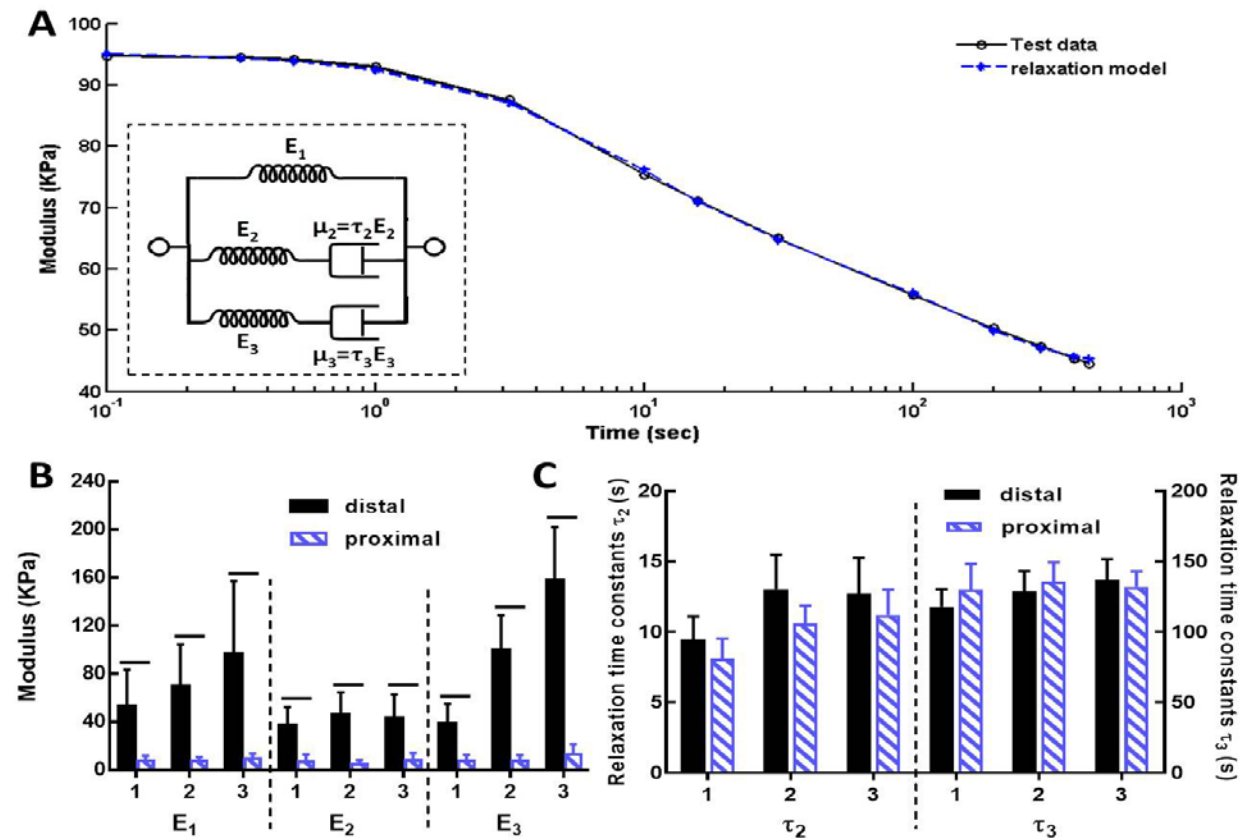


Fig. 3.9 Fitting results of the two-relaxation-time solid linear model for compression tests. (A) Typical model fit to experimental data (shown data is for a distal sample; proximal samples also show good model fits); inset shows schematic of the solid linear model. (B) Elastic moduli of different model components are significantly larger for distal samples at each of three steps (corresponding to compressive clamp strains of 0.08, 0.16, 0.24). (C) Relaxation time constants are very similar for distal and proximal samples at each strain step. (Plots show average +/- standard deviation; $n=9$ /group; horizontal bars indicate significant differences between regions).

between distal and proximal samples at each strain step ($p > 0.05$). Of note, different magnitudes

of relaxation time constants τ_2 and τ_3 demonstrated relaxation behavior at different time-scales for both distal and proximal samples (Fig. 3.9C).

Shear testing. Different regions of bovine flexor tendons also exhibited differences in the mechanical response during shear loading. Force values for both distal and proximal samples increased with increasing applied shear strain (Fig. 3.10A). Distal samples experienced maximum and minimum loads that were much larger (~2-3X) than proximal samples ($p \leq 0.02$). In fact, the equilibrium distal forces were approximately equal to the peak proximal forces at each step ($\gamma = 0.08, 0.16, 0.24$). Maximum and minimum stresses in distal samples were also larger (~2-3X) than proximal samples, with significant differences observed at strains of 0.16 and 0.24 ($p \leq 0.015$, Fig. 3.10B).

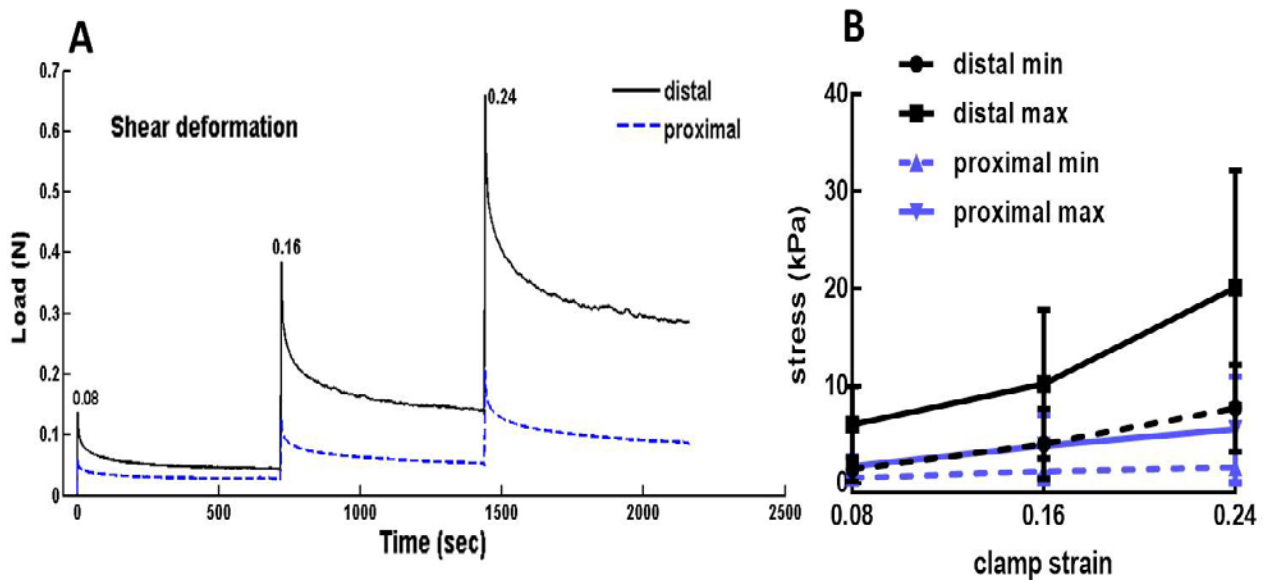


Fig. 3.10 Mechanical response in shear tests. (A) Typical load-time curve during three-step incremental stress-relaxation tests show larger forces for distal than proximal samples. (B) Maximum and minimum stresses are significantly larger for distal samples compared to proximal samples, except minimum stresses at 0.08 strain are not different between regions ($n=14/\text{group}$; average \pm standard deviation).

The normalized relaxation plots (Figure 3.11A) demonstrated fairly consistent relaxation behavior for distal and proximal samples across different strain steps, with stresses decreasing to ~30%-50% of peak values. Average relaxation ratios were similar between distal and proximal

samples ($p>0.1$); however, in contrast to results from compressive testing, relaxation ratios decreased with increased clamp strain (Figure 3.11B). Experimental shear modulus values for

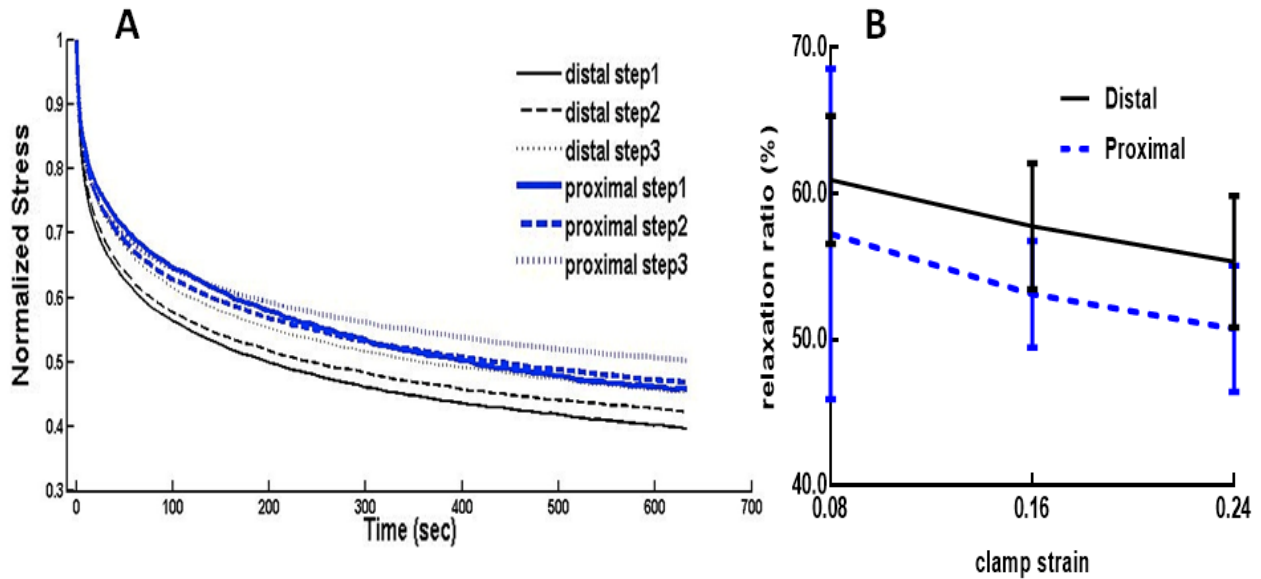


Fig. 3.11 (A) Normalized stress relaxation was evaluated for each strain step of distal and proximal samples in shear tests (curves were averaged by group, error bars not shown for clarity). (B) Relaxation ratios for shear tests decreased slightly with increasing strain, but were not different between regions ($n=14/\text{group}$; average \pm standard deviation).

distal and proximal samples excellently fit to the solid linear model ($R^2 \geq 0.97$). As with compressive testing, distal modulus values in shear were consistently larger than proximal values at each strain step ($p<0.05$, Figure 3.12A). Interestingly, equilibrium moduli (i.e., E_1) were larger than time-dependent modulus values (i.e., E_2 and E_3), and while distal moduli increased with increasing shear strain, proximal values were relatively independent of strain. Proximal and distal samples exhibited similar values for both relaxation time constants, and no differences were found between various strain steps ($p>0.3$, Figure 3.12B). Relaxation time constant τ_2 (~3-5 sec) was an order of magnitude less than relaxation time constant τ_3 (~120-140 sec) demonstrating different time-scales for relaxation behavior of both distal and proximal samples.

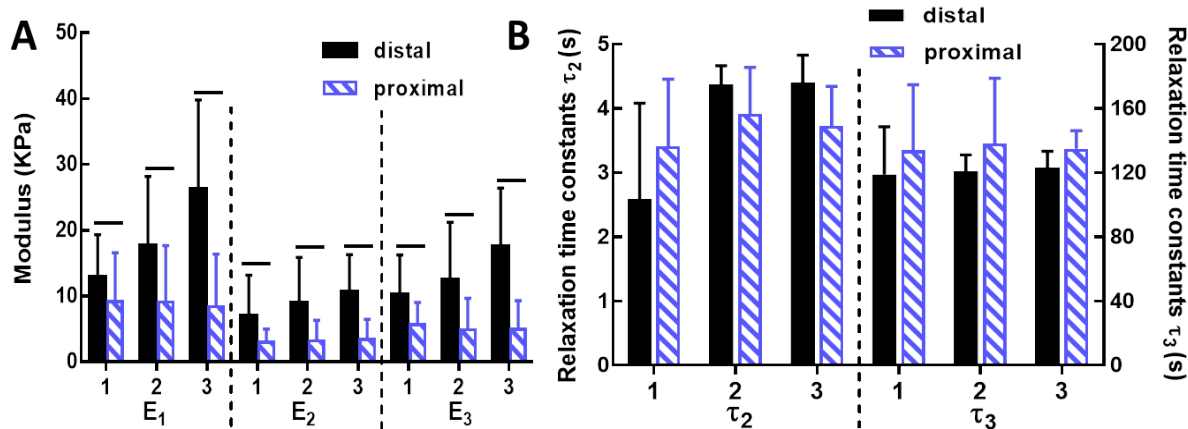


Fig. 3.12 Fitting results of the two-relaxation-time solid linear model for shear tests. (A) Elastic moduli of different model components are significantly larger for distal samples at the second and third strain steps (corresponding to shear strains of 0.16 and 0.24). (B) Relaxation time constants are similar for distal and proximal samples, with differences only at the last strain step. (Plots show average \pm standard deviation; $n=14$ /group; horizontal bars indicate significant differences between regions).

Microscale strain analysis at different locations through thickness. Different anterior-to-posterior locations (i.e., three distinct locations through the sample thickness) in distal or proximal samples did not exhibit different microscale deformation behavior under compression or shear tests (not shown). In shear and compression tests, measured strains, within-row rotations (θ_1 , equation 3.8), and between-row rotations (θ_2 , equation 3.9), were similar among the three different anterior-to-posterior locations for both proximal and distal samples. Since strains and rotations among the three distinct anterior-to-posterior locations were not significantly different, measured parameters from the three locations were grouped together for subsequent analyses.

Strain analysis in different tendon regions. For both distal and proximal samples, measured tissue strains were smaller than applied clamp-to-clamp strains under shear (Fig. 3.13A) and compression (Fig. 3.13B). Local matrix strains were similar to tissue strains in shear (Fig. 3.13A), but smaller than tissue strains in compression (Fig. 3.13B). Nuclei-based strains were slightly smaller than local matrix strains in compression, particularly for the largest strain step (Fig. 3.13B). While all tissue and local matrix strains increased with increasing clamp strains, nuclei-

based values remained relatively constant, especially for proximal samples. While distal and proximal samples exhibited similar results in shear, local matrix and nuclei-based strains were larger for distal samples than for proximal samples in compression. No significant differences of tissue, local matrix, and nuclei-based strains were found distal and proximal samples, except for nuclei-based strain under 0.24 compression clamp strain (Fig. 3.13B).

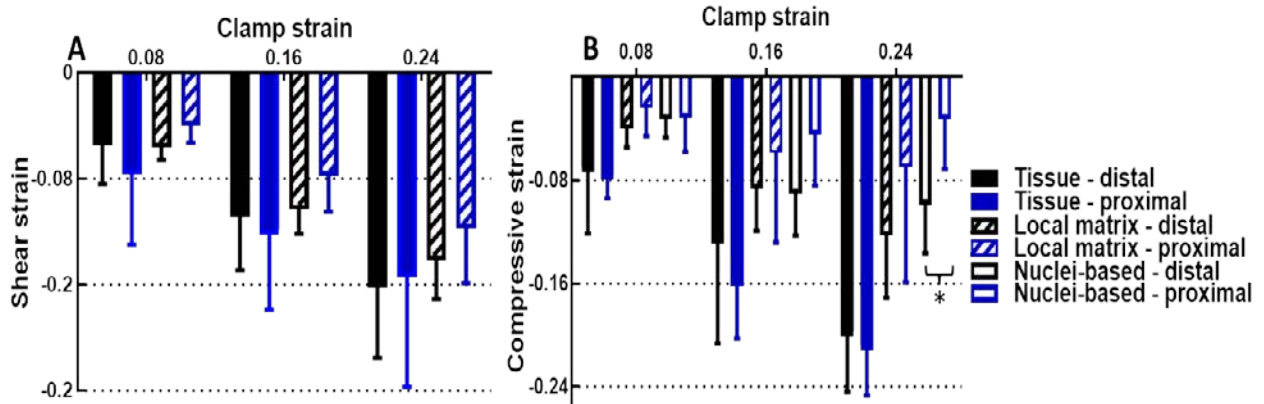


Fig. 3.13 Multiscale strain values of distal and proximal DDFT samples in (A) shear and (B) compression show strain attenuation at smaller length scales (dashed horizontal lines indicate magnitude of applied clamp strains; data are shown as mean \pm 95% confidence intervals; * for $p < 0.05$).

Rotations computed by tracking nuclei centroids were greater between-rows of collagen fibers than those measured within-rows for both distal and proximal samples under shear (Fig. 3.13A). Based on our definitions for these parameters (Fig. 3.6), “between-row rotation” corresponds to sliding between neighboring collagen fibers while “within-row rotation” is indicative of collagen uncrimping and/or realignment. Thus, sliding contributes significantly to the shear response. Both measures of “rotation” were similar (and non-zero) under compression, suggesting that both mechanisms contribute to the response of tendon to compressive loading (Fig. 3.14B). There were only a few significant ($p < 0.05$) distal-proximal differences: between-row rotations in shear (Fig. 3.14A), and within-row rotations under 0.08 and 0.16 compressive strains (Fig. 3.14B). Between-row rotation values were significantly different from within-row

values in shear, but not in compression. Finally, average nuclei-based strains measured *along* fibers (see Fig.3.6B) were ~ 0 in shear and compression (not shown), suggesting minimal stretching of the fibers under these non-tensile loading protocols.

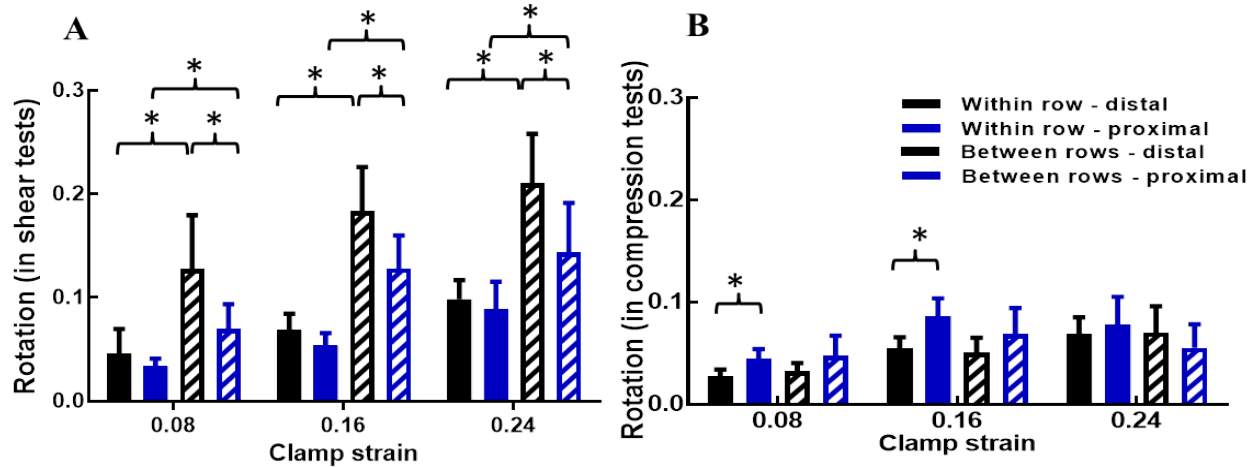


Fig. 3.14 (A) Rotation under shear and (B) compression for distal and proximal samples vs. clamp strain within row and between rows (rotation is computed as shown in Fig. 3.13; data are shown as mean \pm 95% confidence intervals; * for $p < 0.05$).

Distal samples had significantly smaller NAR values than proximal samples before loading, indicating slightly rounder nuclei than proximal samples (Fig. 3.15A). Average Δ NAR values did not increase with increased applied shear strain and were not different between distal and proximal regions (Fig. 3.15B). In contrast, Δ NAR of both distal and proximal samples increased with compressive strain (Fig. 3.15C). Proximal samples also exhibited significantly larger Δ NAR values than distal samples at 0.16 and 0.24 compressive strains ($p < 0.05$).

Strain analysis for photobleaching on single or two subfascicles. After further examination of microscopy images, we observed that photobleached lines were sometimes cast across two subfascicles instead of upon on a single continuous subfascicle. Horizontal breaking of bleached lines often occurred between adjacent subfascicles, but not within a single subfascicle, demonstrating sliding between subfascicles (Fig. 3.16). To explore these differences further,

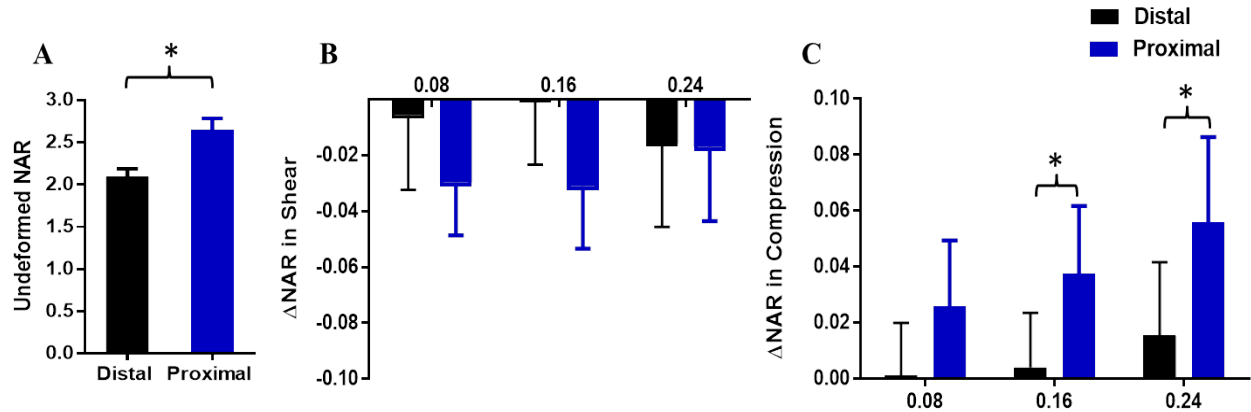


Fig. 3.15 (A) Nuclear aspect ratio of distal and proximal samples before loading; change of nuclear aspect ratio normalized by undeformed NAR under shear (B) and compression (C) for distal and proximal samples after strain applied (data are shown as mean \pm 95% confidence intervals; * for $p < 0.05$).

the strain parameters calculated using photobleached lines were separated into two groups: whether they crossed two subfascicles or were created on a single subfascicle. Although shear strain values were similar in distal samples, shear across two subfascicles was significantly larger than for a single subfascicle in proximal samples (Fig. 3.17A). For compressive loading, strain values of two subfascicles were larger than those of a single subfascicle for both distal (at all strain levels) and proximal samples (at the largest strain step) (Fig. 3.17B). Interestingly, several samples with lines photobleached on a single fascicle showed positive compressive strain; this counter-intuitive result may be due to fibers realigning in the out-of-plane dimension (i.e., fibers moving laterally and getting squeezed out of the imaging plane).

Histology. Viewed under polarized microscope, proximal samples showed consistent staining through the thickness, while distal samples exhibited varying intensity of staining (Fig. 3.18A,C). From the top to the bottom (i.e., anterior to posterior), less intense and less organized

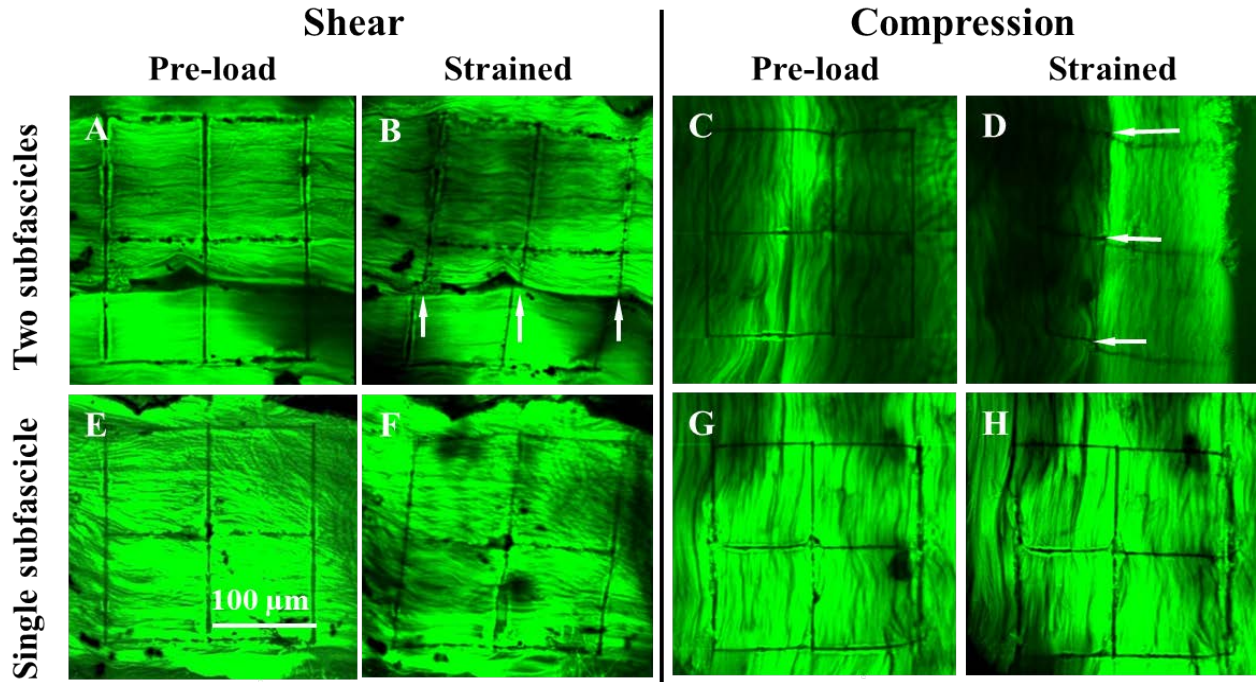


Fig.3.16 Two-photon microscopy images show lines photobleached on two subfascicles under (A) shear pre-load, (B) 0.24 shear strain, (C) compressive pre-load, and (D) 0.24 compressive strain; images in which photobleached lines are on single subfascicle under (E) shear pre-load, (F) 0.24 shear strain, (G) compressive pre-load, and (H) 0.24 compressive strain (white arrows indicate sliding between subfascicles).

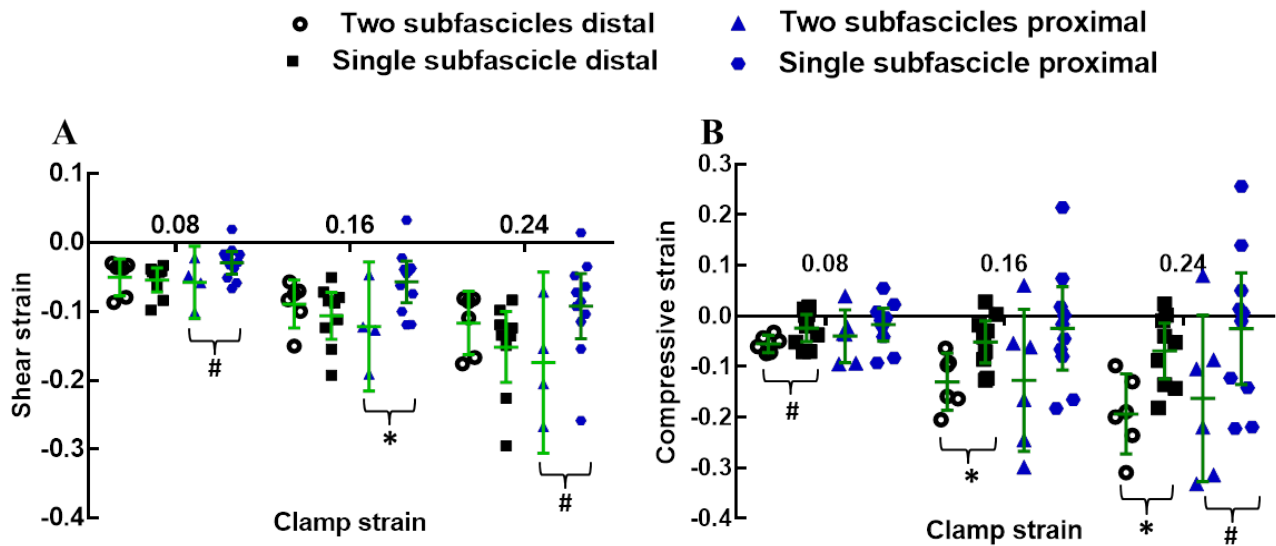


Fig. 3.17 Individual symbols shows strain values for distal and proximal samples grouped according to whether photobleached lines are on two subfascicles or single subfascicles for (A) shear and (B) compressive loading (lines and error bars are mean \pm 95% confidence intervals; * for $p < 0.05$; # for $0.05 \leq p \leq 0.1$).

collagen was observed near the anterior surface. In addition, collagen crimp was more

pronounced in the proximal samples compared to samples from the distal region (Figure 3.18B,D). Distal samples were stained more intensely with alcian blue than proximal samples (Fig. 3.19), suggesting significantly more proteoglycan present in distal samples. In distal samples, alcian blue staining was much more intense near the anterior surface of the tissue, demonstrating increased proteoglycans in this area of less organized collagen.

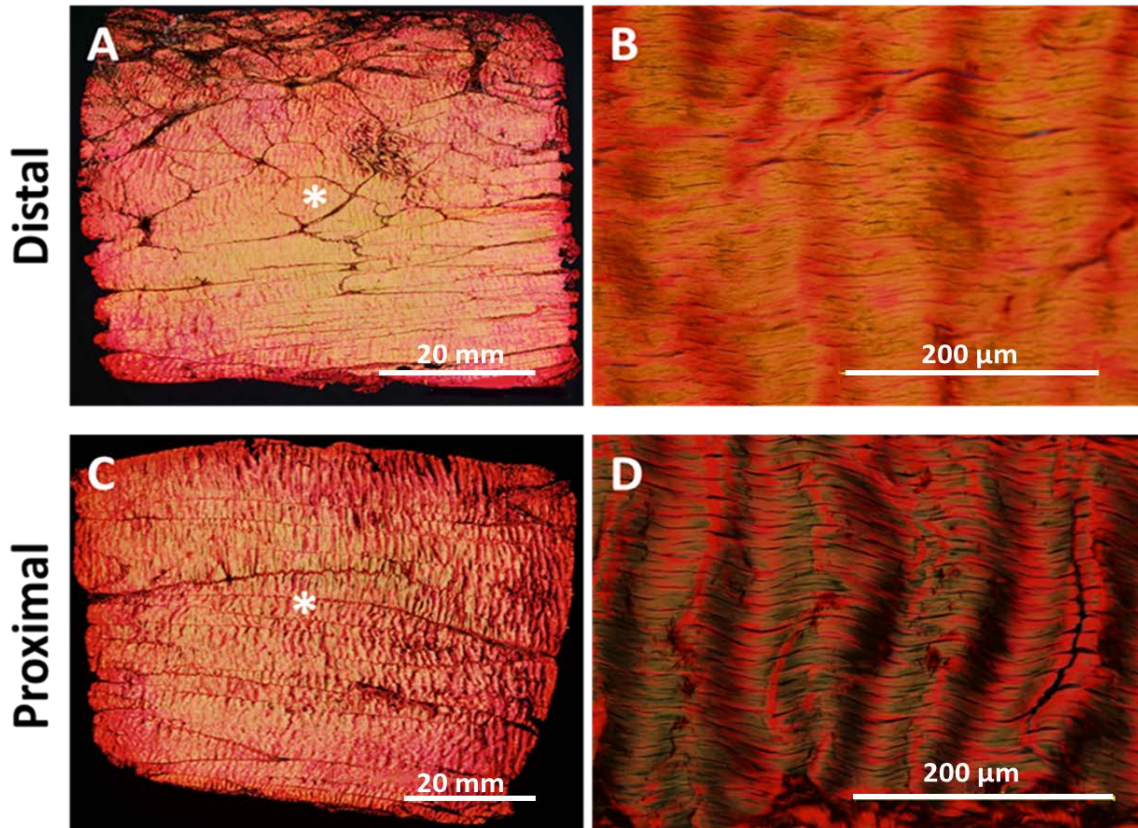


Figure 3.18 Representative picosirius red stained sections of distal (A) and proximal (C) samples by 4X objective of polarized light microscope. Images of distal (B) and proximal (D) samples at 40X, taken at the locations denoted by * in (A) and (B). The distal region shows non-uniform staining through the thickness and less collagen crimping compared to the proximal region. Anterior surface is towards the top of each image.

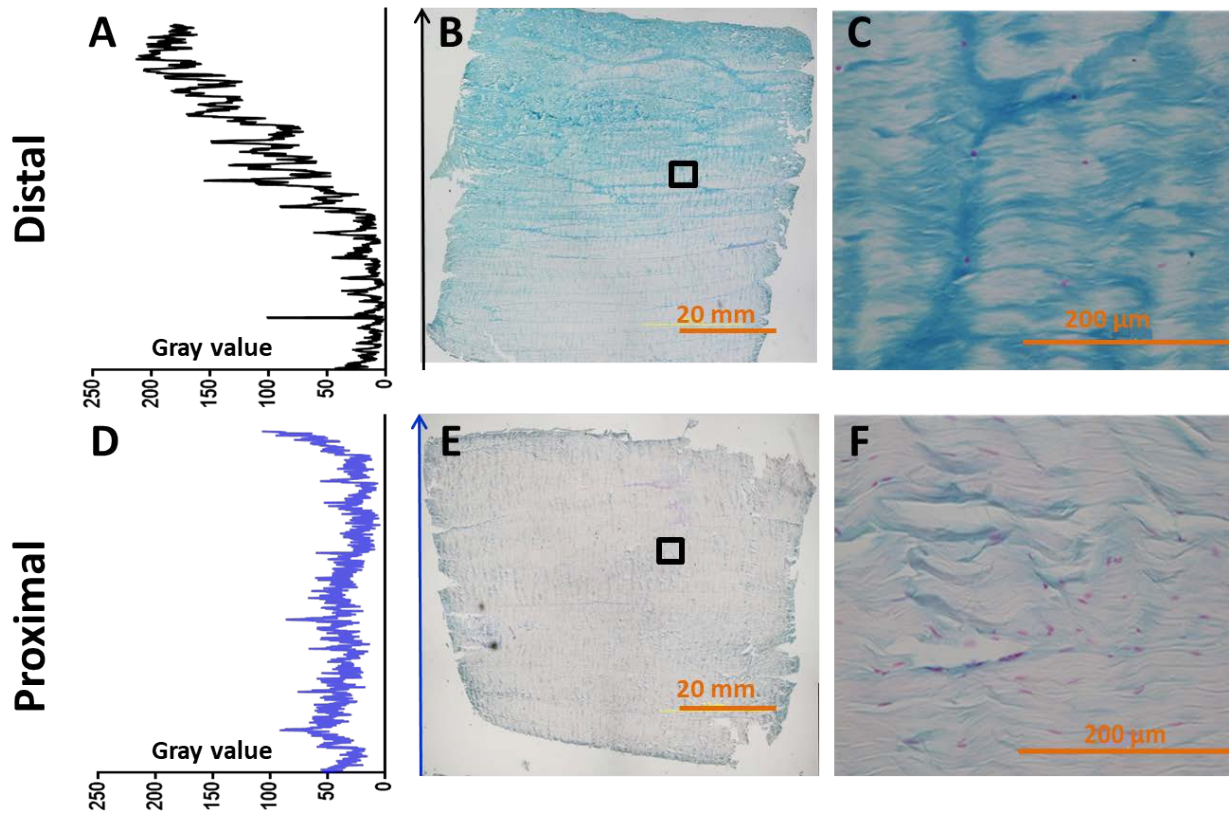


Fig. 3.19 Averaged intensity plots along tendon thickness (shown by arrows) for distal (A) and proximal (D) regions. Representative alcian blue stained sections of distal (B) and proximal (E) samples by 4X objective of white light microscope. Images of distal (C) and proximal (F) samples by 40X objective, taken at the locations denoted by * in (B) and (E). The distal region shows non-uniform staining through the thickness and staining in distal region is greater overall compared to the proximal region. Anterior surface is towards the top of each image.

3.4 Discussion

In this study, distal and proximal samples of bovine DDFT exhibited different mechanical responses during compression and shear loading. In particular, distal samples demonstrated larger compressive and shear stresses than proximal samples as hypothesized. Surprisingly, samples from these two locations had similar relaxation rates and total relaxation ratios, thereby exhibiting similar relaxation behavior under both compression and shear loading, which was contrary to our hypothesis. Strains were moderately attenuated from tissue to local matrix to nuclei-based measures, consistent with previous findings [30]. In addition, between-row rotations were found to be significantly larger than within-row rotations for distal and proximal

samples under shear, while similar under compression, indicating that fiber sliding was more prevalent in shear than compression. Broken photobleached lines further showed that sliding occurred between subfascicles of deformed tendon samples. Changes of nuclear aspect ratio demonstrated that macroscopically applied strains transferred down the hierarchical length scales to the cell nuclei. Comparing different tendon regions, distal and proximal samples exhibited similar strain responses at tissue and local matrix levels, but showed differences in many parameters evaluated at the level of the cell nuclei (Table 3.1). Specifically, differences were observed for between-row rotations, within-row rotations, NAR and Δ NAR in shear or compression, indicating varying microscale behavior for regions of bovine DDFTs that were shown to exhibit differences in mechanical and compositional properties. Staining of proximal samples was relatively homogeneous, but staining of distal samples varied through the thickness, with less organized collagen and increased proteoglycan near the anterior surface of DDFT. Interestingly, these differences between regions appeared to impact only the elastic, and not viscous, mechanical behavior of DDFT.

Table 3.1 Results for samples from the distal region compared to the proximal region for shear and compression testing (\uparrow , \leftrightarrow , and \downarrow represent larger, equivalent, and smaller values in the distal region compared to proximal, respectively; D = distal; P = proximal).

	Tissue strain	Local matrix strain	Nuclei-based strain	Between-row rotation	Within-row rotation	Between-row vs. within-row rotations	NAR	Δ NAR	Local matrix strain: two subfascicles vs. single subfascicle
Shear	\leftrightarrow	\leftrightarrow	N/A	\uparrow	\leftrightarrow	\uparrow (D & P)	\downarrow	\leftrightarrow (D & P) < 0	\uparrow (P only)
Compression	\leftrightarrow	\leftrightarrow	\uparrow	\leftrightarrow	\downarrow	\leftrightarrow (D & P)		\downarrow (D & P) > 0	\uparrow (D & P)

Similar to the current work, several previous studies have shown that biomechanical properties of several tendons vary across different regions or depths. For example, one of the few studies to evaluate tendon under compression showed that compressive stiffness of the

supraspinatus tendon (SST) has a inhomogeneous distribution from anterior to posterior and distal to proximal, which is dependent on its loading environment, architectural microstructure, and biochemical composition [16]. In terms of tensile loading, many studies have analyzed how tendons respond within different regions and across multiple length scales. For example, elastic moduli of human SST under longitudinal tensile testing decrease from medial to anterior to posterior regions, and transverse modulus values exhibit significant thickness-dependence; these regional differences in mechanics correlate with location-specific microstructural organization [5, 10]. In addition to these results for the highly complex SST, the nonlinearity of tendon mechanics, evaluated by hysteresis loss and recovery during incremental tensile loading, was shown to differ between two types of tendons, namely energy-storing and positioning tendons [19]. Collagen fiber re-alignment and crimp certainly contribute to nonlinearity, and differences in tendon's helical structures are proposed to further alter the extension and recoil response [19]. Taken together, these studies and the results presented herein demonstrate that tendon structure plays a large role in dictating biomechanical response under different types of loading.

Besides differences of tendon structure accounting for various mechanical responses, previous studies demonstrate that tendons in different locations often have varying compositional profiles that can also contribute to defining unique biomechanical behaviors. For example, the distal region of bovine DDFT shows evidence of fibrocartilage-like tissue that develops under pressure and frictional forces, with increased content of Type II collagen, glycosaminoglycans/proteoglycans, and rounded chondrocyte-like cells compared to the proximal region [2, 31, 32]. Moreover, the dominant proteoglycan of the distal region is aggrecan, which is rich in chondroitin sulfate and keratin sulfate, while the small proteoglycans decorin and biglycan mainly exist in the proximal region [4, 33, 34]. Since the large negative

charge of aggrecan increases binding of water to retain higher osmotic pressure and provides higher charge repulsive force, increased aggrecan enables the distal region to better resist compression and shear loading [34]. Aggrecan can also contribute to improved sliding between fibrils, which is especially significant when experiencing frictional forces [35]. Our current results confirmed that the distal and proximal regions exhibited different collagen and proteoglycan distributions, and we now also showed distinct mechanical properties under shear and compression loading. However, observed mechanical differences were mainly for elastic behavior in both types of loading; the time-dependent viscous response (i.e., relaxation behavior) was unexpectedly similar between distal and proximal samples, even with structural and compositional differences apparent between these two regions. Proteoglycans have been shown to greatly influence tendon viscoelasticity [34], and fascicles from bovine extensor tendons demonstrated increased stress relaxation after removing glycosaminoglycans (GAG) with chondroitinase ABC [36]. In tendon samples evaluated in the current study, the viscoelastic effect of proteoglycan differences between regions may have been offset by differences in collagen organization and/or density, leading to similar overall relaxation behavior. This topic merits further study.

Along with composition and structural organization, the nature of the *in vivo* mechanical loading environment also influences tendon properties. The specific aspects of physiological loading (i.e., magnitude and direction of forces) dictate changes in tissue properties through cell responses in order to adapt to functional mechanical environment. For example, stretching of muscles for 21 days stimulated synthesis of extracellular matrix proteins and glycosaminoglycan in calcaneal tendons of rats [37]. In contrast, immobilization, a method to reduce physiological compression loading, caused less synthesis of proteoglycans of calcaneal tendons [38]. A prior

study found that segments of bovine DDFT under *in vitro* cyclic compressive loading synthesized greater aggrecan and biglycan mRNA, and tendon segments cultured in transforming growth factor (TGF)- β 1 also stimulated expression and synthesis of aggrecan and biglycan [39]. Therefore, Robbins et al. suggested that mechanical loading caused altered expression of key genes (e.g., TGF- β 1) that led to changes in the ECM and subsequent fibrocartilage formation in the distal region [39].

Previous studies on fascicles from rat tail tendons under tension have demonstrated that the local matrix strain along the direction of fiber alignment was approximately half of the applied strain, and large variability between samples was attributed to inhomogeneous tendon organization [40]. Furthermore, strain transfer was also attenuated from tissue to local matrix to nuclei levels in meniscus and annulus fibrosus, with the level of attenuation dependent on tissue types, species, and ages [12]. Our results concurred with these studies, finding that strain was transmitted less from tissue to local matrix to nuclei levels, albeit under shear and compression loading rather than tension. Strain attenuation was larger under compression than shear, suggesting that different physical mechanisms regulate strain responses in these two types of loading. Additionally, proximal samples had slightly smaller strains transferred from tissue to local matrix than distal samples, which could correlate with compositional and organizational differences between these two regions of the DDFT (i.e., more proteoglycans and less well-organized collagen fibers in distal than proximal regions) [3]. For compression testing, strains calculated by photobleached lines were slightly larger than the strain computed by tracking cell nuclei, which also agrees with previous studies of tendon loaded in tension [41]. Compared with the amount of variability between samples, small differences between strain values obtained by tracking photobleached lines and coordinates of nuclei centroids are small enough that either of

these approaches can be used to characterize microscale strains. However, evaluating differences between micro-level strains computed by photobleached lines and nuclei may provide insight into how fibroblasts interact with fibers under different loading regimes.

Between-row rotations primarily represent sliding between fibers, while within-row rotations represent fiber straightening, uncrimping and/or realignment within a given fiber [42]. Given these interpretations, significant differences between these parameters in shear demonstrated that sliding was the predominant mechanism governing the strain response (Fig. 5A). Larger between-row rotations with the increase of applied strain indicated more sliding, with less dramatic increases for within-row rotations. The same was not true for compression, where between-row and within-row rotations were of similar magnitudes (Fig. 5B). Since (1) strains along individual fibers were ~ 0 (not shown), (2) within-row rotations only showed moderate increases at higher applied clamp strains, and (3) collagen fibers continued to exhibit fiber crimping even at high (shear or compressive) strain (e.g., Figs. 3 and 7), it appears that sliding (in shear) and fiber realignment/reorganization (in shear and compression) contribute more than collagen uncrimping to the response of tendon to non-tensile deformation. Additionally, out-of-plane fiber realignment facilitated by helical sub-structures may contribute to within-row rotations. Previous work has demonstrated the existence of spiral supra-organization in tendon collagen fibers using three-dimensional x-ray tomography and interference microscopy at various sectioning planes [43, 44]. However, additional studies are needed to quantitatively analyze the consequences of helical structures in tendon's response to loading, particularly under physiologically-relevant loading regimes.

Applied strains were transmitted to the level of cell nuclei. Increased NAR values under compression showed that cell nuclei became more elongated as compressive forces squeezed

cells lying between collagen fibers. In contrast, decreased NAR values were observed under shear loading, illustrating different mechanisms governing cell responses. Since sliding dominates the local matrix response to shear loading, sliding between fibers may cause cell rotation leading to slight rounding of cell nuclei. Taken together, the microscale measures based on cell nuclei indicate that fiber sliding, realignment and uncrimping play different roles in regulating tendon behavior and cell responses under variable types of loading.

In our experiments, breaking of photobleached lines often occurred at the interface of subfascicles, which could be attributed to less stiff interfascicular material. It remains unclear how non-fibrillar matrix is distributed amongst subfascicles and how it functions in force transfer when different hierarchical structures assemble to form tendons. It has been suggested that a horseshoe-shaped core protein in proteoglycans binds non-covalently to single collagen triple helices, and that fibrils are then chained together to form fibers [45]. Obvious sliding and strain attenuation among different length scales in our study also suggested collagen fibrils connected in a staggered form. Furthermore, shear loading could not be supported by unconnected collagen fibrils, so must be supported by the transfer of shear stress between collagen fibrils and non-fibrillar matrix. However, previous work demonstrated that the depletion of GAGs from tendon fascicles did not affect dynamic and viscoelastic properties under tensile loading [46]. More recently, other constituent proteins of the ECM such as elastin have been suggested to play a significant role in connecting and transferring load between collagen fibers in connective tissues [47]. Further research is needed to identify key components of the interfascicular matrix and determine how they contribute to the response of tendon to different loading conditions.

This study is not without limitations. First, the thickness of samples loaded in the test system for shear testing were not always kept the same as value measured by the laser system, which

could have caused slight tension or compression prior to applying shear strain. These offsets were minimized using the three-axis positioning system; however, more studies should be conducted to determine the degree to which tension or compression influences mechanical response of tendon during shear loading. Second, cellular strain was not evaluated. However, Δ NAR provides a measure related to cellular deformation. Future work could incorporate both cellular aspect ratios and NAR for elucidating mechanotransduction more completely under shear and compression. Third, macroscale camera and multi-photon microscopy images were not collected simultaneously, but rather for different sets of samples. However, all mechanical tests were performed with the same loading device and protocol, so we expect any differences to be minimal. Finally, although histological analysis showed different distributions of proteoglycan and collagen, we did not quantitatively compare the varieties and amounts in distal and proximal regions. Other techniques such as biochemical analysis could be used to quantify these differences.

3.5 Conclusion

In conclusion, compression and shear tests showed that different regions of bovine DDFT exhibited unique mechanical responses. Specifically, the proximal region had smaller compressive and shear stresses than the distal region although they showed similar relaxation rates and ratios. When evaluated using a two relaxation-time solid linear model, proximal and distal regions exhibited similar relaxation behavior under compression and shear loading, even though moduli of different components was significantly smaller for the proximal region. DDFT samples had attenuated strains from macro- to micro- length scales (from the tissue to local matrix to nuclei levels) in both shear and compressive loading. Variability in measured strains was indicative of microstructural inhomogeneity of tendon. Sliding along fibers was more

pronounced in shear than compression. Breaking of photobleached grid lines demonstrated more relative motion between subfascicles than within single subfascicles. The nuclear aspect ratio decreased in shear, but increased in compression, suggesting that different mechanisms govern interaction between fibers and cells for these regimes of multiaxial loading. Distal and proximal regions of DDFt demonstrated similar behavior at larger length scales, but differences in microscale responses to non-tensile loading. Regional differences in the *in vivo* loading environments (e.g., tensile vs. combined/multiaxial loading) are likely responsible for the location-specific mechanical properties, which correlated with microstructural organization and compositional content. These findings provide additional details of tendon structure-function relationships under multiaxial loading conditions and have important implications for evaluating the mechanobiologic response of tendon by quantifying the microscale (i.e., cell level) deformations experienced during physiologically-relevant non-tensile loading. In addition, results provide insight into how multiscale strains may be altered following compositional/organizational ECM changes that accompany injury/degeneration, which has implications in tendon healing and repair. Finally, experimental data from this study will help establish design criteria for engineered tendon replacements that are capable of proper function in complex *in vivo* loading environments.

3.6 References

1. Zhu, Y., et al., A finite viscoelastic-plastic model for describing the uniaxial ratchetting of soft biological tissues. *J Biomech*, 2014. 47(5): p. 996-1003.
2. Vogel, K.G., Tendon structure and response to changing mechanical load. *J Musculoskelet Neuronal Interact*, 2003. 3(4): p. 323-5; discussion 333-325.
3. Koob, T.J. and K.G. Vogel, Site-related variations in glycosaminoglycan content and swelling properties of bovine flexor tendon. *J Orthop Res*, 1987. 5(3): p. 414-424.

4. Koob, T.J. and K.G. Vogel, Proteoglycan synthesis in organ cultures from regions of bovine tendon subjected to different mechanical forces. *Biochem J*, 1987. 246(3): p. 589-598.
5. Lake, S.P., et al., Effect of fiber distribution and realignment on the nonlinear and inhomogeneous mechanical properties of human supraspinatus tendon under longitudinal tensile loading. *J Orthop Res*, 2009. 27(12): p. 1596-1602.
6. Bey, M.J., et al., Intratendinous strain fields of the intact supraspinatus tendon: the effect of glenohumeral joint position and tendon region. *J Orthop Res*, 2002. 20(4): p. 869-874.
7. Huang, C.Y., et al., Inhomogeneous mechanical behavior of the human supraspinatus tendon under uniaxial loading. *J Orthop Res*, 2005. 23(4): p. 924-930.
8. Matuszewski, P.E., et al., Regional variation in human supraspinatus tendon proteoglycans: decorin, biglycan, and aggrecan. *Connect Tissue Res*, 2012. 53(5): p. 343-348.
9. Riley, G.P., et al., Tendon degeneration and chronic shoulder pain: changes in the collagen composition of the human rotator cuff tendons in rotator cuff tendinitis. *Ann Rheum Dis*, 1994. 53(6): p. 359-366.
10. Lake, S.P., et al., Tensile properties and fiber alignment of human supraspinatus tendon in the transverse direction demonstrate inhomogeneity, nonlinearity, and regional isotropy. *J Biomech*, 2010. 43(4): p. 727-732.
11. Buckley, M.R., et al., Distributions of types I, II and III collagen by region in the human supraspinatus tendon. *Connect Tissue Res*, 2013. 54(6): p. 374-379.
12. Han, W.M., et al., Macro- to microscale strain transfer in fibrous tissues is heterogeneous and tissue-specific. *Biophys J*, 2013. 105(3): p. 807-817.
13. Screen, H.R., S. Toorani, and J.C. Shelton, Microstructural stress relaxation mechanics in functionally different tendons. *Med Eng Phys*, 2013. 35(1): p. 96-102.
14. Thorpe, C.T., et al., Fascicles from energy-storing tendons show an age-specific response to cyclic fatigue loading. *J R Soc Interface*, 2014. 11(92): p. 20131058.
15. Miller, K.S., et al., Characterizing local collagen fiber re-alignment and crimp behavior throughout mechanical testing in a mature mouse supraspinatus tendon model. *J Biomech*, 2012. 45(12): p. 2061-2065.
16. Lee, S.B., et al., The bursal and articular sides of the supraspinatus tendon have a different compressive stiffness. *Clin Biomech (Bristol, Avon)*, 2000. 15(4): p. 241-247.
17. Zhang, Z.J. and S.N. Fu, Shear Elastic Modulus on Patellar Tendon Captured from Supersonic Shear Imaging: Correlation with Tangent Traction Modulus Computed from Material Testing System and Test-Retest Reliability. *PLoS One*, 2013. 8(6): p. e68216.
18. Cheng, V.W., Screen, H. R., The micro-structural strain response of tendon. *Journal of Materials Science*, 2007. 42(21): p. 8957-8965.
19. Thorpe, C.T., et al., Helical sub-structures in energy-storing tendons provide a possible mechanism for efficient energy storage and return. *Acta Biomater*, 2013. 9(8): p. 7948-7956.

20. Arnoczky, S.P., et al., In situ cell nucleus deformation in tendons under tensile load; a morphological analysis using confocal laser microscopy. *J Orthop Res*, 2002. 20(1): p. 29-35.
21. Fang, F., A.S. Sawhney, and S.P. Lake, Different regions of bovine deep digital flexor tendon exhibit distinct elastic, but not viscous, mechanical properties under both compression and shear loading. *J Biomech*, 2014. 47(12): p. 2869-2877.
22. Buckley, M.R., et al., Mapping the depth dependence of shear properties in articular cartilage. *J Biomech*, 2008. 41(11): p. 2430-2437.
23. Evanko, S.P. and K.G. Vogel, Proteoglycan synthesis in fetal tendon is differentially regulated by cyclic compression in vitro. *Arch Biochem Biophys*, 1993. 307(1): p. 153-164.
24. Szczesny, S.E., R.S. Edelman, and D.M. Elliott, DTAF dye concentrations commonly used to measure microscale deformations in biological tissues alter tissue mechanics. *PLoS One*, 2014. 9(6): p. e99588.
25. Bruehlmann, S.B., P.A. Hulme, and N.A. Duncan, In situ intercellular mechanics of the bovine outer annulus fibrosus subjected to biaxial strains. *J Biomech*, 2004. 37(2): p. 223-231.
26. Lake, S.P., E.S. Hald, and V.H. Barocas, Collagen-agarose co-gels as a model for collagen-matrix interaction in soft tissues subjected to indentation. *J Biomed Mater Res A*, 2011. 99(4): p. 507-515.
27. Lake, S.P. and V.H. Barocas, Mechanical and structural contribution of non-fibrillar matrix in uniaxial tension: a collagen-agarose co-gel model. *Ann Biomed Eng*, 2011. 39(7): p. 1891-1903.
28. Thomopoulos, S., G.M. Fomovsky, and J.W. Holmes, The development of structural and mechanical anisotropy in fibroblast populated collagen gels. *J Biomech Eng*, 2005. 127(5): p. 742-750.
29. Beer, F., E. Johnston, and J. DeWolf, *Mechanics of Materials*. 2006. The McGraw-Hill Companies Publishing.
30. Sherif, A.M., Accelerated versus conventional corneal collagen crosslinking in the treatment of mild keratoconus: a comparative study. *Clin Ophthalmol*, 2014. 8: p. 1435-1440.
31. Carvalho, H.F., et al., Identification, content, and distribution of type VI collagen in bovine tendons. *Cell Tissue Res*, 2006. 325(2): p. 315-324.
32. Feitosa, V.L., et al., Comparative ultrastructural analysis of different regions of two digital flexor tendons of pigs. *Micron*, 2006. 37(6): p. 518-525.
33. Vogel, K.G., What happens when tendons bend and twist? Proteoglycans. *Journal of Musculoskeletal and Neuronal Interactions*, 2004. 4(2): p. 202-203.
34. Yoon, J.H. and J. Halper, Tendon proteoglycans: biochemistry and function. *J Musculoskelet Neuronal Interact*, 2005. 5(1): p. 22-34.

35. Thorpe, C.T., et al., The role of the non-collagenous matrix in tendon function. *Int J Exp Pathol*, 2013. 94(4): p. 248-259.
36. Legerlotz, K., G.P. Riley, and H.R. Screen, GAG depletion increases the stress-relaxation response of tendon fascicles, but does not influence recovery. *Acta Biomater*, 2013. 9(6): p. 6860-6866.
37. de Almeida, F.M., et al., Effects of stretching on morphological and biochemical aspects of the extracellular matrix of the rat calcaneal tendon. *Cell Tissue Res*, 2010. 342(1): p. 97-105.
38. Aro, A.A., et al., Structural and biochemical analysis of the effect of immobilization followed by stretching on the calcaneal tendon of rats. *Connect Tissue Res*, 2008. 49(6): p. 443-454.
39. Robbins, J.R., S.P. Evanko, and K.G. Vogel, Mechanical loading and TGF-beta regulate proteoglycan synthesis in tendon. *Arch Biochem Biophys*, 1997. 342(2): p. 203-211.
40. Shepherd, J.H., G.P. Riley, and H.R. Screen, Early stage fatigue damage occurs in bovine tendon fascicles in the absence of changes in mechanics at either the gross or micro-structural level. *J Mech Behav Biomed Mater*, 2014. 38: p. 163-172.
41. Screen, H.R., et al., An investigation into the effects of the hierarchical structure of tendon fascicles on micromechanical properties. *Proc Inst Mech Eng H*, 2004. 218(2): p. 109-119.
42. Screen, H.R., Bader, D. L., Lee, D. A., Shelton, J. C., Local Strain Measurement within Tendon. *STRAIN*, 2004. 40: p. 157-163.
43. de Campos Vidal, B., Image analysis of tendon helical superstructure using interference and polarized light microscopy. *Micron*, 2003. 34(8): p. 423-432.
44. Kalson, N.S., et al., Fibre bundles in the human extensor carpi ulnaris tendon are arranged in a spiral. *J Hand Surg Eur Vol*, 2012. 37(6): p. 550-554.
45. Scott, J.E., Proteodermatan and proteokeratan sulfate (decorin, lumican/fibromodulin) proteins are horseshoe shaped. Implications for their interactions with collagen. *Biochemistry*, 1996. 35(27): p. 8795-8799.
46. Fessel, G. and J.G. Snedeker, Evidence against proteoglycan mediated collagen fibril load transmission and dynamic viscoelasticity in tendon. *Matrix Biol*, 2009. 28(8): p. 503-510.
47. Henninger, H.B., et al., Effect of elastin digestion on the quasi-static tensile response of medial collateral ligament. *J Orthop Res*, 2013. 31(8): p. 1226-1233.

Chapter 4: Multiscale Mechanical Integrity of Human Supraspinatus Tendon in Shear after Elastin Depletion³

4.1 Introduction

The supraspinatus tendon (SST), part of the rotator cuff in the shoulder, passes underneath the acromion such that interactions with surrounding bones/tissues cause multiaxial loading (i.e., tension, shear, compression). Study of SST mechanical behavior under different loading scenarios could help determine how tendon modulates its structure and composition to support multiaxial loading, and potentially inform how degeneration or injury occurs due to such loading. Previous studies have reported unique and highly inhomogeneous mechanical, structural, and compositional properties for human SST under tensile loading [1, 2]. The medial SST exhibits properties typical of tendon while the lateral region (i.e., the area of likely multiaxial loading) shows planar mechanical isotropy, disorganized collagen fibers, and extracellular matrix (ECM) composition more similar to fibrocartilage [2-5]. These data imply complex multiaxial *in vivo* loading of SST, however much remains unknown regarding SST properties under such non-tensile loads.

Biomechanical tensile testing combined with confocal imaging has been utilized to examine tendon mechanics and physical mechanisms underlying tendon behavior. For example, photobleached grids created on rat-tail tendons showed both rotation and stretch under tension, which indicated collagen fiber sliding and elongation as the predominant modes of local matrix

³ Reprinted from Fang, F. and Lake, SP., 2016, "Multiscale mechanical integrity of human supraspinatus tendon in shear after elastin depletion." *J Mech Behav Biomed Mater.* 63, 443-455.

deformation contributing to tendon response under tension [6, 7] Tendon viscosity and elasticity in tension are also facilitated by this microscale deformation (i.e. sliding between collagen fibers and fiber elongation) for avoiding injury [6, 8, 9]. In our Chapter 3, sliding between collagen fibers and fiber reorganization were found to modulate the response of bovine deep digital flexor tendons in shear loading [9]. Although strain transfer in tendon has been evaluated, it remains generally unknown which tissue constituents facilitate force transfer, particularly under non-tensile and/or multiaxial loading.

While long known to be important in cardiovascular mechanics, recent work has suggested that elastin may play a mechanical role in orthopaedic tissues such as tendon and ligament [10-15]. For example, elastin has been shown to sustain tensile loading in the toe-region and assist in load transfer of porcine ligament [11]. Additionally, decreased mechanical parameters of ligaments after elastin depletion under both shear and transverse tensile loading verified that elastin also provided support for transverse elongation and shear deformation [12], which has also been demonstrated for bovine annulus fibrosus under dynamic shear loading [14]. Interestingly, both rat-tail and human palmaris longus tendons showed lower tensile strength and failure strain following elastin degradation, and larger wavelength of crimp pattern under tension [10]. To date, elastin has been shown to distribute along collagen fibers in tendon, with fibrillin-1 and fibrillin-2 coexisting with elastin as measured by immunohistochemistry [16-19]. However, it remains unclear how elastin is distributed within and throughout tendon, how it interacts with collagen fibers, and how elastin contributes to tendon mechanical behavior under multiaxial loading.

The aims of this study were (1) to quantitatively evaluate region-specific mechanical properties of human SST under shear using biomechanical testing in combination with

multiphoton microscopy imaging, and (2) to examine the role of elastin in SST response to shear through targeted enzyme treatments. We hypothesized that (1) both anterior and posterior regions of SST would exhibit larger shear stresses and smaller local matrix strains than the medial region due to less organized collagen in these regions, and (2) SST samples would show smaller shear stresses but larger microscale strains following elastin degradation, thereby demonstrating that elastin contributes to maintain tendon mechanical integrity under multiaxial loading.

4.2 Materials and methods

Elastase treatment protocol. The efficiency of elastase on SST was examined in concentration- and time-dependent testing. Small tissue segments (n=15), weighing 40-50 mg (approximate dimensions of 1×0.5×0.5mm), were obtained from the anterior region of a single SST. To hinder proteolysis caused by elastase impurity, all segments were equilibrated in 15 ml PBS with 0.1 mg/ml soybean trypsin inhibitor (SBTI, SB903, Elastin Product Company) for 15 min at room temperature. These segments were randomly divided into five groups (n=3 for each) and incubated in 15 ml PBS with 0, 1, 5, 10, and 20 units/ml elastase (trypsin-free porcine pancreatic elastase with high purity, EC134, Elastin Products Company) for 6 hours at room temperature to evaluate the effect of elastase concentration. Similar small tissue segments (n=15) were prepared from the anterior region of another SST and treated similarly with soybean trypsin inhibitor, as stated above. After divided into five groups (n=3 for each), segments were incubated in 30 ml PBS with 5 units/ml elastase for 0, 1, 4, 6, 12 hours at room temperature to evaluate the effect of incubation time. Following elastase treatment, the elastin content of all segments was quantified using the biochemical analysis described below. Results of the concentration- and

time-dependent testing indicated an elastase treatment protocol of 15-minute incubation in 0.1 mg/ml SBTI solution followed by incubation for 8 hours in 5 units/ml elastase in PBS.

Due to the relatively large size of our samples for biomechanical testing and the method used to attach samples to shear clamps discussed below, the depth at which elastase could penetrate into the tissue for digestion was evaluated. Bovine deep digital flexor tendons (DDFTs), as a representative tendon tissue with a better known (and constant) distribution of elastic fibers [17], were used for this assessment. Samples (n=4) with the same size as the ones used for biomechanical testing were cut from the proximal region of four bovine DDFTs, similar to previous studies [9, 17, 20]. An additional set of adjacent samples (n=4) was also obtained from the corresponding flexor tendons for control. Samples were glued to shear clamps and the clamps-sample assemblies were incubated in PBS for 8 hours, consistent with the time used for sample preparation and biomechanical testing before elastase treatment. After PBS incubation, the clamps-sample assemblies were treated according to the elastase treatment protocol. The control clamps-sample assemblies were incubated in PBS but without elastase for the same amount of time. The surface of samples touching the bottom of beaker during treatment was defined as the bottom. Following treatment, thin pieces of samples weighing 40-50 mg were acquired at five locations evenly spaced along the sample thickness in the z-direction (Fig. 4.1A) for biochemical analysis. Normalized elastin content was reported as the ratio of elastin in treated samples relative to corresponding controls.

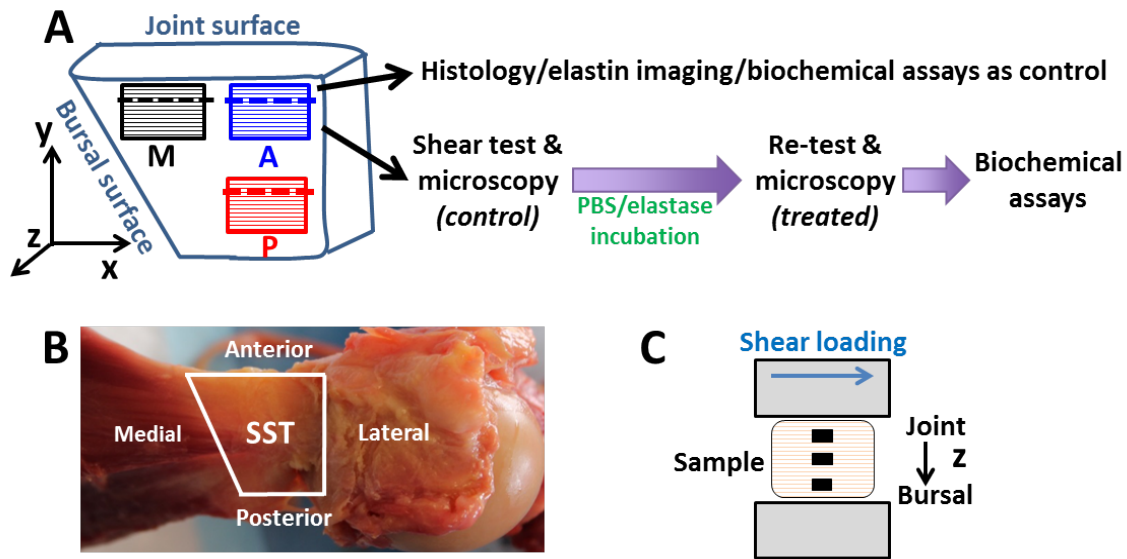


Fig. 4.1 The experimental design. (A) Samples (black, blue, and red blocks, lines inside showing alignment of collagen fibers), obtained from medial (M), anterior (A), and posterior (P) regions of SST used for biomechanical testing and compositional analysis. (B) Representative supraspinatus tendon (SST) specimen showing anatomical orientation. (C) Bursal and joint surfaces of SST sample mounted to clamps. Solid black blocks indicate three locations for photobleaching during multiphoton imaging; blue arrow shows shear loading direction and the black arrow shows the z-axis of the sample (through thickness).

Biochemical analysis. A non-equilibrium competitive enzyme-linked immunosorbent assay (ELISA) was adopted from established techniques to quantify the crosslinking desmosine as a marker of elastin [21, 22]. A ninhydrin-based assay was used to measure total protein [23]. Briefly, prepared 40-50 mg segments were dehydrated in a refrigerated vapor trap (RVT 4014, Thermo Fisher Scientific, St. Louis, MO), hydrolyzed in 6N HCl for 48 hours, then subjected to the competitive ELISA protocol [21]. Total elastin amount was converted from desmosine content using a conversion factor of 43.7 nano-moles desmosine per microgram of elastin [24]. Our preliminary data suggested that elastase treatment did not significantly alter the amount of total remaining protein (not shown). Therefore, elastin amount was normalized by total protein [24, 25]. Dimethylmethylene blue colorimetric assay was conducted to determine the effect of elastase treatment on proteoglycan (PG), composed of a core protein and attached glycosaminoglycan (GAG) chain [10, 12, 26]. After tissue segments were digested by papain

(papain from papaya latex, P4762, Sigma-Aldrich), 1-9-dimethylmethylene blue (DMMB, 341088, Sigma-Aldrich) was added to the digested tissue solution. GAG content was determined by spectrophotometry at 595 nm wavelength and normalized by sample wet weight [27].

Biomechanical testing. SSTs (n=12) were harvested from fresh frozen human cadaver shoulders (average age: 73.2 ± 12.8 years) without evidence of damage or tears. Full-thickness samples (10 mm long, 8 mm wide) were obtained from three SST regions (i.e., anterior, posterior, and medial), similar to previous studies (Fig. 4.1B) [3, 28]. A small specimen (2×1 mm L×W) adjacent to each mechanical test sample was acquired and used for histology, fluorescence imaging, or biochemical analysis to determine elastin content (Fig. 4.1B). For the mechanical test specimens, full-thickness surfaces along the direction of collagen fibers (xz plane in Fig. 4.1A) were leveled slightly on a microtome as described previously [9]. Thickness values (the length along z axis in Fig. 1) and cross-sectional areas (xy plane in Fig. 4.1) were measured with a non-contact laser scanning system.

Samples were incubated for 30 min in a 0.1M sodium bicarbonate buffer with 100 $\mu\text{g/ml}$ 5-DTAF and 1 $\mu\text{g/ml}$ DAPI to stain collagen and nuclei, respectively [9]. Following PBS washes, clamps-sample assemblies (Fig. 4.1C) were mounted in a micromechanical test device secured to the stage of a Zeiss multiphoton confocal microscope system [9]. The same shear testing and imaging protocol from Chapter 3. Briefly, after applying a 0.005N pre-load, four adjacent squares (100×100 μm , Fig. 4.2) were photobleached at a depth of $\sim 50\mu\text{m}$ (y axis in Fig. 1B) at three locations lying evenly along the bursal-to-joint thickness. Due to less organized collagen fibers in some regions, the photobleached location of some grid lines were adjusted slightly to guarantee clear visibility of intersections among lines. Incremental three-step stress-relaxation shear testing (8% strain steps separated by 12-minute relaxation periods) was applied and multi-

channel z-stacks were collected eight minutes after the application of each strain step, as described previously (Fig. 4.2) [9]. The shear strain was defined as the arctangent value of the ratio of applied displacement to sample thickness. Then, clamps were locked together to maintain the initial thickness and detached from the testing device. A power analysis

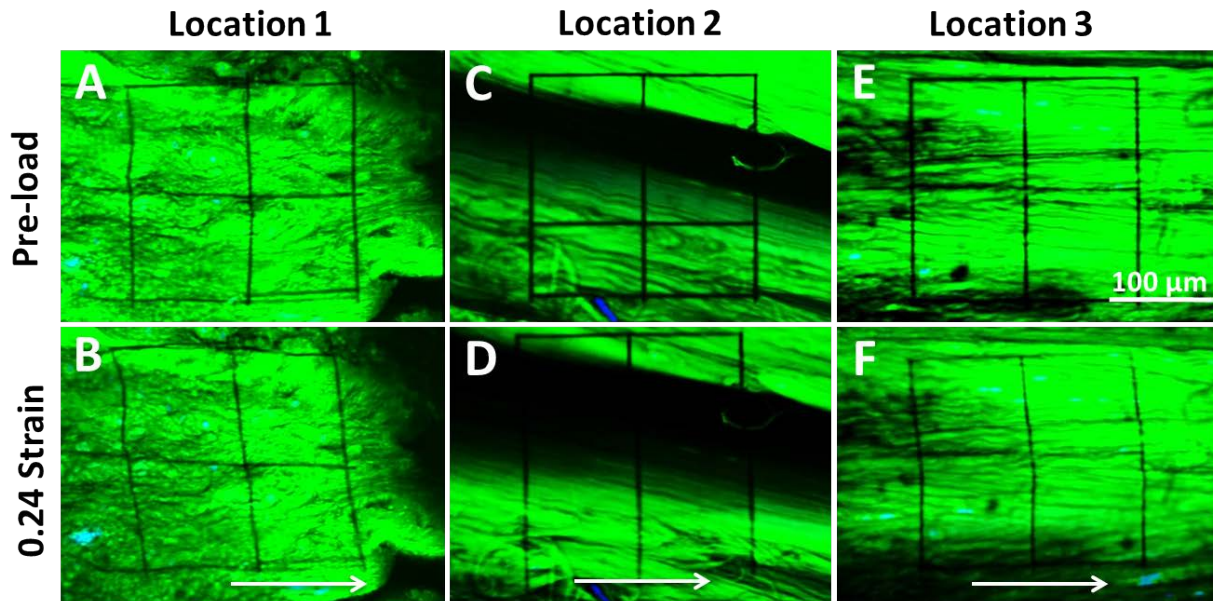


Fig. 4.2 Typical microscopy images from three locations in the same SST sample (from medial region) under pre-load and 0.24 shear strain, demonstrating that organization and deformation of local matrix differ within one sample from a single region. The white arrows show shear loading direction. Location 1 is from the bursal side, location 2 from the central zone, location 3 from the joint side. Scale bar =100 μm .

(power=0.8; $\alpha=0.05$) using results from our previous multiscale studies of bovine flexor tendon (Fang and Lake, 2015; Fang et al., 2014) suggested a sample size of seven to be sufficient to detect differences between regions and before/after enzyme digestion; the remaining samples were designated for use as control. For elastase-treated samples (n=7 per SST region), the clamps-sample assemblies were treated with the elastase protocol described earlier, namely 15-minute incubation in 0.1 mg/ml SBTI solution followed by 8 hours incubation in 5 units/ml elastase. For PBS-incubated samples (n=5 per SST region), the clamps-sample assemblies were incubated in PBS with 0.1 mg/ml soybean trypsin inhibitor for 15 min and then PBS for 8 hours

at room temperature. Following incubation, four adjacent squares were again photobleached on samples at the same three (or adjacent) bursal-joint locations and all samples were retested with the same shear loading protocol and image acquisition using multiphoton microscopy. After the completion of mechanical testing, ten samples were randomly selected and three tissue segments weighing 40-50 mg were taken from each sample evenly along the bursal-joint thickness to quantify elastin content via biochemical analysis. Similarly, another set of five samples after mechanical testing was used and three segments weighing 40-50 mg were taken from each of them to quantify GAG content.

Structure Analysis. Specimens obtained from each of the three SST regions (i.e., anterior, posterior, medial) from four mechanically-tested tendons were evaluated by histology and fluorescent microscopy. For histological examination, specimens were fixed in 4% paraformaldehyde for 24 hours, dehydrated in 70% ethanol, and embedded in paraffin. Paraffin sections (5- μ m thickness) were obtained and stained with hematoxylin and eosin (H&E), Alcian blue, and Verhoeff-Van Gieson (VVG) stain, then imaged using bright field microscopy with 20 \times and 40 \times objectives. Standard images representative of collagen organization and the distribution of cells, proteoglycans and elastic fibers were selected. Image J was used to adjust images of VVG stain acquired by 40 \times objective.

For fluorescent imaging, specimens were prepared using the same microtome to obtain smooth imaging surfaces. The specimens were incubated in 0.5 mg/ml sulforhodamine B (SRB) solution for 1 min since SRB has been shown fluorescently stain elastic fibers [29, 30]. After washing with PBS three times, 1 μ g/ml DAPI solution was applied for 10 mins to stain nuclei [6, 9]. The Mai Tai broadband infrared multiphoton laser of Zeiss multiphoton confocal microscope system was set to 800 nm excitation, and signals from elastic fibers and nuclei were collected at

565-600 nm and 450-490 nm, respectively, by utilizing 40× high NA (numerical aperture) oil-immersion objectives [9, 30]. Image z-stacks were acquired with 0.5-μm spacing and collapsed to form composite images.

Data analysis. Force values recorded immediately after the application of each step-strain were divided by cross-sectional areas (dimensions in xy plane in Fig 1B) and taken as peak stresses. Equilibrium stresses were computed as force values after each 12-minute stress-relaxation period normalized by cross-sectional areas. Peak/equilibrium reduced ratio was defined as:

$$\text{Peak/equilibrium reduced ratio} = \{1 - (\text{peak/equilibrium stress after PBS incubation or elastase treatment}) / (\text{peak/equilibrium stress before incubation or treatment})\} * 100\%$$

Local matrix-based strains, “between-row rotations”, and “within-row rotations” were calculated as done in previous studies [9, 20]. Briefly, collagen and nuclei channels were separated from collapsed z-stacks for evaluating local matrix strain and nuclei-based strain. 2D Lagrangian strains were calculated by tracking

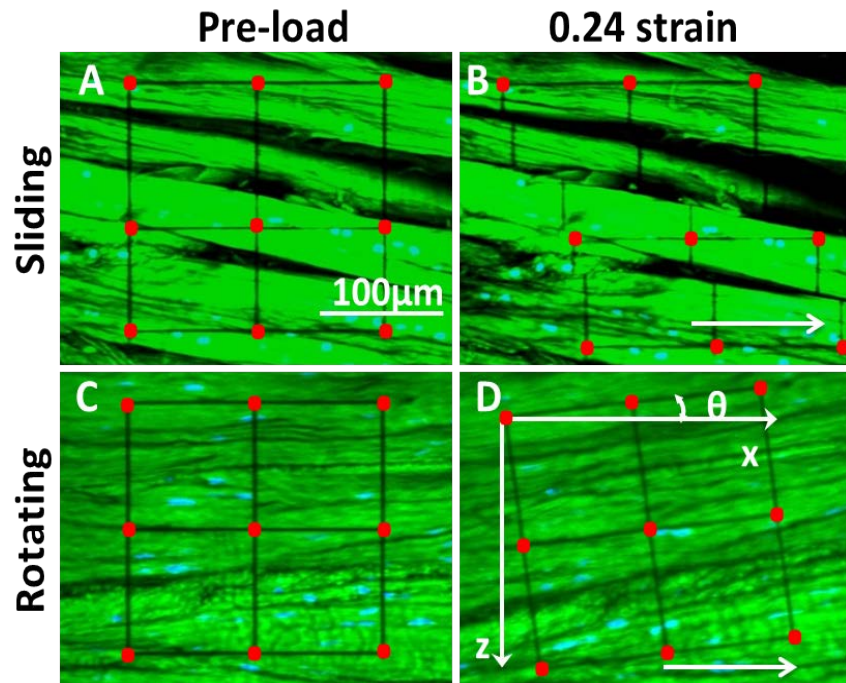


Fig. 4.3 Typical microscopy images from three locations in the same SST sample (from medial region) under pre-load and 0.24 shear strain, demonstrating that organization and deformation of local matrix differ within one sample from a single region. The white arrows show shear loading direction. Location 1 is from the bursal side, location 2 from the central zone, location 3 from the joint side. Scale bar =100 μm.

photobleached lines in multiphoton images (Fig. 4.3A&B) and taken as local matrix strains. Nuclei coordinates were obtained by Image J (1.47, National Institute of Health, Bethesda, MD) to compute within-row rotation and between-rows rotation [9]. Mechanical metrics from the first shear test were considered as control and compared to results from tests conducted after PBS- or enzyme-incubation. Normalized stresses were computed by dividing the re-tested data by the overall peak stress value from the corresponding sample in the (pre-incubation) first mechanical test. To quantify rigid body motion of photobleached lines visualized in multiphoton microscopy images, rotation of lines was calculated as the angle between deformed horizontal photobleached lines and the image x-axis (Fig. 4.3C&D). Between-rows and within-row rotations, indicating sliding between collagen fibers and reorganization within collagen fibers, respectively, were calculated as described previously [9]. Grid-based strains (i.e., local matrix strains) and nuclei-based deformation measures (i.e., within-row and between-rows rotations) are both valuable metrics as they represent different length scales and behaviors, and because the specific interaction between local extracellular matrix and cells is not well known.

All data are shown as mean \pm standard deviation (SD). Paired *t*-tests were used to evaluate mechanical differences between control and elastase-treated or PBS-incubated samples, while unpaired *t*-tests were used to evaluate local matrix-based strains and rotations. One-way ANOVAs with Bonferroni post-hoc tests were used to evaluate differences in output parameters by SST regions (anterior, posterior, and medial). Statistical significance was set at $p < 0.05$ while $0.05 \leq p \leq 0.1$ were taken as trends towards statistical significance.

4.3 Results

Biochemical analysis of samples. Following treatment, elastin content remaining in SST was inversely proportional to elastase concentration with a relatively consistent decrease across all concentrations evaluated (Fig. 4.4A). For different incubation times, elastin content decreased initially with time but appeared to mostly plateau after 6 hours (Fig. 4.4B). The two SSTs used for these experiments had different overall elastin amounts, such that elastin content was slightly higher for the samples used to evaluate different concentrations (Fig.4.4A) compared to the samples used to evaluate different incubation times (Fig.4.4B). Due to the high cost of elastase

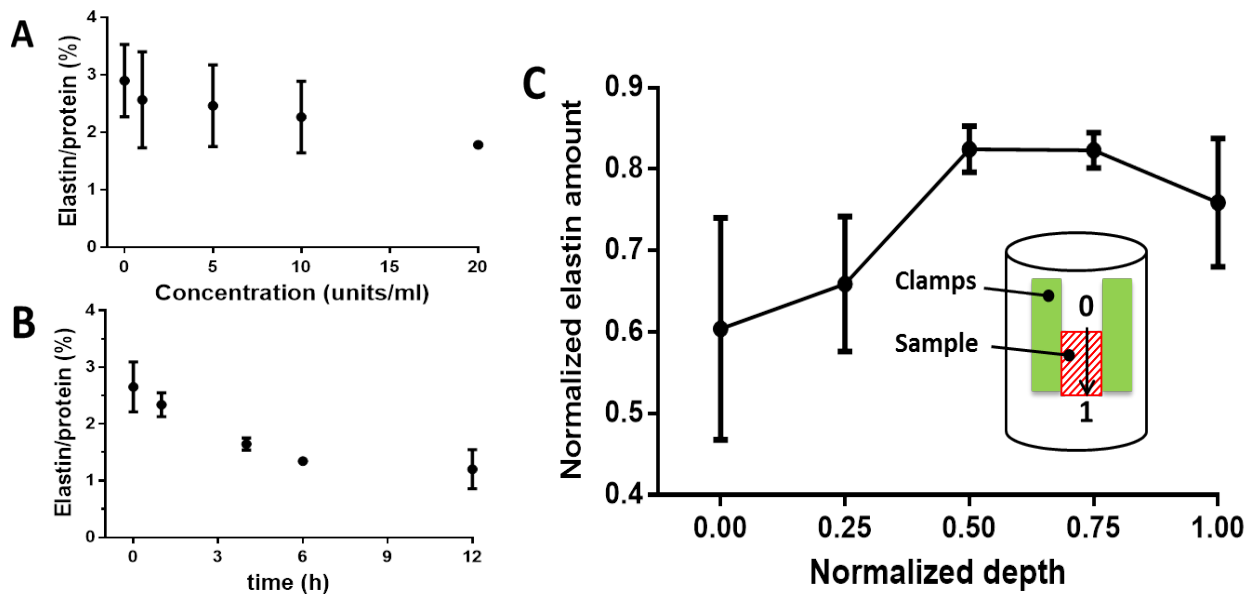


Fig. 4.4 The quantity of elastin in samples treated with different concentrations of elastase for six hours (A) or with 5 units/ml elastase for different times (B). (C) Remaining elastin content along the sample depth; inset shows a sample (red block) attached to clamps (green blocks) incubated in elastase solution. The normalized depth is defined as 0 (top) to 1 (bottom).

and relatively small decrease of elastin with the increase of elastase concentration from 5 to 20 units/ml, a treatment protocol of 5 units/ml elastase in PBS for 8 hours was used as the elastase protocol. Evaluation of elastase penetration using bovine flexor tendon samples illustrated that $39.6 \pm 7.9\%$ elastin was depleted near the top of surface of DDFT samples, which decreased to only $17.6 \pm 1.3\%$ depletion at 50-75% depth (Fig. 4.4C). Since the bottom surface of samples did

not completely contact the test device, depleted elastin increased slightly to $24.1\pm 3.9\%$ at the bottom compared to the middle location. Thus, due to limitations in diffusion and enzyme penetration, there was a gradient of elastin distribution after elastase treatment. Without enzyme treatment, anterior, posterior, and medial regions of control human SST had $2.63\pm 0.51\%$, $2.77\pm 0.32\%$, and $2.94\pm 0.46\%$ elastin normalized by the total protein amount, which were not significantly different by regions. For mechanically-tested SST samples, $52.0\pm 8.0\%$, $16.0\pm 5.5\%$, and $30.4\pm 4.9\%$ from the top, middle, and the bottom of samples, respectively, were removed.

Elastase-treated and control samples had $27.3\pm 4.8\%$ and $29.1\pm 3.2\%$ total protein normalized by wet weight; since the main protein in tendon is collagen, collagen content was therefore assumed not to be altered dramatically by elastase digestion [5, 31]. Similarly, GAG content normalized by sample wet weight was $0.30\pm 0.03\%$ and $0.32\pm 0.05\%$ in elastase-treated and control samples, without which was not significantly different between groups.

Contribution of elastin to tendon mechanics. Control samples (i.e., before treatment) consistently exhibited larger stresses than both elastase-treated and PBS-incubated samples in all three SST regions (Fig. 4.5). Peak stresses were significantly smaller for elastase-treated anterior and medial regions at lower strains ($p < 0.040$; Fig. 4.5A). The posterior region showed trends towards decreased peak stresses for all strain steps ($p < 0.07$). No significant differences of peak stresses between control and PBS-incubated samples were detected except for posterior samples at 0.16 strain (Fig. 4.5B). Only the anterior region showed significantly decreased equilibrium stresses after enzyme treatment at lower strains ($p < 0.020$), while the posterior and medial regions showed trends towards decreased stresses ($p < 0.08$) at lower strains (Fig. 4.5C).

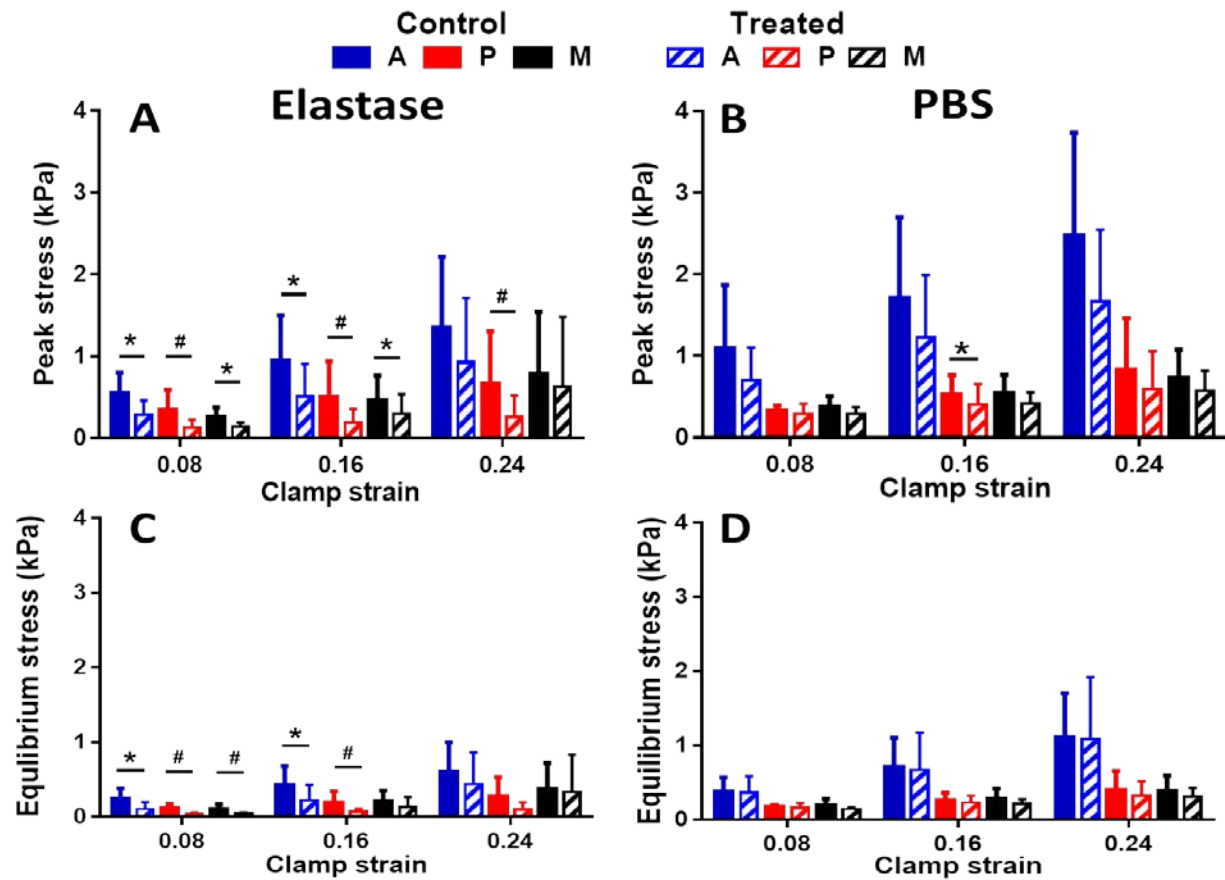


Fig. 4.5 Peak and equilibrium stresses of samples from SST anterior (A), posterior (P), and medial (M) regions for elastase treatment (A&C) and PBS incubation (B&D). Data are shown as mean \pm SD; * for $p < 0.05$; # for $0.05 \leq p \leq 0.1$.

Control and PBS-incubated samples exhibited similar equilibrium stresses for all SST regions (Fig. 4.6A&B). Stresses of elastase-treated samples decreased more than corresponding stresses of PBS-incubated samples (Fig. 4.6C&D). Although not reaching a level of statistical significance, the anterior region had larger values than both posterior and medial regions for both peak and equilibrium stresses.

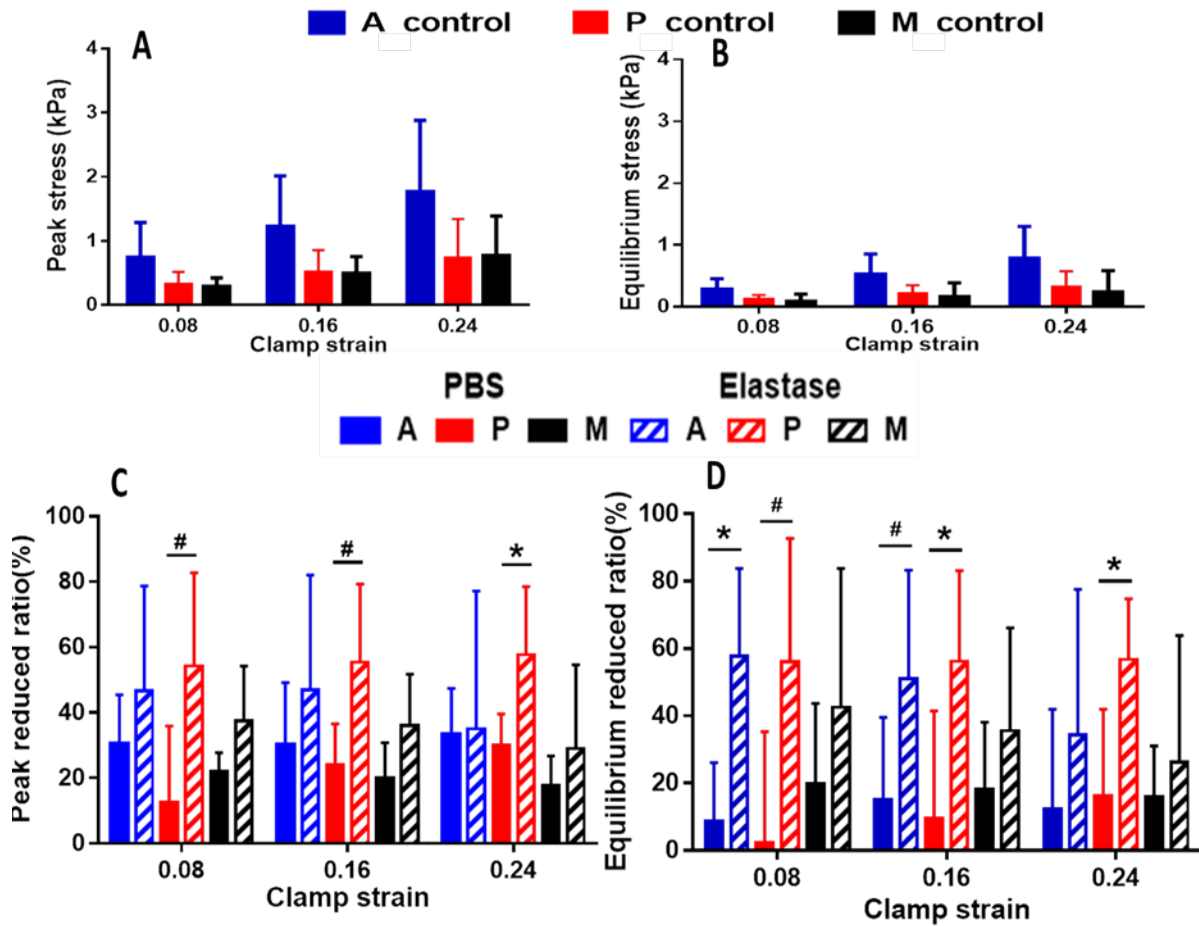


Fig. 4.6 Peak (A) and equilibrium (B) stresses of each region before treatment/incubation by grouping PBS-incubated and elastase-treated samples together. Peak (C) and equilibrium (D) reduced ratio, calculated using the equation above, demonstrated stress decrease more after elastase treatment than PBS incubation.

Average normalized stress-time curves were plotted by averaging normalized stresses of all samples within corresponding groups and illustrate how shear stresses of samples throughout the test protocol changed after enzyme treatment or PBS incubation (Fig. 4.7). Elastase treatment led to larger decreases in stresses than PBS incubation for all SST regions, but with a particularly dramatic effect for samples from the posterior region. All SST regions exhibited obvious stress relaxation, with consistently larger normalized stresses for the medial region compared to the other two regions.

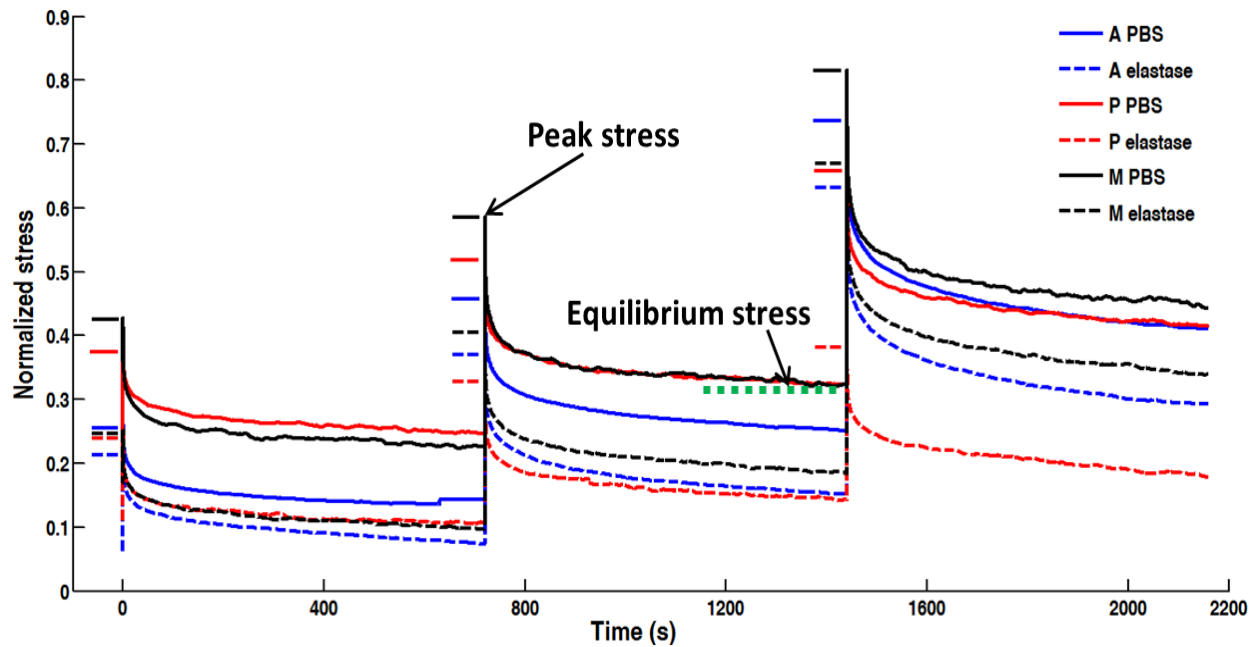


Fig. 4.7 Averaged stress-time curves of elastase-treated and PBS-incubated samples from anterior (A), posterior (P), and medial (M) regions, normalized by corresponding control stresses. The short dash and solid lines show normalized peak stresses for each group.

On the microscale, no consistent qualitative differences in structural appearance of collagen fibers (i.e., crimp pattern, fiber diameter, spacing between fibers) after both elastase treatment and PBS incubation were observed relative to pre-treatment and pre-incubation during the examination of multiphoton images. Different SST samples, and sometimes even different locations inside the same sample, had quite variable structure of collagen fibers (Fig. 4.2). In multiphoton microscopy images, collagen crimping was not obvious in any regions of the SST, in contrast to our previous observations of bovine DDFT [9]. Breaking of photobleached lines and rigid rotation of the entire grid were observed in some samples from all three SST regions (Fig. 4.3). Local matrix strains were highly variable, but were generally smaller than applied clamp strains (Fig. 4.8), demonstrating strain attenuation at smaller length scales. There were no significant differences in local matrix strain values between PBS-incubated or elastase-treated and control samples and no differences observed between the three SST regions. Rotation of the

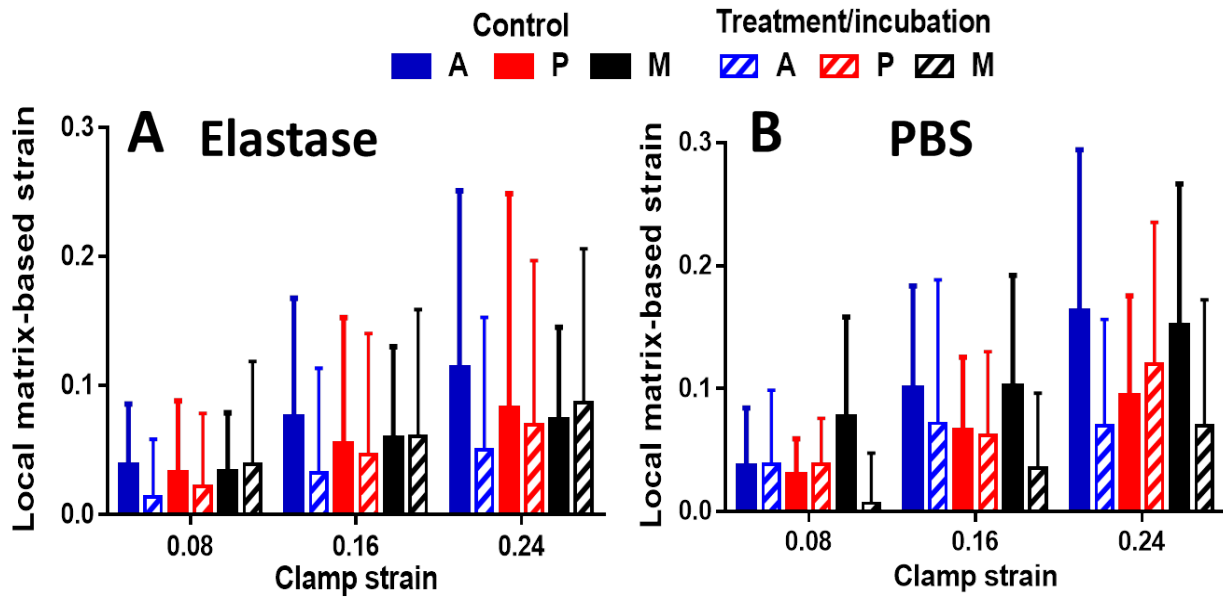


Fig. 4.8 Local matrix-based strain values of samples from SST anterior (A), posterior (P), and medial (M) regions before and after (A) elastase treatment or (B) PBS incubation. Data are shown as mean \pm SD; no statistical differences were found between elastase- and PBS-treated samples.

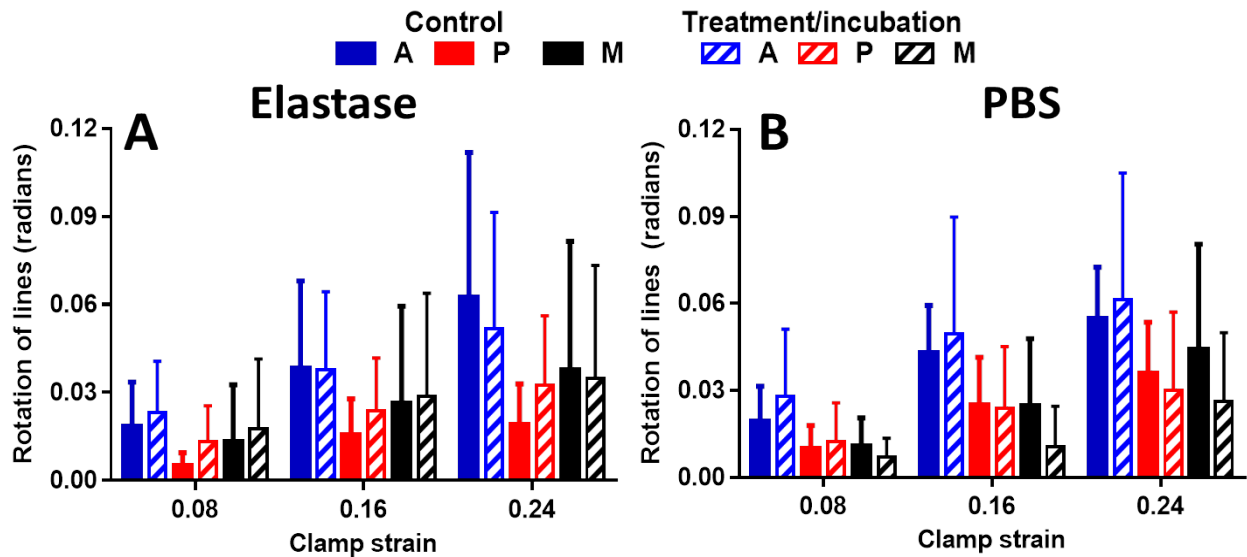


Fig. 4.9 Rotation calculated using deformed photobleached grids of samples from SST anterior (A), posterior (P), and medial (M) regions before and after (A) elastase treatment or (B) PBS incubation. Data are shown as mean \pm SD; no statistical differences were found between elastase- and PBS-treated samples.

photobleached grids increased with the increase of applied strains (Fig. 4.9); average rotation values were generally greater in the anterior region than posterior and medial regions, however no regional differences were statistically significant. No significant difference of rotation was

found between control and elastase treatment, which was also true for PBS incubation. Between-rows and within-row rotations were also calculated to evaluate sliding between collagen fibers and fiber reorganization, respectively. Since it was difficult to determine which nuclei were situated in the same row of collagen fibers in microscopic images with highly disorganized collagen fibers (Fig. 4.3A), only nuclei in images with relatively aligned collagen fibers were considered for computing these two parameters. The cutoff criterion for deciding whether collagen was aligned sufficiently for parameter computation was that collagen fibers could be tracked visually for at least a 100- μm long segment. Between-rows rotation increased slightly with the increase of clamp strain, while in contrast, within-row rotation remained relatively constant at each strain level

(Fig. 4.10). Consistent with previous studies, between-rows rotation was significantly greater than within-row rotation in control samples at low strains (i.e., 0.08, 0.16) ($p < 0.027$). Samples after elastase treatment also exhibited greater between-

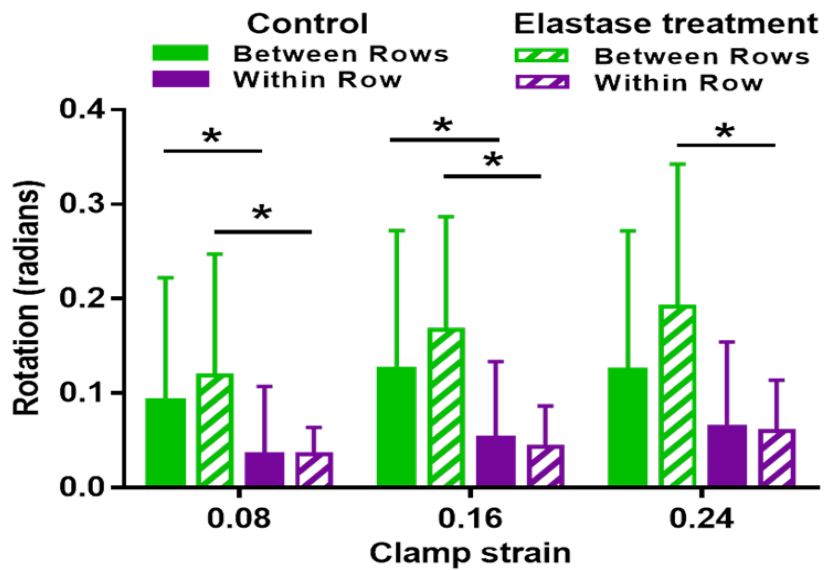


Fig. 4.10 Between-rows rotations (indicative of fiber sliding) and within-row rotations (indicative of fiber uncrimping/reorganization) vs. clamp strain for control and elastase-treated samples. Data are shown as mean \pm SD; * for $p < 0.05$; # for $0.05 \leq p \leq 0.1$.

rows rotation than within-row rotation ($p < 0.003$). Between-rows rotation in control samples showed a trend towards significance from elastase-treated samples at low strains ($p < 0.083$).

SST structure. There were no obvious structural and compositional (i.e., collagen fibers, cellularity, distribution of PGs) differences among SST regions as assessed via H&E, alcian blue, and VVG histological evaluation (Fig. 4.11). However, sub-regions of tissue exhibiting organized, less organized, and totally disorganized collagen fibers were observed in each of the anterior, medial, and posterior regions of the two SSTs examined histologically. There were relatively few cells and limited PG situated within/between organized collagen fibers (Fig. 4.11A&D). Cellularity and PG content increased qualitatively in locations with increasing fiber disorganization (Fig. 4.11B-F). For example, a band of less organized collagen fibers with increased PG content was obvious between organized collagen fibers (Fig. 4.11 B&E). Fluorescent staining with SRB showed elongated elastic fibers located along organized collagen fibers (Fig. 4.12A&B). In the locations of less organized collagen fibers, both long and short elastic fibers were visible (Fig. 4.12B). Only short elastic fibers were observed in regions of greatly disorganized collagen (Fig. 4.12C). Distributions of elastic fibers examined by VVG histology staining showed similar observations to fluorescent SRB images (Fig. 4.12D-F), demonstrating inhomogeneous organization of elastic fibers inside SST. In summary, histological and fluorescent evaluation of SST sections demonstrated a high degree of structural/organizational heterogeneity within all regions of SST.

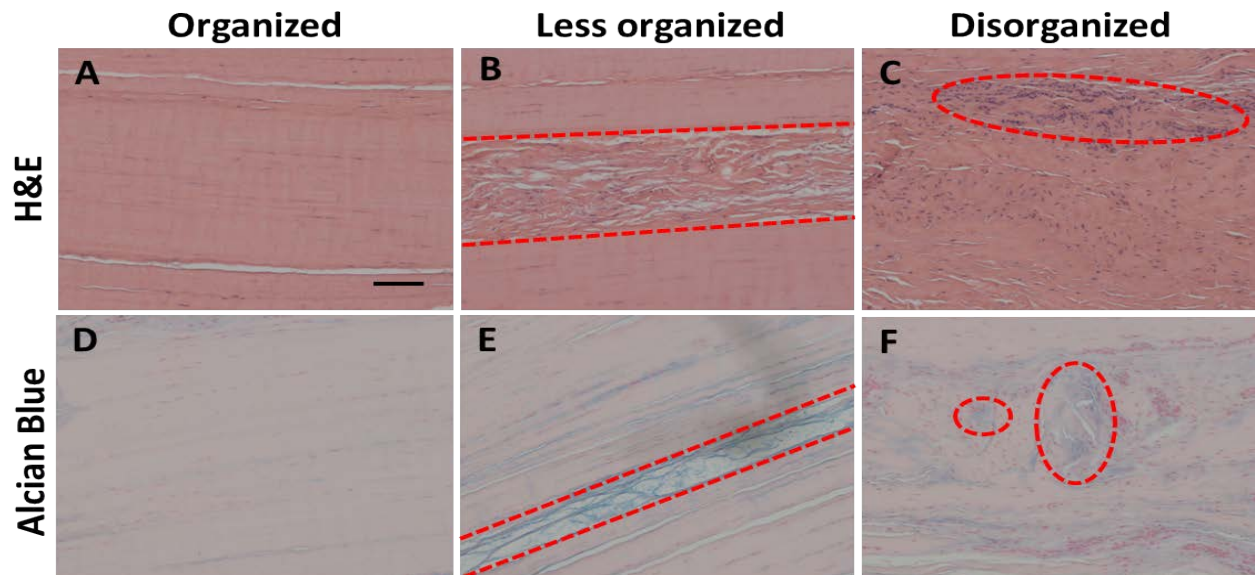


Fig. 4.11 Representative H&E and alcian blue histological sections show different collagen organization even inside the same cadaveric tendon. (A&D) Highly organized collagen fibers and low cellularity were apparent in some microscale locations. (B&E) Less organized collagen fibers (highlighted by red lines) were situated between bundles of organized collagen fibers, with increased proteoglycans between organized fibers. (C&F) Disorganized collagen fibers (highlighted by red circles) were also found with increased cellularity and PGs. Images acquired with 20X objective; scale bar = 100 μ m.

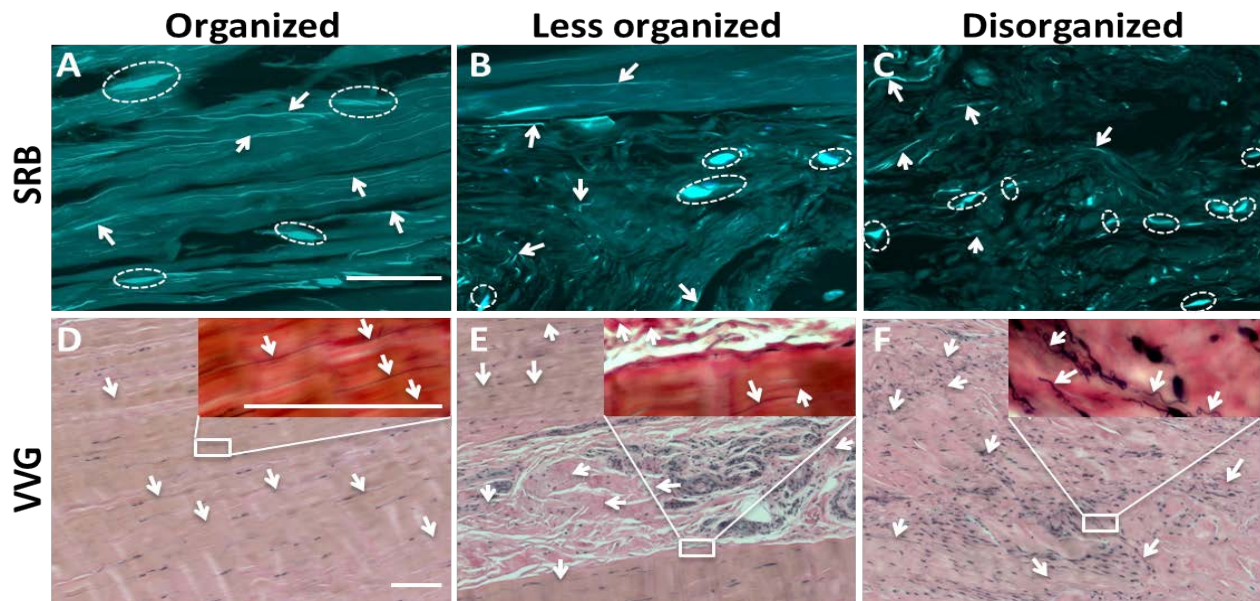


Fig. 4.12 Distribution of elastic fibers shown by fluorescent SRB stain (top row) and histological VVG stain (bottom row). Relatively long elastic fibers (highlighted by white arrows) localized along well-organized collagen fibers (A&D). In locations of somewhat less organized collagen fibers, both short disorganized and long organized elastic fibers were observed (B&E). In locations of several disorganized collagen fibers, elastic fibers were short and disorganized (C&F). To differentiate elastic fibers from nuclei in fluorescent SRB images, nuclei are circled with dotted ellipses. Images acquired with 40 \times objective for SRB and 20 \times and 40 \times objectives for VVG stain; scale bars = 100 μ m.

4.4 Discussion

In this study, multiscale mechanical behavior of SST under shear loading was examined and the contribution of elastin to SST mechanical integrity was evaluated by comparing mechanical parameters of the same samples before and after elastase treatment. SST exhibited decreased shear stresses after elastase enzyme treatment (at 0.08 and 0.16 strains), implying that elastin plays a role in tendon mechanical behavior in shear at low strains. Several evaluated metrics of microscale deformation were similar before and after treatment, and all parameters were similar among the three SST regions. SST shear stresses only showed small increases with increasing strain, similar to a previous report of tendon under incremental stress-relaxation tensile testing [32], which is likely due to the significant relaxation that occurs following each strain step. Overall magnitude of shear stresses in this study were small, similar to the observation that SST tensile mechanical properties are lower than other tendons [3, 26, 28, 32].

Multiphoton microscopy and histology images demonstrated significant tissue heterogeneity in SST samples with variable collagen fiber organization not only inside every SST region, but also in different microscale sub-locations. Heterogeneous micro-structure of cadaveric SST samples (i.e., collagen fiber organization, distribution of cells, PGs, and elastin) likely contributes to similar properties among regions, especially similar deformation among SST three regions. Large strain attenuation of SST from the tissue scale to micron scale was detected and local matrix-based strain did not increase proportionally with the increase of applied strain, which is also true for tendon in tension [7, 32, 33]. The slight increase of microscale strain after each subsequent strain step was due, at least in part, to the partial recovery of collagen fibers after stress relaxation. Rotation of photobleached grid lines in locations with both organized fibers and relatively disorganized fibers demonstrates that fiber reorganization functions as

tendon response to shear loading. Greater values of between-rows rotation than within-row rotation and visualized broken photobleached lines also illustrate that fiber sliding contributes to the response of tendon to shear loading.

Human SST exhibits region-specific mechanical properties (e.g., stresses, fiber realignment) under both longitudinal and transverse tensile loading [3, 28], which contrasts with our results of SST in shear. Similar to other tendons, collagen type I is the primary component that supports tensile loading in SST, and variable fiber collagen alignment and realignment correlates with region-specific SST mechanics under tensile loading [3, 28]. Other extracellular matrix constituents (i.e., collagen type II, PGs, elastic fibers) have been hypothesized to function as linking components between type I collagen, and could be involved in maintaining tendon integrity in shear loading [9, 17, 31]. Elastic fibers shown in our images locate both around visible cells and also between collagen fibers without cells, different from previous work showing that elastic fibers only disperse around nuclei [16]. This discrepancy may be due to differences in staining technique: immunostaining with an antibody that specifically binds to elastin and SRB dye used in our experiment that targets elastic fibers. Other tissue constituents show regional variability in human SST. For example, the posterior and anterior regions have greater biglycan and aggrecan [5, 34]. Compared to the other regions of SST, the insertion is shown to have more collagen type II, whose amount is suggested to be inversely correlated with tensile modulus and collagen alignment [5, 34]. However, the combination of different fiber organization and variable distribution of minor tissue constituents could contribute to the lack of region-specific mechanical properties measured in shear loading in the current study. Specifically, our imaging and histological results demonstrated that some tendon locations show typical tendon-like structure with highly organized collagen fibers with relatively few cells,

while others locations exhibit more fibrocartilage-like structure with disorganized collagen fibers and increased cellularity. Importantly, these variations in properties did not follow consistent region-specific trends. It is possible that such heterogeneity has a larger impact on shear mechanics than results in tensile loading. In addition, although SSTs with obvious tears were excluded, cadaveric human tendons used in this study may have varying degrees of less obvious levels of degeneration and damage. Heterogeneous structural and compositional properties on the microscale resulting from such variability should certainly be considered when examining the results presented in this study.

The results of this study demonstrate a role of elastin in tendon mechanics, which is consistent with previous studies of soft tissues [10-12, 14]. For human lumbar annulus fibrosus under shear and tensile loading, elastin was shown to enhance mechanical properties in the radial orientation perpendicular to collagen fiber organization, based on the observation of decreased modulus and increased extensibility after elastin depletion [14, 15]. Ligament, which has relatively similar structure and composition to tendon, was also shown to have smaller stresses and greater strain after elastin digestion under tensile, transverse tensile, and shear loading [11, 12]. Another study described greater extensibility and loss of elastic behavior in human palmaris longus tendons after elastase treatment [35]. Consistently, our studies showed decreased stress values, however we did not measure greater local matrix-based strain after elastin degradation as in previous studies; differences may be due to various amounts and distribution of elastin and/or limitations in the portion of elastin we were able to degrade in our samples. In our previous study of DDFT [9], two tissue regions with distinct biochemical composition showed significantly different stresses but relatively similar local matrix strains under shear loading, which fits with results in this study for samples before and after elastase treatment. Our results from VVG stain

and fluorescent dye demonstrate that normal SST has non-uniform distribution of elastic fibers inside/among regions. Locations of disorganized collagen fibers have short elastic fibers, similar to elastin fragments inside ligament after elastase treatment shown in a recent study [12]. These short elastic fibers possibly do not contribute as significantly to tendon mechanical behavior as do longer elastin segments parallel to more organized collagen fibers. Additional work is needed to further evaluate these potential interactions/mechanisms.

To evaluate the mechanical contribution of specific extracellular matrix molecules, enzyme treatment has been widely used in combination with biomechanical testing [10-12, 14, 15, 35-39]. For degrading elastin, elastase treatment is relatively convenient to conduct and efficient to degrade elastin under optimum treating environments. Elastase functions through the cleavage of peptide bonds on tropoelastin, instead of desmosine and isodesmosine crosslinks [12, 40]. This potentially hinders the evaluation of elastin's mechanical role in two aspects: (1) intact crosslinks remaining or trapped in digested tissues may bridge collagen fibers or strengthen tissue stiffness such that mechanical properties would not be influenced by elastase treatment; (2) the examination of elastase efficiency on depleting elastin would be inaccurate based on the common biochemical assay that uses desmosine as a marker to quantify elastin content in tissues [15, 21]. Furthermore, the sources (i.e., neutrophil elastase, pancreatic elastase), types (i.e., elastase I, elastase II), and purity of elastase also influence substrate specificity [10, 40]. Some studies have demonstrated that elastase degrades laminin, fibronectin, collagen type IV, and cleaves long GAG chains from PGs [38-41]. In contrast, the same elastase and similar treating protocol used in our study were confirmed by Henninger et al. [11, 12] to have no appreciable effect on degradation of collagen in ligament. Our results suggested that elastase used in this study only caused a 6.2% decrease of average GAG quantities in tendon.

Since relative hydration in connective tissues directly relates to tissue viscoelasticity, the influence of enzyme treatment/incubation on tendon mechanical behavior should also be evaluated from the perspective of tissue swelling. PBS buffer has been most commonly used for elastase treatment during mechanical testing [10-12, 15, 16]. Compared to fresh tissue after harvesting, tissues soaked in PBS have higher water content, causing increased fibril diameter and inter-fibrillar space, but decreased fibril crimping on tendon [10, 41, 42]. These structural changes contribute to decreased tensile modulus and stresses, which makes it difficult to ascertain whether mechanical properties are affected by swelling through incubation or the specific removal of a targeted protein. One strategy to overcome this challenge is to compare tissue mechanical properties after enzyme treatment with samples incubated in PBS for the same time [13, 43]. In biomechanical tests of SST after PBS incubation, our study found decreased shear stress, likely due to tissue swelling, consistent with previous reports [41, 44]. However, elastin-depleted SST exhibited lower shear stress than PBS incubation alone, demonstrating that elastin influences SST mechanical integrity. The other strategy that could be adopted to eliminate swelling is through the use of other buffers such as Dulbecco's modified Eagle medium (DMEM), PBS with 10% sucrose, and Tris buffer with 7.5% polyethylene glycol [10, 41, 42]; in this case, the catalytic activity of enzyme in these buffers should be validated to guarantee efficiency of component removal, and any potential swelling due to buffer treatment alone should be also quantified.

This study is not without limitations. Elastase treatment could possibly have cleaved other crosslinks in addition to those found in elastin; however we used the same elastase formulation that was demonstrated to be quite specific in previous work [11, 12]. In addition, elastin was not completely digested from human SST, due to both the relatively large size of our samples and

limitations of elastase penetration [10, 12]. However, even with partial depletion of elastin, SST exhibited decreased stresses in shear, enabling our evaluation of elastin contribution to tendon biomechanics. The high concentration of 5-DTAF used to stain collagen fibers in tendon could change mechanical properties [32]. Since both control and elastase-treated samples were subjected to the same concentration of 5-DTAF stain, we expect no overall effect when comparing mechanics between groups. Finally, the cadaveric tendons evaluated in this study were relatively old; compositional and structural alternation caused by age- or use-related degeneration could influence multiscale tendon behavior.

4.5 Conclusion

This study demonstrates that even moderate disruption of the elastin protein (via targeted enzymatic treatment) leads to SST altered mechanical properties, thereby suggesting a mechanical role of elastin in tendon mechanics. SSTs do not have regional-specific mechanical properties under shear loading, perhaps due to the heterogeneous structure observed in our tested samples, which may be evidence of a highly complex physiological loading environment. Breakage of photobleached lines, relative displacement of nuclei, and rigid rotation in multiphoton images demonstrate that both sliding and reorganization of collagen fibers are deformation modes on the microscale that respond to shear strain applied on the tissue scale. Evaluation of the role of tissue constituents present in tendon in small quantities (e.g., elastin) complements our understanding of functional properties in healthy conditions and mechanical changes that occur in states of degeneration/damage.

4.6 References

1. Bey, M.J., et al., Intratendinous strain fields of the intact supraspinatus tendon: the effect of glenohumeral joint position and tendon region. *J Orthop Res*, 2002. 20(4): p. 869-874.

2. Ahmadzadeh, H., et al., Determining the contribution of glycosaminoglycans to tendon mechanical properties with a modified shear-lag model. *J Biomech*, 2013. 46(14): p. 2497-2503.
3. Lake, S.P., et al., Tensile properties and fiber alignment of human supraspinatus tendon in the transverse direction demonstrate inhomogeneity, nonlinearity, and regional isotropy. *Journal of biomechanics*, 2010. 43(4): p. 727-732.
4. Marturano, J.E., et al., Characterization of mechanical and biochemical properties of developing embryonic tendon. *Proceedings of the National Academy of Sciences*, 2013. 110(16): p. 6370-6375.
5. Buckley, M.R., et al., Distributions of types I, II and III collagen by region in the human supraspinatus tendon. *Connect Tissue Res*, 2013. 54(6): p. 374-379.
6. Screen, H.R., Bader, D. L., Lee, D. A., Shelton, J. C., Local Strain Measurement within Tendon Strain, 2004. 40(4): p. 157-163.
7. Szczesny, S.E., et al., Quantification of Interfibrillar Shear Stress in Aligned Soft Collagenous Tissues via Notch Tension Testing. *Scientific reports*, 2015. 5.
8. Cheng, V.W., Screen, H. R., The micro-structural strain response of tendon. *Journal of Materials Science*, 2007. 42(21): p. 8957-8965.
9. Fang, F. and S.P. Lake, Multiscale strain analysis of tendon subjected to shear and compression demonstrates strain attenuation, fiber sliding, and reorganization. *Journal of Orthopaedic Research*, 2015. 33(11): p. 1704-1712.
10. Grant, T.M., et al., The Mechanical, Structural, and Compositional Changes of Tendon Exposed to Elastase. *Annals of biomedical engineering*, 2015: p. 1-10.
11. Henninger, H.B., et al., Effect of elastin digestion on the quasi-static tensile response of medial collateral ligament. *Journal of Orthopaedic Research*, 2013. 31(8): p. 1226-1233.
12. Henninger, H.B., et al., Elastin governs the mechanical response of medial collateral ligament under shear and transverse tensile loading. *Acta biomaterialia*, 2015. 25: p. 304-312.
13. Jacobs, N.T., et al., Effect of orientation and targeted extracellular matrix degradation on the shear mechanical properties of the annulus fibrosus. *Journal of the mechanical behavior of biomedical materials*, 2011. 4(8): p. 1611-1619.
14. Michalek, A.J., et al., Measurement of local strains in intervertebral disc anulus fibrosus tissue under dynamic shear: contributions of matrix fiber orientation and elastin content. *Journal of biomechanics*, 2009. 42(14): p. 2279-2285.
15. Smith, L.J., et al., Elastic fibers enhance the mechanical integrity of the human lumbar annulus fibrosus in the radial direction. *Annals of biomedical engineering*, 2008. 36(2): p. 214-223.
16. Thakkar, D., et al., Distribution and expression of type VI collagen and elastic fibers in human rotator cuff tendon tears. *Connective tissue research*, 2014. 55(5-6): p. 397-402.
17. Grant, T.M., et al., Elastic fibres are broadly distributed in tendon and highly localized around tenocytes. *Journal of anatomy*, 2013. 222(6): p. 573-579.

18. Ritty, T.M., K. Ditsios, and B.C. Starcher, Distribution of the elastic fiber and associated proteins in flexor tendon reflects function. *The Anatomical Record*, 2002. 268(4): p. 430-440.
19. Feitosa, V., et al., Variations in the glycosaminoglycan content, swelling properties and morphological aspects of different regions of the superficial digital flexor tendon of pigs. *Cell. Mol. Biol*, 2002. 48: p. 359-367.
20. Fang, F., A.S. Sawhney, and S.P. Lake, Different regions of bovine deep digital flexor tendon exhibit distinct elastic, but not viscous, mechanical properties under both compression and shear loading. *Journal of biomechanics*, 2014. 47(12): p. 2869-2877.
21. Watanabe, T., et al., An enzyme-linked immunosorbent assay (ELISA) for the quantitation of urinary desmosine. *The Tokai journal of experimental and clinical medicine*, 1989. 14(4): p. 347-356.
22. Gunja-Smith, Z., An enzyme-linked immunosorbent assay to quantitate the elastin crosslink desmosine in tissue and urine samples. *Analytical biochemistry*, 1985. 147(1): p. 258-264.
23. Starcher, B., A ninhydrin-based assay to quantitate the total protein content of tissue samples. *Analytical biochemistry*, 2001. 292(1): p. 125-129.
24. Schwartz, E., F.A. Cruickshank, and M. Lebowitz, Determination of desmosines in elastin-related skin disorders by isocratic high-performance liquid chromatography. *Experimental and molecular pathology*, 1990. 52(1): p. 63-68.
25. Osakabe, T., Y. Seyama, and S. Yamashita, Comparison of ELISA and HPLC for the determination of desmosine or isodesmosine in aortic tissue elastin. *J Clin Lab Anal*, 1995. 9(5): p. 293-296.
26. Svensson, R.B., et al., Tensile force transmission in human patellar tendon fascicles is not mediated by glycosaminoglycans. *Connect Tissue Res*, 2011. 52(5): p. 415-421.
27. Zheng, C. and M. Levenston, Fact versus artifact: avoiding erroneous estimates of sulfated glycosaminoglycan content using the dimethylmethylene blue colorimetric assay for tissue-engineered constructs. *European cells & materials*, 2015. 29: p. 224-236.
28. Lake, S.P., et al., Effect of fiber distribution and realignment on the nonlinear and inhomogeneous mechanical properties of human supraspinatus tendon under longitudinal tensile loading. *Journal of orthopaedic research: official publication of the Orthopaedic Research Society*, 2009. 27(12): p. 1596-1602.
29. Ricard, C., et al., In vivo imaging of elastic fibers using sulforhodamine B. *Journal of biomedical optics*, 2007. 12(6): p. 064017-064017-8.
30. He, B., et al., Microstructural analysis of collagen and elastin fibres in the kangaroo articular cartilage reveals a structural divergence depending on its local mechanical environment. *Osteoarthritis and Cartilage*, 2013. 21(1): p. 237-245.
31. Fang, F. and S.P. Lake, Modelling approaches for evaluating multiscale tendon mechanics. *Interface Focus*, 2016. 6(1): p. 20150044.

32. Szczesny, S.E., R.S. Edelman, and D.M. Elliott, DTAF dye concentrations commonly used to measure microscale deformations in biological tissues alter tissue mechanics. *PLoS One*, 2014. 9(6): p. e99588.
33. Han, W.M., et al., Macro- to microscale strain transfer in fibrous tissues is heterogeneous and tissue-specific. *Biophys J*, 2013. 105(3): p. 807-817.
34. Matuszewski, P.E., et al., Regional variation in human supraspinatus tendon proteoglycans: decorin, biglycan, and aggrecan. *Connect Tissue Res*, 2012. 53(5): p. 343-348.
35. Millesi, H., et al., Biomechanical properties of normal tendons, normal palmar aponeuroses, and tissues from patients with Dupuytren's disease subjected to elastase and chondroitinase treatment. *Clinical Biomechanics*, 1995. 10(1): p. 29-35.
36. Carta, L., et al., Discrete contributions of elastic fiber components to arterial development and mechanical compliance. *Arteriosclerosis, thrombosis, and vascular biology*, 2009. 29(12): p. 2083-2089.
37. Le, V.P., et al., Fibulin-5 null mice with decreased arterial compliance maintain normal systolic left ventricular function, but not diastolic function during maturation. *Physiological reports*, 2014. 2(3): p. e00257.
38. Wagenseil, J.E., et al., Effects of elastin haploinsufficiency on the mechanical behavior of mouse arteries. *American Journal of Physiology-Heart and Circulatory Physiology*, 2005. 289(3): p. H1209-H1217.
39. Hirano, E., et al., Functional Rescue of Elastin Insufficiency in Mice by the Human Elastin Gene Implications for Mouse Models of Human Disease. *Circulation research*, 2007. 101(5): p. 523-531.
40. Vered, M., Y. Burstein, and A. Gertler, Digestion of elastin by porcine pancreatic elastase I and elastase II. *International journal of peptide and protein research*, 1985. 25(1): p. 76-84.
41. Chimich, D., et al., Water content alters viscoelastic behaviour of the normal adolescent rabbit medial collateral ligament. *Journal of biomechanics*, 1992. 25(8): p. 831-837.
42. Lujan, T.J., et al., Contribution of glycosaminoglycans to viscoelastic tensile behavior of human ligament. *Journal of Applied Physiology*, 2009. 106(2): p. 423-431.
43. Fessel, G. and J.G. Snedeker, Evidence against proteoglycan mediated collagen fibril load transmission and dynamic viscoelasticity in tendon. *Matrix Biology*, 2009. 28(8): p. 503-510.
44. Screen, H.R., et al., The influence of swelling and matrix degradation on the microstructural integrity of tendon. *Acta biomaterialia*, 2006. 2(5): p. 505-513.

Chapter 5: Multiscale Mechanical Evaluation of Human Supraspinatus Tendon in Shear after Glycosaminoglycan Reduction⁴

5.1 Introduction

Injury, disease and age-related degeneration of tendon often lead to deteriorated mechanical properties and loss of function [1]. To address the origins of altered mechanical behavior, the structural and compositional properties of tendons in healthy or diseased states have been characterized to elucidate how these factors contribute to mechanical function [2, 3]. In addition, treatment strategies for tendon injuries seek to promote the formation of normal structural and compositional properties in order to restore a suitable environment to promote cell-mediated tissue remodeling and sustain *in vivo* mechanical loading. Therefore, tendon structure and function not only dictate mechanical properties, but also are key indicators to help evaluate treatment efficiency.

Previous literature has established that tendon is mainly composed of collagen type I, with minor amounts of other extracellular matrix (ECM) components, including other types of collagen, glycoproteins, elastin, and proteoglycans (PGs) [3]. Although collagen type I is the principal tendon component that supports mechanical loading, other constituents, especially elastin and PGs, have been suggested to contribute to tendon mechanics [4, 5]. PGs, consisting of a core protein with attached glycosaminoglycan (GAG) sidechains, are observed in the

⁴ Reprinted from Fang, F., and Lake, SP., 2017, "Multiscale mechanical evaluation of human supraspinatus tendon under shear loading after glycosaminoglycan reduction." *J Biomech Eng.* 139(7): 071013.

interfascicular matrix of tendons and in specific regions of some tendons (i.e., flexor tendon, supraspinatus tendon) that experience multiaxial loading [6, 7]. Besides being present in healthy tendon, increased GAGs have been shown to collocate with disorganized collagen fibers, and expression of PGs (e.g., aggrecan and biglycan) are prominently upregulated in injured tendons [8, 9]. Therefore, evaluation of PG/GAG quantity and distribution have been regarded as an essential task to address tendon structure-function relationships [10, 11].

Knockout animal models and degradation via enzyme treatment have been adopted as two common approaches to examine the role of PGs and GAG side chains in tendon function from both biochemical and mechanical perspectives [9, 12-17]. Using such techniques, small leucine-rich PGs (i.e., decorin, biglycan) have been shown to modulate the functional activity of growth factors and cell surface receptors, and provide regulatory effects (e.g., collagen fibrillogenesis) in tendon that often have mechanical implications [15, 16, 18]. Another study suggested that decorin and biglycan bind calcium ions and promote mineralization of tendon collagen fibrils [19]. Regarding direct mechanical contributions, PGs undoubtedly help sustain compressive loading in tendon (e.g., through water bound to the GAG sidechains of the large PG aggrecan) [20, 21], similar to their demonstrated role in cartilage [22-25]. However, tensile testing of enzymatically-treated tendon/ligament showed that GAG degradation did not alter mechanical parameters, suggesting that GAGs do not contribute directly to tensile mechanics of tendon/ligament [26-28]. These results contradict a previously proposed theoretical mechanism wherein PG core proteins bind to collagen fibrils and GAGs crosslink fibrils to increase tensile strength of connective tissues [29], as well as previous results showing that GAGs contribute to the mechanics of other soft tissues such as arterial wall and sclera [30, 31].

Determining whether GAGs play a role in tendon mechanical properties under other non-

tensile loading conditions (i.e., shear, torsion) represents an important additional approach to fully consider their potential contribution to tendon function. One previous study of human medial collateral ligament showed unaltered shear stresses before and after GAG digestion via chondroitinase B treatment [28]. Still, it remains unclear whether GAGs play a mechanical role at both macro- and micro-scales in tendons that experience significant non-tensile loading during normal physiological function. Human supraspinatus tendon (SST), the most commonly injured tendon of the rotator cuff in the shoulder [32], is subjected to complex multiaxial loading (i.e., tension, shear, compression) *in vivo*, including intratendinous shear strain through the tendon thickness during glenohumeral abduction [33]. The complex mechanical nature of the physiological SST environment likely contributes to the unique region-specific tensile mechanical properties, collagen organization, and PG distribution of this tissue [33-35]. While Chapter 4 showed that elastin depletion altered shear mechanics of SST [9], it is unknown if PGs and corresponding GAG sidechains also facilitate the mechanical response of SST to shear loading. Moreover, even with only moderate/minor changes in macroscale shear mechanics following GAG depletion, microscale deformations of treated tendons could potentially exhibit differences due to disrupted microstructural integrity of collagenous matrix and adjacent GAGs. Therefore, using a multiscale experimental approach to simultaneously evaluate macroscale mechanical properties and microscale deformation of SSTs with intact or digested GAGs can help address mechanisms governing the behavior/role of GAGs in the shear behavior of tendons which experience significant non-tensile physiologic loads.

The goal of this study was to quantify multiscale mechanical behavior of human SST before and after removing GAGs to understand how GAGs contribute to this shear response of this complex and unique tendon. Biomechanical shear tests through the tendon thickness were

performed on samples from specific regions of human SST with microscale deformation modes simultaneously recorded via two-photon microscopy. Based on the previous proposition that GAGs might bridge adjacent collagen fibrils and consequently help stress transfer to the higher-scale fibers, and that SSTs are suggested to have greater amounts of GAG content compared to other connective tissues, we hypothesized that GAG depletion in SST would lead to inferior mechanical properties on the macro- and micro-scales, including decreased peak/equilibrium stresses and increased local-matrix based measures of deformation (i.e., strain and rotation).

5.2 Materials and methods

Chondroitinase ABC treatment protocol. A series of concentration- and time-dependent tests were conducted to determine an appropriate treatment protocol using chondroitinase ABC (ChABC), which can degrade GAG chains from tendon. The medial region of a single SST was used to obtain small tissue specimens (n=15) with approximate dimensions of 1×0.5×0.5mm and weights of 40-50 mg. To optimize enzyme concentration, specimens were randomly assigned to be incubated in 30 ml pH=8 buffer containing 50 mM Tris, 60mM sodium acetate, 0.02% bovine serum albumin with 0 (control), 0.1, 0.2, 0.3, and 0.4 units/ml ChABC (n=3 for each concentration, C2905, Sigma-Aldrich, St. Louis) for 6 hours at room temperature [9]. To optimize enzyme incubation time, similar specimens (n=15) were harvested and incubated in 30 ml buffer with 0.2 units/ml ChABC for 0 (control), 1, 3, 8, 16 hours at room temperature. After ChABC treatment, a dimethylmethylene blue colorimetric assay was used to quantify GAG content, reflecting PG amount, in all specimens [12, 13, 29]. After tissue digestion via papain (papain from papaya latex, P4762, Sigma-Aldrich), 1-9-dimethylmethylene blue (DMMB, 341088, Sigma-Aldrich) was added to the tissue solution in standard 96-well plates. Intensity of 595 nm wavelength light was quantified for each sample by spectrometry and compared to

standard curve data to determine GAG content, which was normalized by sample wet weight [36].

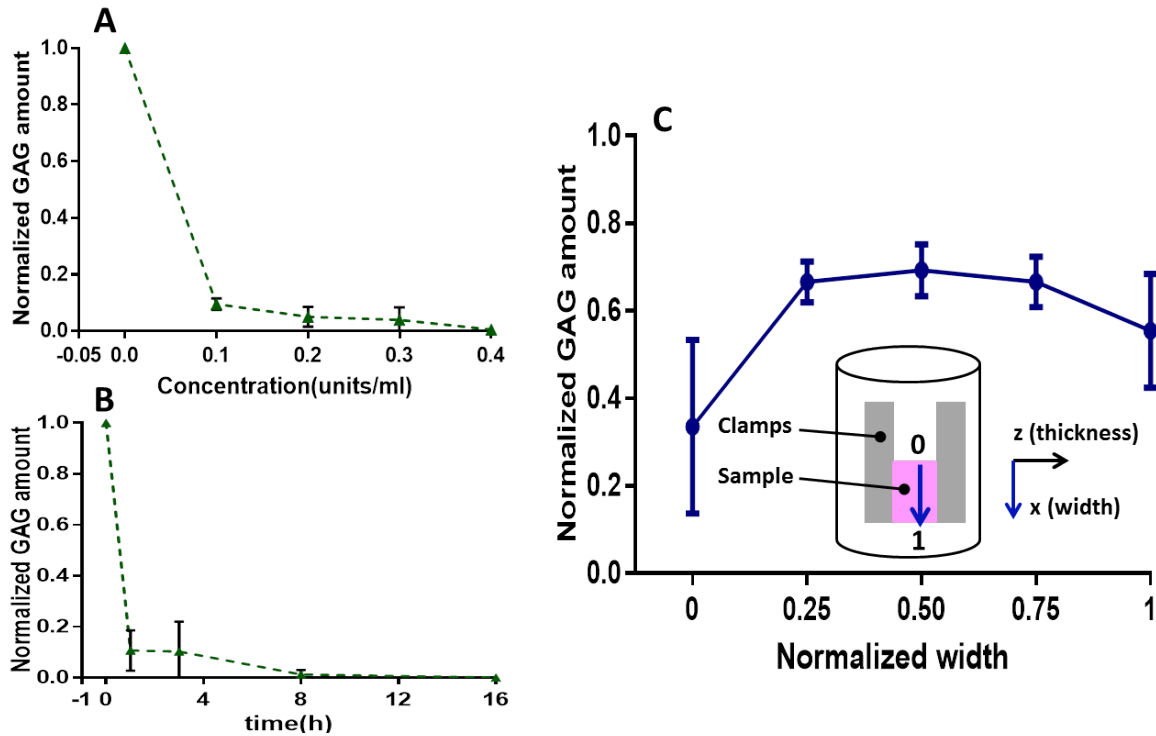


Fig. 5.1 Normalized GAG amounts in SST samples treated for 6 hours with different concentrations of ChABC buffer (A) or with 0.2 units/ml ChABC buffer for different durations of incubation (B). (C) GAG amount within DDFT after ChABC treatment exhibited a gradient distribution along the sample width; inset displays how clamps (gray blocks) and attached sample (pink block) are secured for incubation and the subsequent mechanical test, where the normalized width is shown as 0 (top) to 1 (bottom) and is indicated as the x axis in the plot.

Since the attachment of relatively large mechanical test samples to shear clamps partially blocks enzymatic solution from contacting sample surfaces during incubation, the penetration of ChABC into full-size clamped samples was also evaluated. Human SST exhibits heterogeneous collagen organization and GAG distribution, making it challenging to evaluate penetration of enzymatic degradation [5]. Our preliminary data found that bovine deep digital flexor tendon (DDFT) had a constant distribution of GAGs ($0.21 \pm 0.02\%$ normalized by wet weight) in the proximal region, consistent with previous studies [7, 37]. Therefore, the proximal region of

DDFT was used as a representative model for this quantification. Two adjacent and paired samples (n=4) with the same size as mechanically tested samples were harvested from the proximal region of four bovine DDFTs, as done previously [6, 7, 38]. Samples were glued to shear test clamps; one clamps-sample assembly was incubated in PBS for 8 hours as the control, and the other incubated in 0.2 units/ml ChABC buffer for 8 hours. After incubation, thin pieces of specimens weighing 40-50 mg were carefully collected at five locations evenly spaced along the treating buffer depth from treated/incubated samples for biochemical analysis. The normalized sample width (marked by the blue arrow, Fig. 5.1C) was taken as 1 and the sample surface was defined as 0. Normalized GAG content was computed as the ratio of GAGs in treated samples relative to corresponding controls along the sample width.

Biomechanical tests. Using results from our previous multiscale studies of bovine flexor tendon [6, 7], a power analysis (power=0.8; $\alpha=0.05$) determined that a sample size of n=7 would be sufficient to find differences in stress and microscale strain values of at least 4kPa and 4%, respectively, before and after enzyme depletion. Seven cadaveric shoulder specimens (mean age: 61.3 ± 14.6 years) with no evidence of tendon damage were dissected to harvest SSTs. As described in previous studies [9, 34, 35], full-thickness samples were obtained from anterior, posterior, and medial regions of SST for biomechanical tests, and an adjacent specimen was harvested from each sample as control tissue for biochemical or histological analysis. After the surfaces of mechanically tested samples were leveled on a freezing-stage microtome, cross-sectional area and thickness were measured by a non-contact laser scanning system (Keyence, Elmwood Park, NJ) [9].

Samples, stained with 5-DTAF and DAPI to visualize collagen and nuclei as done previously [6, 9], were mounted in a biomechanical test device combined with a Zeiss two-photon confocal

microscope [6, 9]. The test system, applied shear loading protocol, and image acquisition settings/timings were adopted from Chapter 3 and 4 [9], which compared the mechanical response of human SST in shear after elastase treatment. Accordingly, after preloading samples, photobleached grids were created with four adjacent $100 \times 100 \mu\text{m}$ squares at a depth of $50 \mu\text{m}$ at each of the three locations evenly spaced along the sample thickness (Fig. 5.2). Step-increases of 0.08, 0.16, and 0.24 shear strains with 12-minute relaxation periods between each strain value

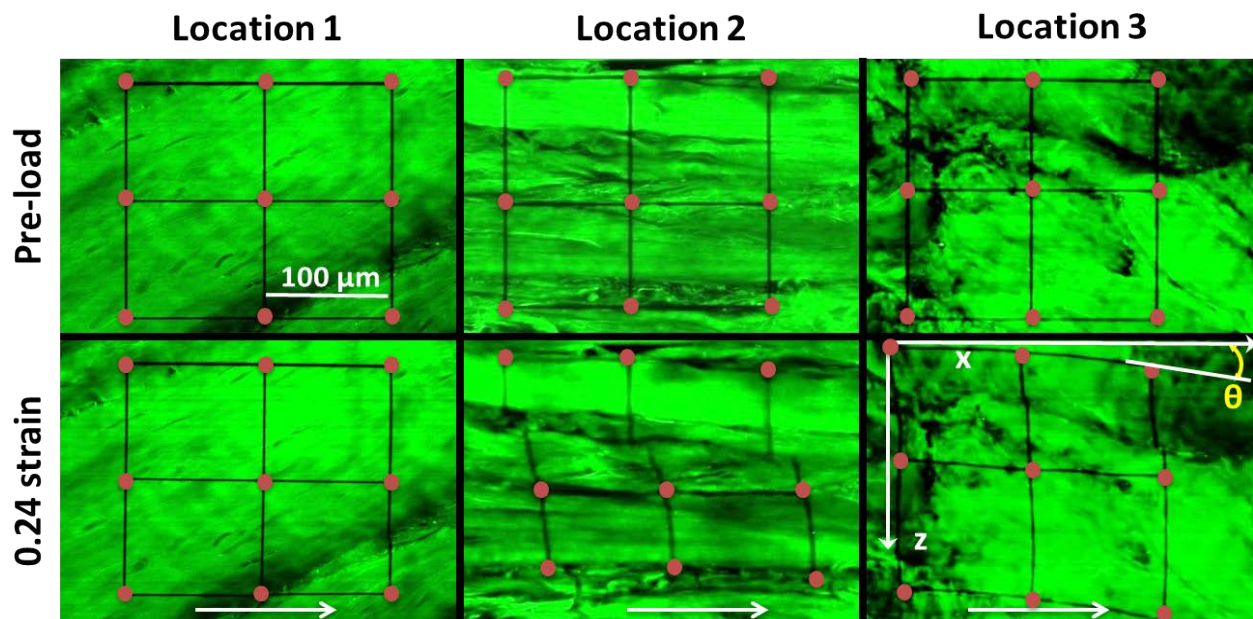


Fig. 5.2 Microscopy images from three locations of the same sample before and after application of 0.24 shear strain. Different locations within one sample from a single SST region showed heterogeneous organization of collagen fibers and different modes of deformation: no obvious deformation at Location 1; fiber sliding at Location 2; fiber reorganization at Location 3. Rotation angle, θ , was calculated as the angle between the horizontal axis of images and deformed photobleached grids. Grid intersection points (red dots added for visualization purpose only) were used to calculate local matrix-based strain, while white arrows show shear loading direction.

were incrementally applied. Multi-channel z-stacks of photobleached squares were collected after preload and eight minutes after each incrementally applied strain [6, 9]. Following the test protocol, samples were kept attached to clamps and clamp-sample assemblies were treated with the previously optimized enzyme protocol (see results section), namely 0.2 units/ml ChABC

buffer for 8 hours. Following ChABC treatment, photobleached squares were recreated again on the same three sample locations (or on nearby locations if the previous photobleached grids were not sharp) for image analysis. The shear loading protocol and image acquisition were then performed again for all treated samples. Control data from our prior study [9], namely shear test data of SST samples before and after PBS incubation (without enzyme treatment), were employed here to compare the effects of PBS incubation and GAG depletion on SST mechanical properties.

Evaluation of treatment efficiency. After the completion of biomechanical tests, ten samples and corresponding controls were randomly selected for DMMB assay. Three tissue segments weighing 40-50 mg were collected from each sample evenly along sample width to quantify GAG content, as discussed in section 5.1. The efficiency of ChABC treatment was also evaluated using histological analysis of mechanically tested samples and paired controls from three regions of each of two SSTs (i.e., anterior, posterior, medial). Samples were fixed in 4% paraformaldehyde for 24 hours, dehydrated in 70% ethanol, and embedded in paraffin. Paraffin sections (5- μ m thickness) were obtained from both the top surface and middle portion of mechanically tested samples. From location-matched control samples, histological sections were taken from the paired/mirrored surface that was opposite to the analyzed/imaged surface of mechanically tested samples. Sections were stained with hematoxylin and eosin (H&E) or Alcian blue and imaged via bright field microscopy with 10 \times and 40 \times objectives. Typical images representative of collagen organization and GAG distribution were selected for presentation.

Data analysis. For biochemical data, GAG amounts from tendon specimens/samples after ChABC treatment were normalized by GAG content of corresponding (non-incubated) controls.

Peak (σ_p) and equilibrium (σ_e) stresses were calculated as force values immediately after each strain step and each 12-minute stress-relaxation period, respectively, divided by cross-sectional areas. Normalized stresses were computed by dividing stresses from the second shear tests of ChABC treated samples by the peak stress value (at 0.24 strain) from the first shear test (i.e., before incubation) of the same sample. The relaxation percent, peak reduced ratio, and equilibrium reduced ratio were evaluated as follows:

$$\text{Relaxation percent (\%)} = 100 \frac{\sigma_p - \sigma_e}{\sigma_p} \quad (5.1)$$

$$\text{Peak reduced ratio (\%)} = 100 \frac{\sigma_{p2} - \sigma_{p1}}{\sigma_{p1}} \quad (5.2)$$

$$\text{Equilibrium reduced ratio (\%)} = 100 \frac{\sigma_{e2} - \sigma_{e1}}{\sigma_{e1}} \quad (5.3)$$

Where σ_{p2} and σ_{p1} are peak stresses for the first and second shear tests, and σ_{e2} and σ_{e1} are equilibrium stresses for the first and second shear tests.

As shown in our previous studies [6, 9], local-matrix based strains were calculated as 2D Lagrangian strains by tracking photobleached squares visualized in microscopic images. Rotations, which characterize rigid body motion of photobleached squares, were defined as the average angle between the image x-axis and deformed horizontal photobleached grids (Fig. 2). Prism software (GraphPad Software, Inc. CA, USA) was used to perform statistical analysis. Differences in output parameters by SST regions (anterior, posterior, and medial) were evaluated by one-way ANOVAs and post-hoc comparisons with Bonferroni corrections. Mechanical differences (i.e., peak stress, equilibrium stress, relaxation percent) before and after ChABC treatment were determined by paired *t*-tests. To evaluate local matrix-based strains and rotations,

unpaired *t*-tests were used; a few issues in acquiring image stacks for the same samples before and after treatment precluded paired analysis. Unpaired *t*-tests were also used to compare mechanical parameters (peak reduced ratio, equilibrium reduced ratio) for PBS- and ChABC-incubated samples. All data are shown as mean \pm standard deviation (SD) and statistical significance was set at $p < 0.05$.

5.3 Results

Quantification of treatment efficiency. Untreated human SSTs had $0.282 \pm 0.0383\%$ GAGs (% of wet weight) and no significant differences of GAG content were found by SST region (anterior, posterior, and medial). For the small tissue specimens, all enzyme treatment protocols decreased GAG quantities dramatically (Fig. 5.1A&B). In terms of increasing enzyme concentration, GAG content appeared to plateau (at $\sim 5\%$ remaining) by 0.2 units/ml ChABC buffer (Fig. 5.1A). In terms of increasing incubation duration, no change in GAG quantity was apparent after 8 hours of incubation. Based on these results, 0.2 units/ml ChABC buffer for 8 hours was adopted as the treatment protocol. In the relatively large bovine DDFT samples, a gradient distribution of remaining GAGs was found after ChABC treatment, with $33.5 \pm 17.2\%$ left at the top of samples and $\sim 65\%$ remaining in the middle of samples (Fig. 5.1C). The contact between the container and sample surface possibly contributed to the increase of remaining GAGs to $55.4 \pm 11.3\%$ adjacent to the sample bottom. For the biomechanically tested SSTs, samples contained $48.0 \pm 10.5\%$ GAGs after ChABC treatment compared to the corresponding controls without enzyme treatment.

Based on qualitative histological assessment, collagen density, collagen organization, and crimp of collagen fibers remained unchanged on the top and middle of samples after treatment, as evidenced by H&E-stained sections (Fig. 5.3A-C). In contrast, sections from both the top and

middle of treated samples showed less GAGs than corresponding sections of controls, as shown by Alcian blue stain (Fig. 5.3D&E). Consistent with biochemical results demonstrating a gradient in GAG distribution, histological analysis showed that more GAGs were retained in the middle of treated samples (i.e., darker blue stain) than the top (Fig. 5.3E&F). Interestingly, GAG-rich pericellular matrix was observed around some fibroblasts in SST controls (Fig. 5.3G). ChABC treatment appeared to digest most pericellular GAGs from sections of the top and middle of samples following enzyme incubation (Fig. 5.3H&I).

SST mechanics after GAG depletion. For all samples before ChABC treatment, there were no statistically significant differences detected by tendon region (i.e., anterior, posterior, medial) for peak and equilibrium stresses (Fig. 5.4A&B). All regions showed increased stresses at larger strain steps, while large differences between magnitudes of peak and equilibrium stresses clearly demonstrated that significant stress relaxation occurred. For evaluating the mechanical effect of enzyme treatment, normalized stress-relaxation curves were calculated to reduce the effect of mechanical variation of samples from different donors. ChABC treatment of samples from all three regions led to larger reductions of normalized stresses for the whole loading period compared to PBS-incubated samples (Fig. 5.5), demonstrating some evidence of a mechanical effect due to enzymatic GAG degradation. As no statistically significant differences in peak/equilibrium stresses or time-dependent relaxation were observed by SST region (anterior, posterior, medial), all regions were grouped together for further analysis to examine the influence of GAG depletion on tendon mechanics.

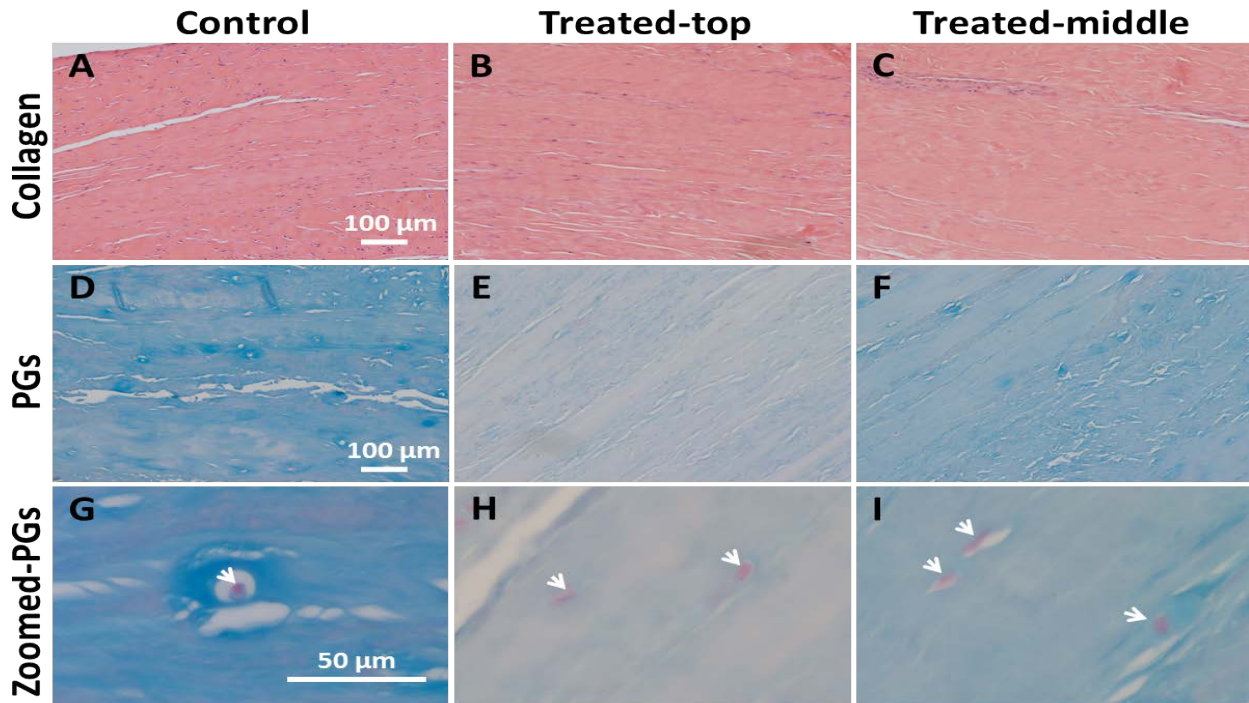


Fig. 5.3 Typical histological images of paired control and treated SST samples, which were stained by H&E and Alcian blue to show collagenous extracellular matrix (pink, A-C) and GAGs (blue, D-I), respectively. After ChABC treatment, the ECM was not visibly disrupted. GAG amount decreased differentially by location within each sample (demonstrated by varying intensity of staining in E and F compared to D), and GAG-rich pericellular matrix was observed to have been particularly degraded. Images A-F were acquired by 10× objective and images G-I by 40× objective. Treated-top and treated-middle are sections from the top and middle of treated samples, respectively. Arrows in images G-I denote cell nuclei.

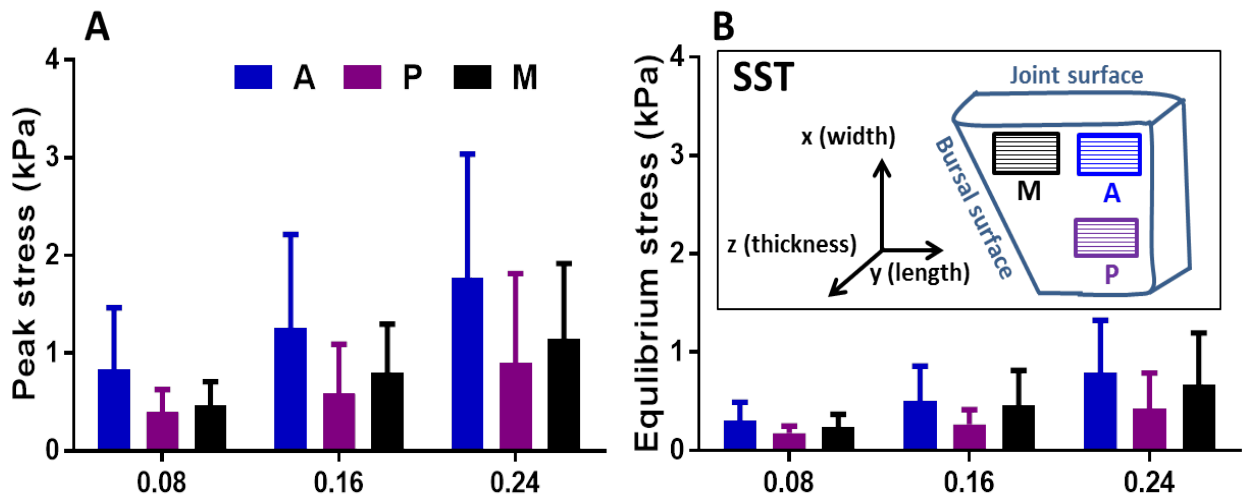


Fig. 5.4 Peak (A) and equilibrium (B) stresses for control (untreated) samples increased at larger strain steps, but were not significantly different across three SST regions; inset shows three regions (M = medial; A = anterior; P = posterior) in SSTs.

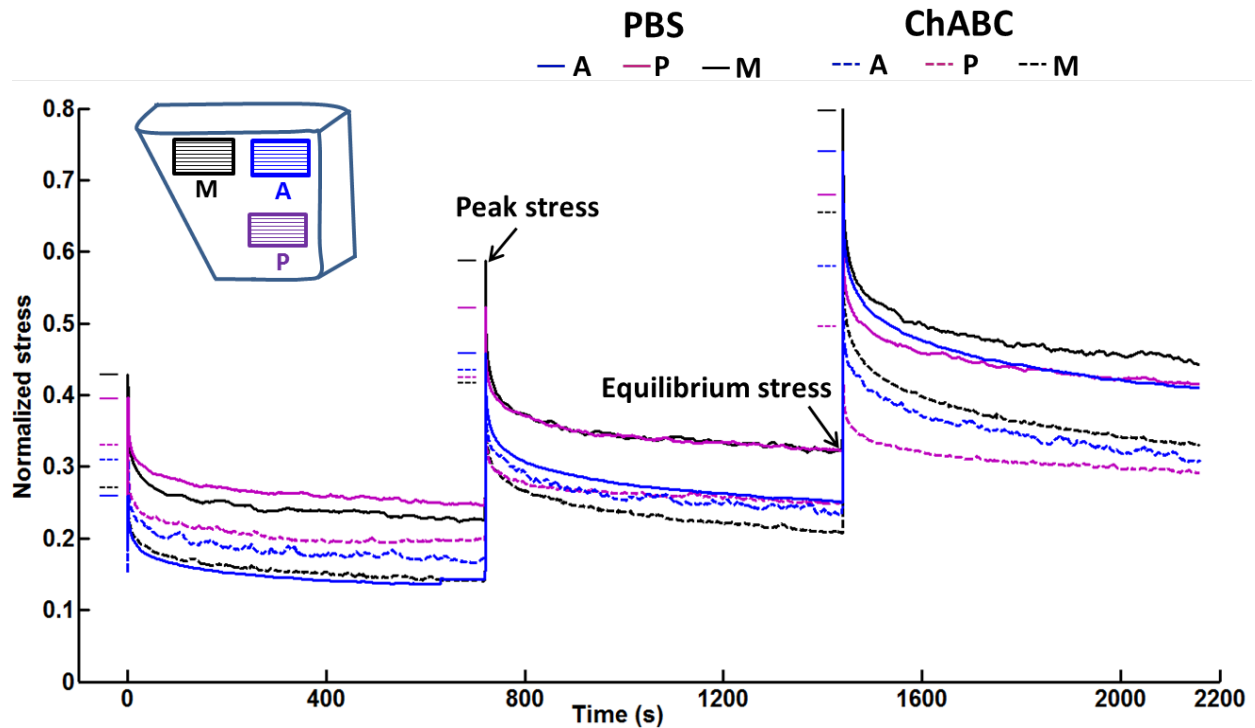


Fig. 5.5 Averaged stress–time curves of SST samples from anterior (A), posterior (P), and medial (M) regions after PBS incubation and ChABC treatment, normalized by corresponding peak stresses from the 0.24 strain step of mechanical test conducted before incubation or treatment. Samples subjected to ChABC treatment showed larger decreases in stress than samples following PBS incubation. Short solid and dashed lines show normalized peak stresses for each group.

No significant differences were found for peak and equilibrium stress values computed for samples before and after ChABC treatment (Fig. 5.6A&B). Relaxation percent was also similar between samples before and after treatment, and decreased slightly at increasing strain steps (Fig. 5.6C). Peak and equilibrium reduced ratios were larger for samples treated by ChABC buffer than for control samples incubated in PBS, suggesting some mechanical effect of GAG degradation to tendon mechanics (i.e., larger reductions in stresses); however these differences did not reach the level of statistical significance (Fig. 5.7). There was no apparent effect of strain-level on peak or equilibrium reduced ratios for PBS-incubated or ChABC-treated samples. For microscale deformation, enzyme treatment did not alter local matrix-based strain and rotation values (i.e., no differences when comparing samples before or after treatment); as expected, all samples exhibited increased local matrix-based strain and rotation at greater strain

levels (Fig. 5.8).

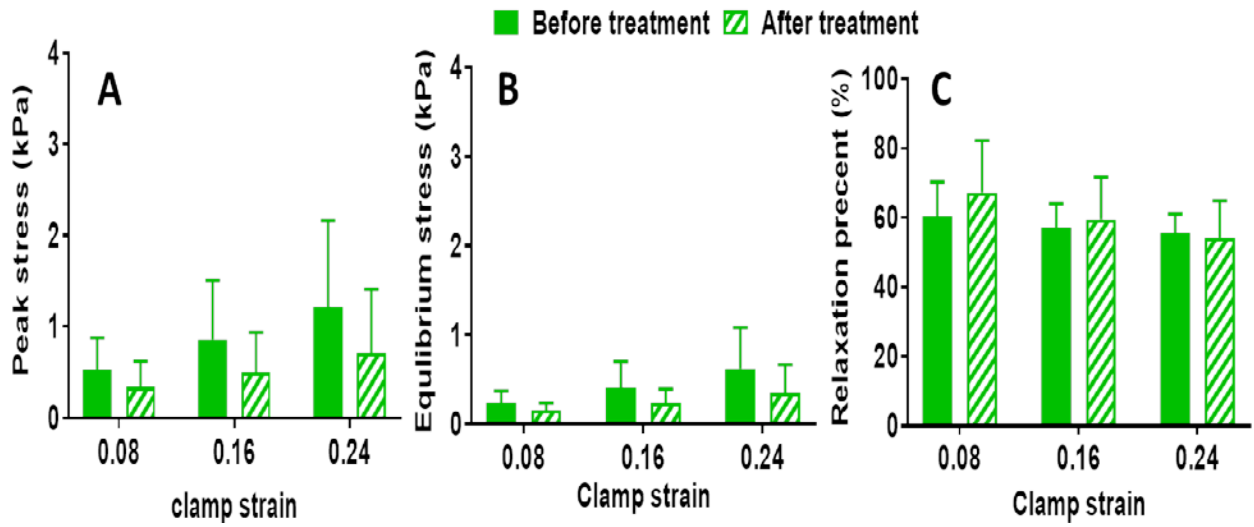


Fig. 5.6 Group peak stresses (A), equilibrium stresses (B), and stress relaxation percent (C) showed moderate changes at increasing strain steps, but were similar before and after ChABC treatment.

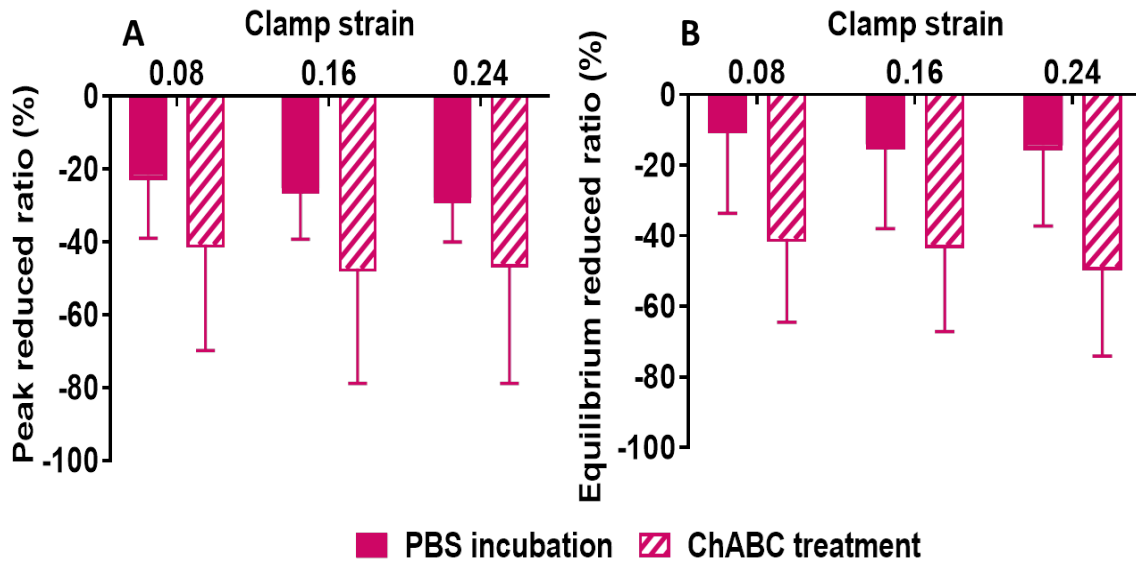


Fig. 5.7 Larger absolute values of peak (A) and equilibrium (B) reduced ratios after ChABC treatment compared to values following PBS incubation indicate that stresses decreased more after ChABC treatment.

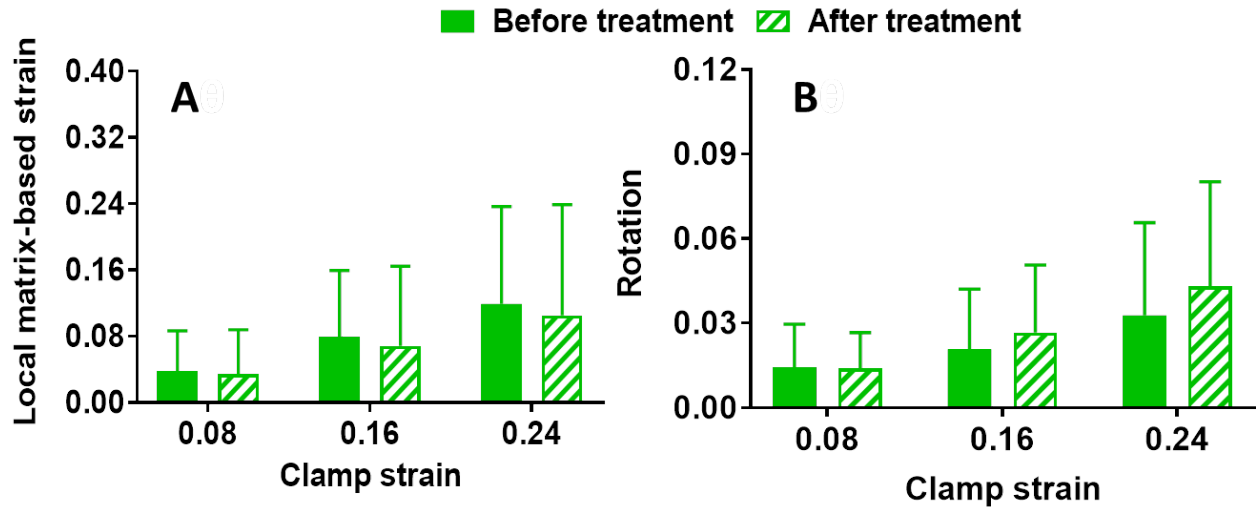


Fig. 5.8 Samples before and after ChABC treatment exhibit similar measures of microscale deformation, namely local matrix-based strain (A) and rotation (B).

5.4 Discussion

In this study, enzymatic treatment using ChABC successfully depleted a large portion of GAGs, indicative of efficient PG degradation, from human SST prepared for shear testing. Although some of the measured values (e.g., peak/equilibrium stresses, reduced stress ratios) were decreased for enzyme-treated samples, there were no statistically significant differences between control and treated samples for any of the mechanical test results or measures of microscale deformation. These results agree with previous reports that GAG depletion from human ligament did not change peak and equilibrium stresses at 0.25 compressive strain and tensile stresses at 0.4 or 0.6 strain [39]. Rat tail tendons in tension also exhibited similar elastic modulus, failure stress, and failure strain before and after GAG depletion [40]. Given (1) the considerable heterogeneity within individual SSTs including particularly heterogeneous collagen organization and modes of deformation observed at different locations of a single SST region (Fig. 5.2), (2) the inherent variability across tendons from different donors including a particularly noticeable variation of GAG amount among different SSTs, and (3) the inability to

fully degrade all GAGs through enzyme treatment, it is possible that some statistically significant results would emerge if more samples were evaluated and/or if more complete GAG degradation could be achieved. Even with these considerations, the data presented in this study support the more likely conclusion that GAGs have little to no role in the mechanical behavior of SST in shear loading, and certainly do not serve as a key tissue constituent to support shear.

Previous studies [10, 12, 14, 16, 26-28, 41-44] on the mechanical effect of GAGs in soft connective tissues have not always been consistent, but have been somewhat dependent on specimen species, types of soft tissues, loading modality and relative tissue health. Consistent with our findings, human medial collateral ligaments, mouse Achilles tendons, and rat tail tendons did not exhibit altered mechanical responses (i.e., stress, strain) in tension or shear after GAG removal [26-29, 41, 43]. Other studies showed that GAG-depleted mouse Achilles tendons had unchanged tensile stiffness, but less microscale reorganization/realignment of collagen fibers at low strains during tensile loading [23, 42, 44]. In contrast, injured equine superficial digital flexor tendons showed increased elastic modulus and ultimate tensile strength under tensile loading after GAG digestion [10, 12, 45]. Previous studies showed that GAGs likely influenced mechanical properties of soft tissues via distinct mechanisms under different loading scenarios, although it remains challenging to explicitly address the specific mechanical function of GAGs. Since highly electronegative GAGs can inhibit water exudation and further cause interstitial fluid pressurization, decreased compressive modulus of tissues such as ligament and cartilage after GAG degradation are most likely attributed to the interaction between PGs and water [12, 24]. For tendon, another proposed mechanism is that GAGs function as a linking structure to bridge adjacent collagen fibrils and provide load support in tension or shear [3]. Previous experimental results from different tissues, which found no change in mechanical properties after GAG

digestion, cannot completely reject this suggested mechanism, but provide no supporting evidence [26, 27]. One possibility is that the bond between PGs and collagen fibrils is weak or slack at low applied strain such that mechanical change due to GAG degradation in tissues is unmeasurable at many of the levels that have been evaluated experimentally [46]. Another possibility is that the influence of GAGs on tendon mechanical behavior depends on applied strain and fibril length relatively to GAG spacing, such that GAG depletion will alter tendon mechanical behavior in tension only when applied strain and the ratio of fibril length to GAG spacing are high enough [47]. A final possibility is that GAGs do not play a role in the tensile or shear mechanical response of tendon.

It is worth noting that a similar loading/analysis protocol were adopted in our prior study to investigate the mechanical role of another tissue constituent present in small quantities, namely elastin [9]. Due to similar physical constraints of the experimental setup, elastin was not fully removed after enzyme treatment; in fact, less elastin was depleted than what was achieved for GAGs in the present study [9]. Even still, SSTs were found to exhibit statistically significant decreases in stresses in shear loading after elastin degradation, particularly at low shear strains [9], similar to a study by another group [13]. Taken together, these data suggest that elastin, compared to GAGs, has a larger contribution to tendon mechanics in shear, further implying that GAGs should not be considered as a key component to regulate tendon mechanical behavior in shear.

As discussed in our prior study [9], high variability among human cadaveric SSTs due to significant natural heterogeneity and/or unknown level of age-related degeneration [9, 34, 35], as well as incomplete digestion of GAGs following ChABC incubation, should be considered when interpreting the current results. For example, previous studies reported higher concentrations of

collagen type II, aggrecan and biglycan in the anterior and posterior SST regions compared to the medial region, while decorin and collagen type I did not have regional variability among different regions [4, 5]. Since the predominant PG in tendon is decorin, this report agrees with our result that the three different regions showed similar overall amounts of PGs and GAGs [3, 5]. SST in this study also exhibited GAG-rich pericellular matrix, similar to what has been reported in cartilage, meniscus, and intervertebral disc [25]. Pericellular matrix could transduce biochemical and biomechanical signals to fibroblasts and simultaneously control/protect them by serving as viscoelastic damper [25, 48]. Nonetheless, even with these potential effects, our ChABC treatment did not visibly alter SST collagen content and structure, but did reduce GAG content, including within the pericellular matrix.

To resolve the limitation of incomplete GAG depletion from tissues by ChABC treatment, genetically modified heterozygous/knockout animal models have been adopted as another approach for evaluation. Unfortunately, reports of the mechanical properties of tendons from specific PG heterozygous/knockout mice (i.e., decorin, biglycan) have been inconsistent, and appear to be influenced by tendon location, animal age, and loading protocol [14-16, 49]. These discrepancies could be partially due to (1) unintended compensatory effects within tissues from these mice, including ameliorated negative influence from increased expression of other PGs in response to the down-regulation of specific targeted PGs, or (2) altered collagen fibrillogenesis due to decreased PGs during development. A combination of experimental approaches may be best suited to address the contribution of PGs and GAGs to tendon mechanics from different perspectives. As illustrated above, by examining macro- and micro-scale mechanical properties and deformation of ChABC treated SSTs under shear loading with two-photon microscopy, GAGs were found to minimally contribute to tendon mechanical behaviors. This study is not

only consistent with several previous studies on the role of PGs and GAGs in tendon under tension [26, 27, 29, 43], but also provides complementary knowledge of GAG function in non-tensile (shear) loading.

Supraspinatus tendons showed only minor changes in mechanical and microstructural properties after ChABC treatment to remove GAGs. Heterogeneity of relatively old donor tissues that were evaluated and incomplete digestion of GAGs may partially contribute to similarities between groups. Although these results may not fully extend to younger tendons and/or tendons following injury or repair, this study provides further evidence for a limited role of GAGs in tendon mechanics, particularly when subjected to shear loading.

5.5 References

1. A, S., R. M, and C. M, Towards an Understanding of the Genetics of Tendinopathy, in *Metabolic Influences on Risk for Tendon Disorders*. 2016, Springer. p. 109-116.
2. Cook, J., et al., Revisiting the continuum model of tendon pathology: what is its merit in clinical practice and research? *British journal of sports medicine*, 2016: p. bjsports-2015-095422.
3. Fang, F. and S.P. Lake, Modelling approaches for evaluating multiscale tendon mechanics. *Interface Focus*, 2016. 6(1): p. 20150044.
4. Buckley, M.R., et al., Distributions of types I, II and III collagen by region in the human supraspinatus tendon. *Connect Tissue Res*, 2013. 54(6): p. 374-379.
5. Matuszewski, P.E., et al., Regional variation in human supraspinatus tendon proteoglycans: decorin, biglycan, and aggrecan. *Connect Tissue Res*, 2012. 53(5): p. 343-348.
6. Fang, F. and S.P. Lake, Multiscale strain analysis of tendon subjected to shear and compression demonstrates strain attenuation, fiber sliding, and reorganization. *Journal of Orthopaedic Research*, 2015. 33(11): p. 1704-1712.
7. Fang, F., A.S. Sawhney, and S.P. Lake, Different regions of bovine deep digital flexor tendon exhibit distinct elastic, but not viscous, mechanical properties under both compression and shear loading. *J Biomech*, 2014. 47(12): p. 2869-2877.
8. Stubendorff, J., et al., Is cartilage sGAG content related to early changes in cartilage disease? Implications for interpretation of dGEMRIC. *Osteoarthritis and Cartilage*, 2012. 20(5): p. 396-404.

9. Fang, F. and S.P. Lake, Multiscale mechanical integrity of human supraspinatus tendon in shear after elastin depletion. *Journal of the Mechanical Behavior of Biomedical Materials*, 2016. 63: p. 443-455.
10. Choi, R.K., et al., Chondroitin sulfate glycosaminoglycans contribute to widespread inferior biomechanics in tendon after focal injury. *Journal of Biomechanics*, 2016. 49(13): p. 2694-2701.
11. Soslowky, L., et al., Neer Award 1999: Overuse activity injures the supraspinatus tendon in an animal model: a histologic and biomechanical study. *Journal of Shoulder and Elbow Surgery*, 2000. 9(2): p. 79-84.
12. Henninger, H.B., et al., Effect of sulfated glycosaminoglycan digestion on the transverse permeability of medial collateral ligament. *Journal of biomechanics*, 2010. 43(13): p. 2567-2573.
13. Grant, T.M., et al., The Mechanical, Structural, and Compositional Changes of Tendon Exposed to Elastase. *Annals of biomedical engineering*, 2015: p. 1-10.
14. Dunkman, A.A., et al., The injury response of aged tendons in the absence of biglycan and decorin. *Matrix Biology*, 2014. 35: p. 232-238.
15. Dourte, L.M., et al., Mechanical, compositional, and structural properties of the mouse patellar tendon with changes in biglycan gene expression. *Journal of Orthopaedic Research*, 2013. 31(9): p. 1430-1437.
16. Dourte, L.M., et al., Influence of decorin on the mechanical, compositional, and structural properties of the mouse patellar tendon. *Journal of biomechanical engineering*, 2012. 134(3): p. 031005.
17. Fang, F. and S.P. Lake, Experimental evaluation of multiscale tendon mechanics. *Journal of Orthopaedic Research*, 2017. 35(7): p. 1353-1365.
18. Iozzo, R.V., The family of the small leucine-rich proteoglycans: key regulators of matrix assembly and cellular growth. *Critical Reviews in Biochemistry and Molecular Biology*, 1997. 32(2): p. 141-174.
19. Landis, W.J. and F.H. Silver, The structure and function of normally mineralizing avian tendons. *Comparative Biochemistry and Physiology Part A: Molecular & Integrative Physiology*, 2002. 133(4): p. 1135-1157.
20. Robbins, J.R., S.P. Evanko, and K.G. Vogel, Mechanical loading and TGF- β regulate proteoglycan synthesis in tendon. *Archives of biochemistry and biophysics*, 1997. 342(2): p. 203-211.
21. Feitosa, V., et al., Comparative ultrastructural analysis of different regions of two digital flexor tendons of pigs. *Micron*, 2006. 37(6): p. 518-525.
22. Nissi, M.J., et al., Multi-parametric MRI characterization of enzymatically degraded articular cartilage. *Journal of Orthopaedic Research*, 2016. 34(7): p. 1111-1120.
23. Schmidt, M.B., et al., Effects of proteoglycan extraction on the tensile behavior of articular cartilage. *Journal of Orthopaedic Research*, 1990. 8(3): p. 353-363.

24. Soltz, M.A. and G.A. Ateshian, Interstitial fluid pressurization during confined compression cyclical loading of articular cartilage. *Annals of biomedical engineering*, 2000. 28(2): p. 150-159.
25. Wilusz, R.E., J. Sanchez-Adams, and F. Guilak, The structure and function of the pericellular matrix of articular cartilage. *Matrix Biology*, 2014. 39: p. 25-32.
26. Fessel, G. and J.G. Snedeker, Evidence against proteoglycan mediated collagen fibril load transmission and dynamic viscoelasticity in tendon. *Matrix Biology*, 2009. 28(8): p. 503-510.
27. Fessel, G. and J.G. Snedeker, Equivalent stiffness after glycosaminoglycan depletion in tendon—an ultra-structural finite element model and corresponding experiments. *Journal of theoretical biology*, 2011. 268(1): p. 77-83.
28. Lujan, T.J., et al., Effect of dermatan sulfate glycosaminoglycans on the quasi-static material properties of the human medial collateral ligament. *Journal of orthopaedic research*, 2007. 25(7): p. 894-903.
29. Svensson, R.B., et al., Tensile force transmission in human patellar tendon fascicles is not mediated by glycosaminoglycans. *Connective tissue research*, 2011. 52(5): p. 415-421.
30. Gandley, R., et al., Contribution of chondroitin-dermatan sulfate-containing proteoglycans to the function of rat mesenteric arteries. *American Journal of Physiology-Heart and Circulatory Physiology*, 1997. 273(2): p. H952-H960.
31. Mattson, J.M., R. Turcotte, and Y. Zhang, Glycosaminoglycans contribute to extracellular matrix fiber recruitment and arterial wall mechanics. *Biomechanics and Modeling in Mechanobiology*, 2016: p. 1-13.
32. Deprés-tremblay, G., et al., Rotator cuff repair: a review of surgical techniques, animal models, and new technologies under development. *Journal of Shoulder and Elbow Surgery*, 2016. 25(12): p. 2078-2085.
33. Bey, M.J., M.L. Ramsey, and L.J. Soslowsky, Intratendinous strain fields of the supraspinatus tendon: effect of a surgically created articular-surface rotator cuff tear. *Journal of shoulder and elbow surgery*, 2002. 11(6): p. 562-569.
34. Lake, S.P., et al., Effect of fiber distribution and realignment on the nonlinear and inhomogeneous mechanical properties of human supraspinatus tendon under longitudinal tensile loading. *Journal of orthopaedic research: official publication of the Orthopaedic Research Society*, 2009. 27(12): p. 1596-1602.
35. Lake, S.P., et al., Tensile properties and fiber alignment of human supraspinatus tendon in the transverse direction demonstrate inhomogeneity, nonlinearity, and regional isotropy. *Journal of biomechanics*, 2010. 43(4): p. 727-732.
36. Zheng, C. and M.E. Levenston, Fact versus artifact: avoiding erroneous estimates of sulfated glycosaminoglycan content using the dimethylmethylene blue colorimetric assay for tissue-engineered constructs. *European cells & materials*, 2015. 29: p. 224-236.

37. Koob, T.J. and K.G. Vogel, Site-related variations in glycosaminoglycan content and swelling properties of bovine flexor tendon. *Journal of orthopaedic research*, 1987. 5(3): p. 414-424.
38. Grant, T.M., et al., Elastic fibres are broadly distributed in tendon and highly localized around tenocytes. *Journal of anatomy*, 2013. 222(6): p. 573-579.
39. Toyjanova, J., et al., 3D Viscoelastic traction force microscopy. *Soft Matter*, 2014. 10(40): 8095-8106.
40. Djuzenova, C.S., et al., Actin cytoskeleton organization, cell surface modification and invasion rate of 5 glioblastoma cell lines differing in PTEN and p53 status. *Exp Cell Res*, 2015. 330(2): p. 346-357.
41. Lujan, T.J., et al., Contribution of glycosaminoglycans to viscoelastic tensile behavior of human ligament. *Journal of Applied Physiology*, 2009. 106(2): p. 423-431.
42. Millesi, H., et al., Biomechanical properties of normal tendons, normal palmar aponeuroses, and tissues from patients with Dupuytren's disease subjected to elastase and chondroitinase treatment. *Clinical Biomechanics*, 1995. 10(1): p. 29-35.
43. Rigozzi, S., R. Müller, and J. Snedeker, Local strain measurement reveals a varied regional dependence of tensile tendon mechanics on glycosaminoglycan content. *Journal of biomechanics*, 2009. 42(10): p. 1547-1552.
44. Rigozzi, S., et al., Tendon glycosaminoglycan proteoglycan sidechains promote collagen fibril sliding—AFM observations at the nanoscale. *Journal of biomechanics*, 2013. 46(4): p. 813-818.
45. Isaacs, J.L., et al., Role of biomolecules on annulus fibrosus micromechanics: Effect of enzymatic digestion on elastic and failure properties. *Journal of the mechanical behavior of biomedical materials*, 2014. 40: p. 75-84.
46. Watanabe, T., et al., Ring-Mesh Model of Proteoglycan Glycosaminoglycan Chains in Tendon based on Three-dimensional Reconstruction by Focused Ion Beam Scanning Electron Microscopy. *Journal of Biological Chemistry*, 2016. 291(45): p. 23704-23708.
47. Ahmadzadeh, H., et al., Determining the contribution of glycosaminoglycans to tendon mechanical properties with a modified shear-lag model. *Journal of biomechanics*, 2013. 46(14): p. 2497-2503.
48. Han, W.M., et al., Microstructural heterogeneity directs micromechanics and mechanobiology in native and engineered fibrocartilage. *Nature materials*, 2016. 15(4): 477-484.
49. Gordon, J., et al., Achilles tendons from decorin- and biglycan-null mouse models have inferior mechanical and structural properties predicted by an image-based empirical damage model. *Journal of biomechanics*, 2015. 48(10): p. 2110-2115.

Chapter 6: The Role of Collagen Crosslinks in Multiscale Mechanics of Rat Supraspinatus Tendon in Tension

6.1 Introduction

As recapitulated previously, tendons mainly sustain tensile loading under *in vivo* physiological loading scenarios [1]. Many kinds of crosslinks are present within collagen inside tendon, which may contribute to tendon strength, aid resistance to chemical or enzymatic breakdown, and prevent weakness and fragility of collagen fibrils [2]. Collagen crosslinks help bridge adjacent collagen molecules/fibrils in tendon on the nano/microscales, and are hypothesized to contribute to mechanical function of tendon [3, 4].

Collagen crosslinks can be categorized into three main groups: immature enzymatic, mature enzymatic and non-enzymatic crosslinks [5, 6]. Non-enzymatic crosslinks in tendons are often produced by glycation related with aging and diabetes. These crosslinks, in the form of advanced glycation end products such as pentosidine, can also be created *in vitro* by incubating tendons in glucose or ribose [7-9]. Since non-enzymatic crosslinks are not prevalent in mature and healthy tendons, they are not the focus of this study. To form enzymatic crosslinks, the copper-dependent enzyme lysyl oxidase (LOX) catalyzes the oxidation of lysine and hydroxylysine residues to form pyridinium and pyrrolic molecules within the N- and C-terminal telopeptides [5]. During this catalysis process, divalent dihydroxylysinonorleucine and hydroxylysinonorleucine are formed as immature enzymatic crosslinks and lysyl pyridinoline (LP) and hydroxylysyl pyridinoline (HP) as mature enzymatic crosslinks [5]. Current studies have demonstrated that the most prevalent type of enzymatic crosslinks in adult tendon is HP and to a lesser degree LP,

which lay within or between collagen molecules, as well as between adjacent microfibrils [10].

Previous studies that have experimentally evaluated the crosslink mechanical contribution on a single length scale yielded results that were not consistent. Some results suggested that more enzymatic crosslinks between and within collagen fibrils contribute to improved tendon tissue-level mechanics [4, 11-14], but the comparison of tendons from different regions indicated that tendon mechanics were not directly correlated with crosslink density inside tissues [15, 16]. For these experimental examinations, several factors which could influence and further counteract potential mechanical contribution of crosslinks. For example, different loading protocols (i.e., stress relaxation, quasi-static loading, creep) [14, 17] have been used; as collagen crosslinks may only govern tendon elasticity instead of viscoelasticity, inconsistent results/conclusions could be drawn from studies using different protocols. Some reports also measured collagen crosslink amounts and related mechanical properties of tendons from different locations, sexes, and/or ages [15-17]. Different types of tendons have varying collagen structure and amounts of other components (i.e., collagen, PG, elastic fibers). Thus, mechanical behavior of these tendons is not only attributed to collagen crosslinks, but also influenced by other compositional and structural elements. Therefore, alternative examination of tendons with altered crosslink density but with similar collagen structure and composition from the same location could help eliminate effects of other contributions to tendon mechanics. For example, approaches such as *in vivo* treatment of soft tissues with β -aminopropionitrile (BAPN, crosslink inhibitor) and *in vitro* culture with lyxyl oxidase (crosslink promoter), could provide a unique way to alter collagen crosslink content in similar tendons and enable comparison of mechanical properties of tendon groups with crosslink content as the only changing variable [3, 4]. Furthermore, since tendon has a complicated hierarchical organization [1, 18] and collagen crosslinks function at smallest scale to bundle

collagen together, crosslinks could potentially impact mechanical signal transfer from the nano to tissue scales [19]. However, it is unknown whether crosslinks regulate mechanical properties among multiple spatial scales. Knowledge of collagen crosslink function could be used for designing optimized biomaterials with required strength for regenerative medicine and also track tissue degeneration/disease using crosslink as a marker of tendon integrity.

This study aimed to examine whether mature enzymatic collagen crosslinks (i.e., HP, LP) contribute to tendon mechanics on both tissue and micron scales and determine how these crosslinks governed tendon microscale deformation. Rat supraspinatus tendons (SSTs) were cultured *in vitro* in lysyl oxidase-like 2 (LOXL-2) medium for two weeks to increase the amount of enzymatic collagen crosslinks. Another group of rats were injected with BAPN to decrease the amount of collagen crosslinks in SSTs. Stress relaxation tensile testing was performed to evaluate mechanical strength of control or cultured/treated SSTs, while simultaneously tracking deformation on the tissue and micron scales monitored via camera and two-photon microscopy. Finally, liquid chromatography-tandem mass spectrometry was used to quantify crosslink amounts. Metrics of multiscale analysis were calculated and compared across different groups of tendons and correlated with crosslink amount. We hypothesized that enzymatic collagen crosslinks would improve mechanical properties by decreasing fiber/fibril sliding and reorganization.

6.2 Materials and methods

Verification of collagen crosslink measurement. Liquid chromatography-tandem mass spectrometry (LC/MS/MS), which has higher resolution and sensitivity compared to high performance liquid chromatography, has been successfully used to measure collagen crosslinks from chicken embryonic tendon and mouse cervical tissue [4, 20]. The protocol for this

technique was adapted from previous reports [20, 21]. Initially, a set of test samples were evaluated to verify the technique: porcine Achilles tendon, bovine patellar tendon, rat SST, mouse Achilles tendon, and mouse SST. Excised samples were incubated into liquid nitrogen and ground into powder with a pestle and mortar after measuring wet weight. Ground powder was put in a suitable vessel (e.g., borosilicate glass with screwed lid, Teflon sealed glass tubes) and hydrolyzed in a volume of 6N chloride acid to give a concentration of approximately 5 mg wet weight of sample per milliliter of acid (i.e., less than 10 mg/ml). The hydrolysis vessels were sealed and heated to 110 °C in the oven for 20-24 hours with time adjusted if the sample was not totally hydrolyzed. All hydrolyzed solutions were passed through 0.2 µm filters to remove debris particles. After filtering, solutions were lyophilized in a refrigerated vapor trap (RVT 4014, Thermo Fisher Scientific, St. Louis) to eliminate all hydrochloric acid. The hydrolysate was re-suspended in a heptafluorobutyric acid buffer and subjected to the analysis on a Waters Xevo TQ MS ACQUITY UPLC system (Waters, Milford, MA) as described to determine HP, LP, and also hydroxyproline [20]. Optimized multiple reaction monitoring (MRM) parameters of positive mass spectrometry and quantification sensitivity were utilized (Table 6.1). The total collagen content was converted from hydroxyproline amount assuming 14% hydroxyproline content per collagen by weight (i.e., 300 mol HYP per 1 mol collagen) [20]. The density of collagen crosslinks HP and LP was obtained by normalizing the amount of HP and LP by total collagen.

Table 6.1 Optimized MRM conditions and quantification limit

Compound	MRM transition (m/z)	Cone Voltage (V)	Collision energy (eV)
Hydroxyproline	132.09>86.07	20	14
HP	429.2>267.1	44	28
LP	413.2>267.1	44	28

Selection of animal models. Rotator cuff tears are very common, causing dysfunction of the shoulder and pain; Due to primary involvement of SST in such conditions the study of SST has high clinical significance [22, 23]. Rat and human share similar shoulder anatomy and similar levels of histologic/morphologic and mechanical properties in overuse injuries to human [23]. Therefore, analysis of rat SST enables examination of the interaction between mechanical loading and structure or composition of tendon and how various factors contribute to tendon degeneration/disease. Since collagen fibers mainly support force transmission under tension, evaluation of enzymatic collagen crosslinks under tensile loading can provide more information about the mechanism of crosslinks modulating tendon multiscale mechanics. Therefore, SSTs from Sprague-Dawley rats were evaluated under tensile loading in this study.

Preliminary in vitro culture to increase collagen crosslinks. Lysyl oxidase (LOX) is an extracellular copper-dependent enzyme that can catalyze aldehyde formation and promote crosslink production to stabilize collagen fibrils. Lysyl oxidase and its four related gene family members (lysyl oxidase homolog 1-4, also named as LOXL1-4)

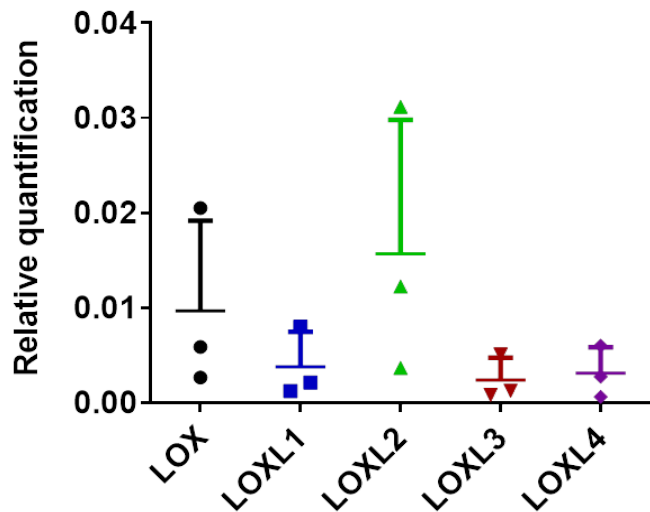


Fig. 6.1 The relative gene expression of LOX and different LOX isoforms in mice Achilles tendon and SST.

have been localized in soft tissues such as arterial walls [24]. Interestingly, expression of LOX and its homologs in mouse aorta depended on mouse age [24]. For mice at developmental time points between embryonic day 14 and postnatal day 60, the main isoform was LOX; expression decreased significantly to similar levels after postnatal day 60 [24]. However, different tissues

and species (i.e., human, rat, mouse) would have different expression of LOX homologs has not been addressed. This information is important for determining the appropriate LOX homolog to be applied in *in vitro* tendon culture to increase collagen crosslinks. Therefore, SSTs and Achilles tendons were harvested from three mice at 14 days old and three rats at 21 days old and subjected to real-time PCR analysis of LOX (Mm00495386_m1), LOXL1 (Mm00804740_m1), LOXL2(Mm00804740_m1), LOXL3(Mm01184865_m1), and LOXL4(Mm00446385_m1) [24]. All LOX levels were normalized to GAPDH. Due to the specificity of these primers/probes to mice and the relatively low expression of GAPDH, LOX levels were only quantified in in two mouse tissues (two SST and one Achilles tendon). Our real-time PCR analysis showed that the primary LOX homolog in mouse SST and Achilles tendon was LOXL2, followed by LOX (Fig. 6.1). In previous studies, lysyl oxidase like 2 enhanced LOX-induced enzymatic collagen crosslinks and finally increased functional properties of bovine articular cartilage explants after 4 weeks culture [3]. Based on these results, LOXL2 was selected as the exogenous enzyme to increase the density of collagen crosslinks *in vitro*. Eight-weeks-old Sprague-Dawley rats (n=3) were sacrificed via CO₂ overdose, and a one unilateral set of SST and Achilles tendon (AT) were harvested immediately. The humerus bone of supraspinatus tendons and calcaneus bone of ATs were attached to a horizontal bar of a custom-built *ex vivo* culture device through 2-0 silk suture (Fig. 6.2). The muscles were attached to a 0.3N weight with a suture, passing under a stainless bar in the same device, so that constant tension was applied to all tendons to partially decrease natural degeneration during *in vitro* culture (Fig. 6.2). To keep the tendon sterile, the bone-tendon-muscle assembly was washed in DMEM (D6046, Sigma-Aldrich) containing 0.1 mg/ml kanamycin (K0129, Sigma-Aldrich) and 0.165 mg/ml gentamicin (15750060, Thermo Fisher), and the whole custom-built device was washed in medium twice. Two unilateral sets of AT and

SST were randomly assigned to culture in DMEM (D6046, Sigma-Aldrich), 0.1 mg/ml penicillin-streptomycin (P4333, Sigma-Aldrich), 2.5 µg/ml amphotericin B (A2942, Sigma-Aldrich), 1× non-essential amino acid (100×, M7145, Sigma-Aldrich), 50 µg/ml L-ascorbic acid (P5607, Sigma-Aldrich), 100 µg/ml sodium pyruvate (S8636, Sigma-Aldrich), 4 mM L-glutamine (G7513, Sigma-Aldrich), 1× ITS+ (insulin, transferrin, selenium) premix (I3146, Sigma-Aldrich), 100 nM dexamethasone (D4902, Sigma-Aldrich), L-proline 50 µg/ml (P5607, Sigma-Aldrich), 0.146 mg/ml DL-5-hydroxylysine (H0377, Sigma-Aldrich), and copper sulfate (451657, Sigma-Aldrich) with 0 ng/ml (control), 0.015 ng/ml (low), 0.15 ng/ml (high) LOXL2 [3]. The culturing devices were placed in the incubator and maintained under 5% CO₂ at 37°C for 2 weeks with culturing medium changed every other day.

Tendon cell viability after a two-week culture period was evaluated with LIVE/DEAD™ viability/cytotoxicity kit (L3224, ThermoFisher Scientific, Waltham, MA), where green-fluorescent calcein-AM indicates intracellular esterase activity of live cells and red-fluorescent ethidium homodimer-1 indicates loss of plasma membrane integrity of dead cells.

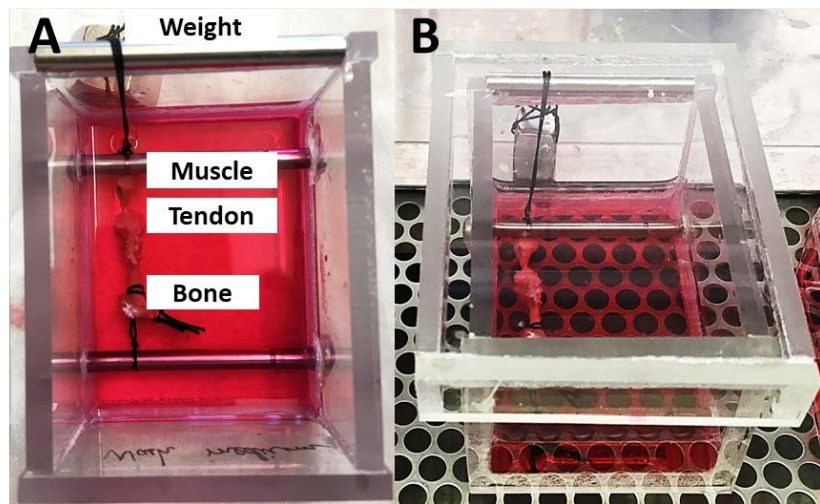


Fig. 6.2 Bone-tendon-muscle assembly cultured in the custom-built device. (A) Constant tension was applied by the weight to the tendon. (B) Culture medium was covered to prevent contamination

Cultured tendons were sliced as thin as possible with a blade and incubated in PBS solution with

4 μM ethidium homodimer and 10 μM calcium AM for 40 min, followed by efficient washing. To acquire cellular images of tendon, a Zeiss multiphoton confocal microscope system was set to 514 nm excitation, and signals from live and dead cells were collected at 477-554 nm and 596-740 nm, respectively, using 20 \times NA objectives.

Evaluation of in vitro cultured tendons. After *in vitro* culture, all tendons were marked with ink and tested with a standard tensile loading protocol [25]. Briefly, tendons were preloaded to 0.1N, preconditioned with 10 cycles of 1% strain followed by a 300-second dwell, and then ramped to 6% strain followed by a 300-second dwell, and ramped to failure at a constant strain rate of 0.1% strain per second. Images were acquired during testing to track tissue deformation.

In vivo treatment to decrease enzymatic collagen crosslinks. A previous study showed that BAPN inhibited LOX activity such that BAPN fed rats had less collagen crosslinks in their tail tendons [11]. Additionally, incisor periodontal ligament from Wistar rats with daily subcutaneous

injection of BAPN exhibited greater shear stress than that without treatment [26]. In a preliminary study,

eight-week-old Sprague-Dawley rats

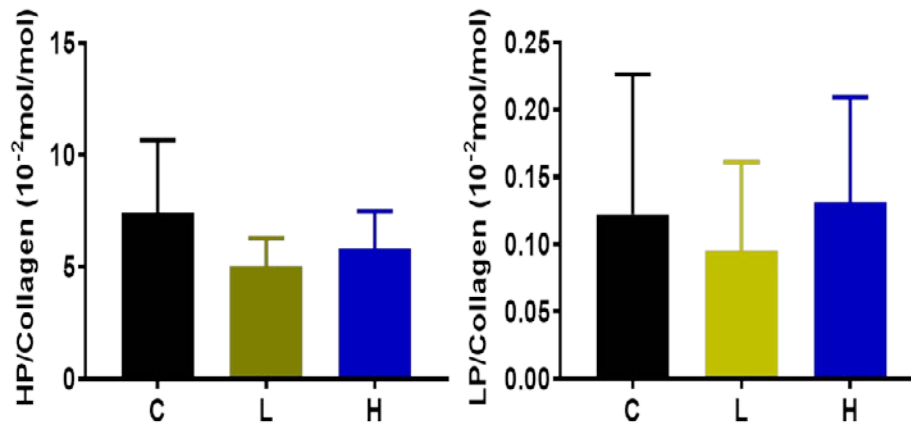


Fig. 6.3 HP and LP contents normalized by collagen amount in tendons of rats which started at eight-weeks old to be injected with no (C), low dose (L), and high dose (H) BAPN for four weeks. HP and LP did not decrease with treatment.

(n=15) were divided into three groups and each group was injected subcutaneously daily for four weeks with saline containing 0 mg/kg (control, C), 350 mg/kg (low dose, L), and 500 mg/kg

(high dose, H) BAPN. BAPN treatment did not significantly decrease mature crosslinks HP and LP (Fig. 6.3). We determined that eight-week old rats may already well-formulated collagen fibrils so that the crosslinks among them can not be significantly altered with BAPN treatment. Supporting this hypothesis, collagen fibrils in rat tendon between 10-30 days primarily grow transversely, with perhaps more crosslinks binding collagen fibrils to build greater diameter [27]. Therefore, we modified our daily BAPN injection protocol to use four-week old rats (n=15). These rats were divided into three groups (n=5 for each group) for control, low dose, and high dose as stated above. All rats were injected for four weeks. Our results (Fig. 6.15) showed that BAPN treatment successfully increased collagen crosslinks in SST.

Tensile testing with two-photon microscopy of in vivo treated tendons. SSTs were harvested from rat shoulders following *in vivo* treatment. Tendons were measured by a non-contact laser system to determine cross-section area, stained with 5-DTAF and DAPI, marked with Verhoeff-Van Gieson stain solution for tracking tissue length-scale strain, and finally attached to the tensile testing device (Fig. 6.4 and 6.5). 100 μm ×100 μm photobleached grids were created at two locations with obvious collagen fiber alignment along tendon. Tendons were subjected to a three-step (6% strain for each step) incremental stress-relaxation tensile test protocol with 12 minutes relaxation time after each strain step. Camera and microscopy images were collected at 1 and 4 minutes, respectively, after each strain step was applied. After biomechanical testing, all samples were used for crosslink quantification. Parameters (peak

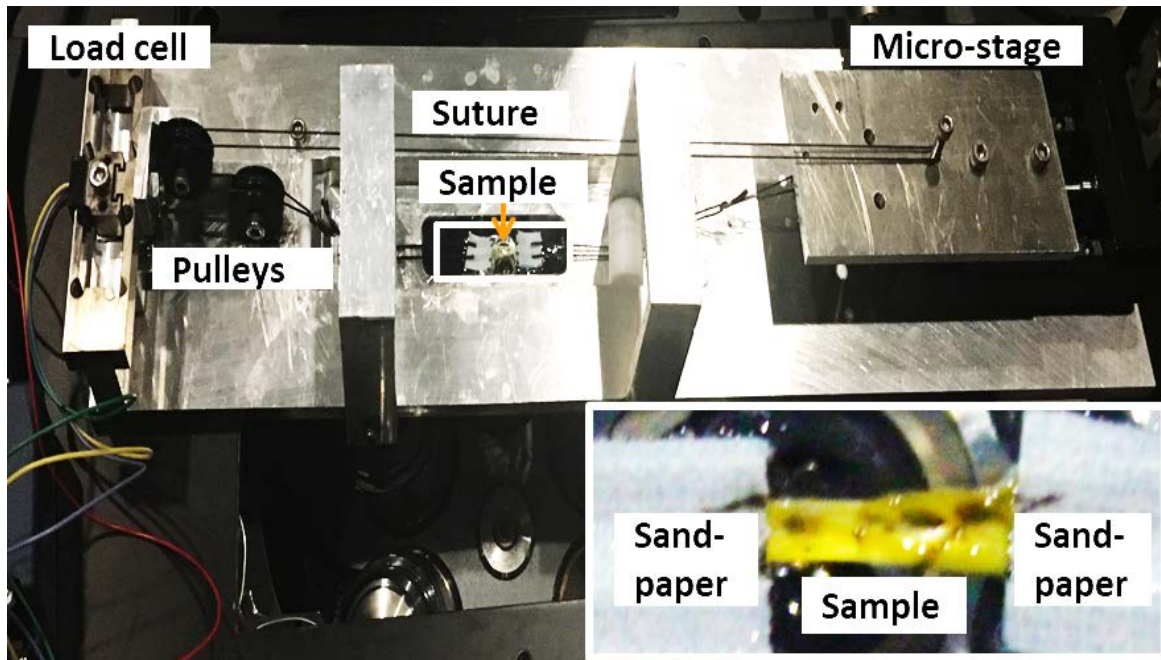


Fig. 6.4 Tensile mechanical testing device. The inset, denoted by the white rectangle, shows rat SST glued to sandpaper tabs, which are then connected to the micro-stage by suture.

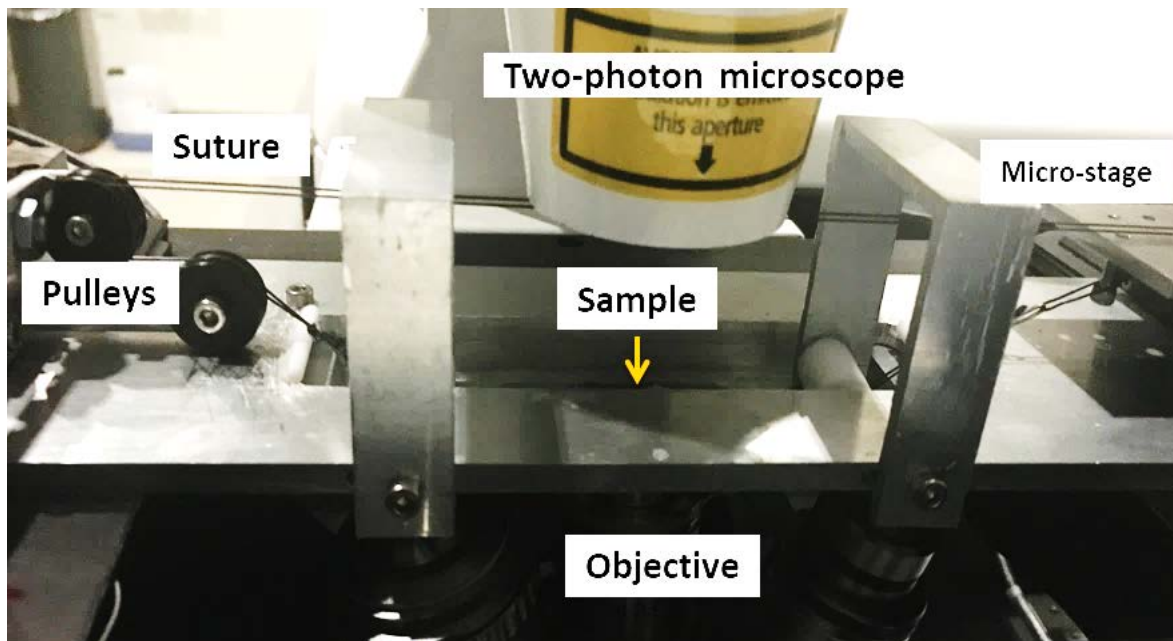


Fig. 6.5 Tensile mechanical testing device mounted on the two-photon microscopy stage.

stresses, equilibrium stresses, side-by-side difference, microscale tensile strain along collagen fibers, microscale shear strain) were calculated by using stress-strain curves, camera, and microscopic images. Side-by-side difference was defined as

$$\text{Difference} = \left| \frac{\sigma_L - \sigma_R}{(\sigma_L + \sigma_R)/2} \right| \quad (6.1)$$

Where σ_L is the stress of left SST and σ_R is the stress of right SST from the same rat.

Data analysis. Parameters (i.e., stress, side-to-side differences of peak/equilibrium stresses, strain in different length scales) were compared among different culturing/treating groups with one-way ANOVAs. For all ANOVAs, when significance was detected ($p < 0.05$), differences between specific groups were evaluated by post-hoc t -tests with Bonferroni corrections. Tissue strain computed with camera pictures was correlated with tendon peak stresses and equilibrium stresses by linear regressions. All data are shown as mean \pm SD.

6.3 Results

Crosslink measurement of different types of tendons. HP and LP contents from different types of tendons were evaluated preliminarily and compared with the values of HP and LP from literature to verify this method. The values of HP in different samples varied subtly and were in the range of data from previous studies which evaluated crosslink analysis of different tissues through several techniques (i.e., high performance liquid chromatography) (Fig. 6.6) [3, 4, 15, 16, 28-34]. Results were similar for LP values in our study (Fig. 6.7), although less LP data was available for comparison. HP density was found to be approximately two orders of magnitude greater than LP density, which was also consistent with previous reports. Based on these preliminary observations, the method and protocol used here were determined to be appropriate.

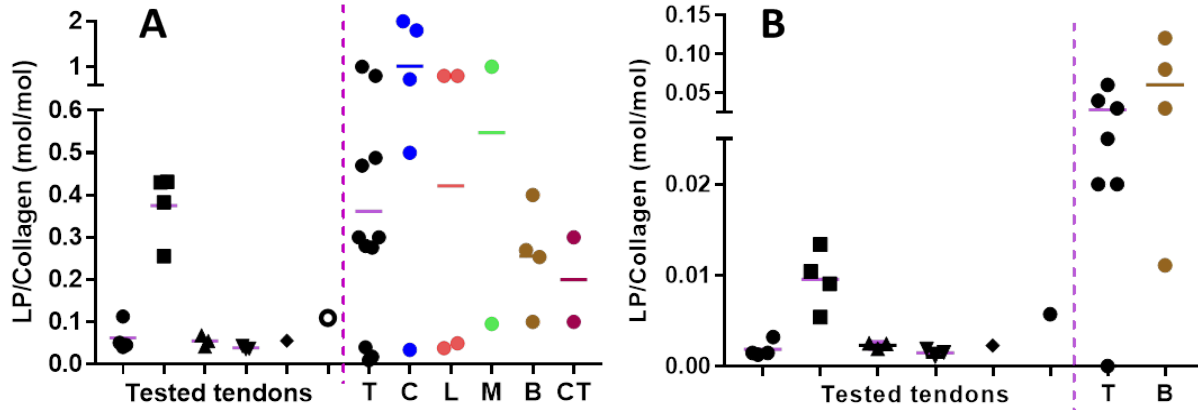


Fig. 6.6 HP (A) and LP (B) amounts in different types of tendons (porcine Achilles tendon, bovine patellar tendon, rat SST, mouse Achilles tendon, and mouse SST) quantified by our technique described in Section 6.2 (left side of the dash line) and further compared with HP (A) and LP (B) densities in tissues from literature (right side of the dash line, T: tendon, C: cartilage, L: ligament, M: meniscus, B: bone, CT: cervical tissue).

Preliminary data of in vitro cultured tendons. After two-week culture, man cells survived in both AT and SST, although some cells died (Fig. 6.7). Interestingly, some cells were stained red for nuclei and blue for cytoplasm, which may be due to esterase still distributed inside the cell cytoplasm when the cells lost their membrane property, such that the ethidium homodimer could still penetrate into cells.

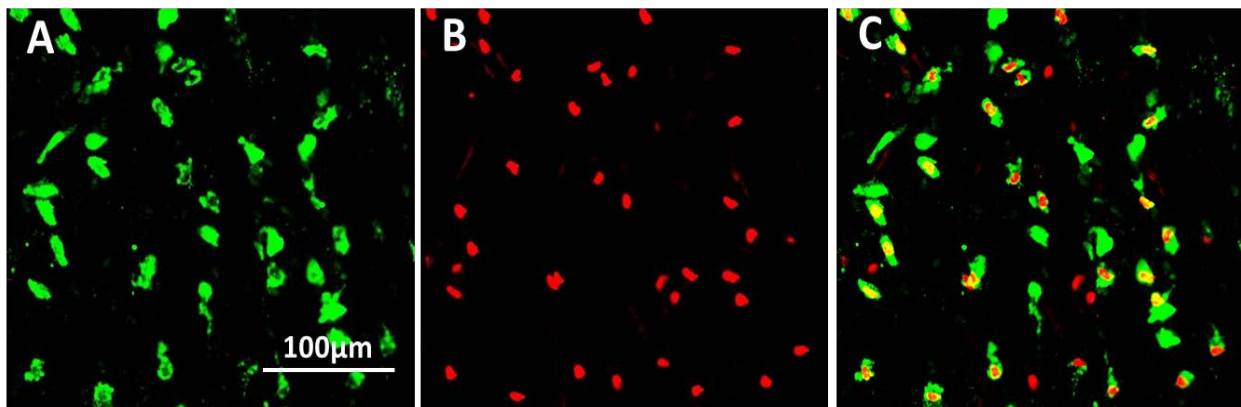


Fig. 6.7 Cell viability of tendons after two-week culture. (A) Live cells were stained green. (B) Dead cells were stained red. (C) Composite channels showed both live and dead cells.

Mechanical response of in vitro cultured tendons in tension. Surprisingly, compared to SST groups cultured without LOXL2 (control), SSTs cultured with low and high concentrations of

LOXL2 showed smaller peak stresses (Fig. 6.8). Linear and toe modulus for control groups were slightly smaller than the high concentration group, which was not true for the low concentration group. Due to the small sample size (n=3) for each group in this preliminary study, statistical analysis was not performed. Evaluation of collagen crosslink density in these groups will be conducted to verify culturing efficiency. These results are preliminary, but suggest that *in vitro* culture in LOXL2 at high concentration may increase tendon mechanical properties.

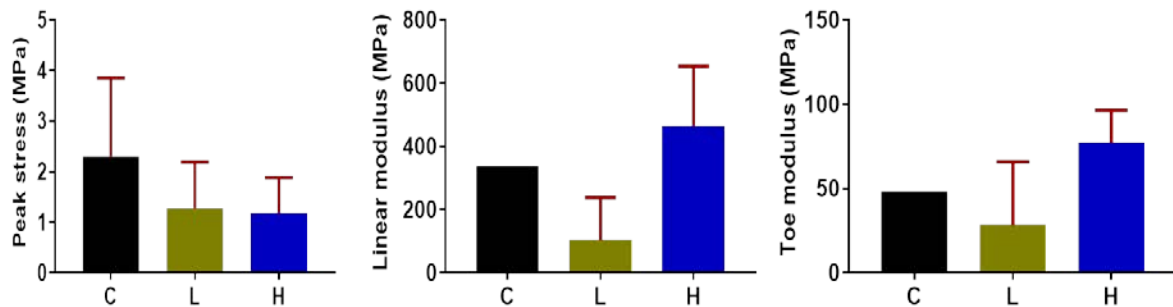


Fig. 6.8 Peak stress (N=2 for control, N=4 for other groups), linear, and toe modulus (N=1 for control, N=4 for other groups) of *in vivo* cultured tendons. C, L, and H are SST groups cultured with no, low, or high LOXL2 concentration, respectively.

Mechanical response of in vivo treated tendons in tension. During *in vivo* treatment, rat body

weight was measured every day and normalized by initial body weight. Groups injected with saline, Low, or high doses of BAPN showed similar normalized weights with no significant differences among groups (Fig. 6.9). Peak and equilibrium stresses increased with the increase of

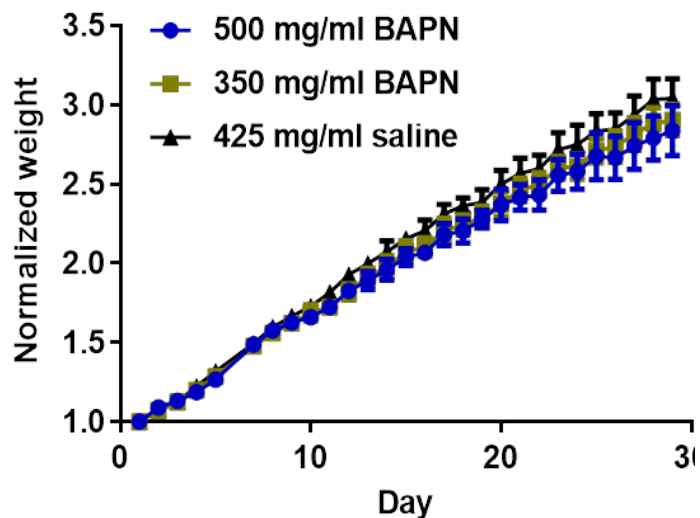


Fig. 6.9 Rat weight during four weeks of injection normalized by day 0 body weight.

applied strain (Fig. 6.10). Equilibrium stress was significantly smaller than peak stress, demonstrating obvious stress relaxation during the loading process. Both low dose and high dose groups exhibited slightly smaller peak stresses than the control group for all three applied strain steps.

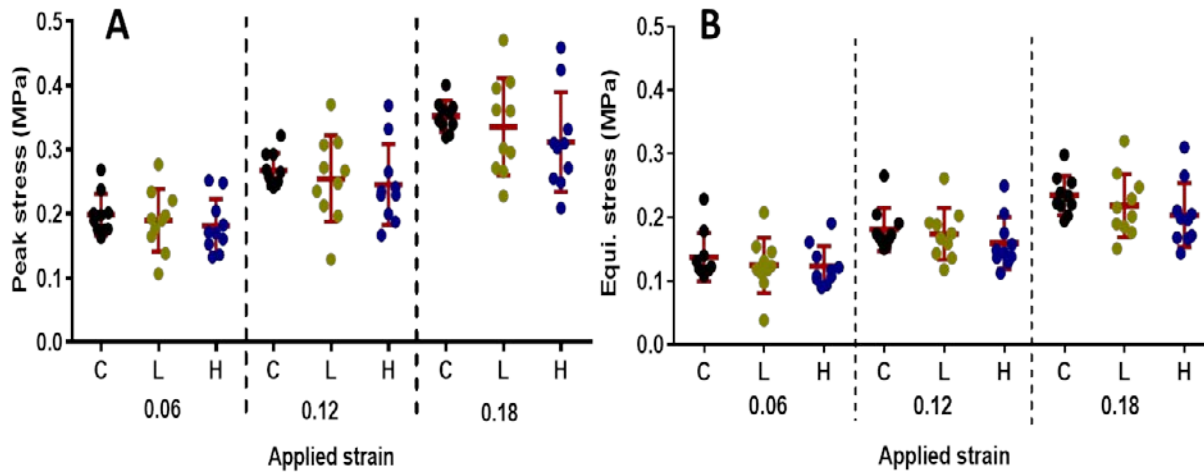


Fig. 6.10 Peak (A) and equilibrium stresses (B) of *in vivo* treated tendons from control (C), low dose (L), and high dose (H) groups. 0.06, 0.12, and 0.18 are applied step strains during mechanical testing.

Although group-group differences did not reach significant levels, peak and equilibrium stresses appear to be dose-dependent. Interestingly, peak and equilibrium stresses in BAPN treated groups were more variable than the control group. After further examining the stress data, side-to-side (limb specific) differences were found. The control group exhibited much smaller side-to-side differences in peak and equilibrium stresses than either the low dose or high dose BAPN groups (Fig. 6.11), and also more variable than control group. Side-to-side differences were relatively consistent across different strain steps.

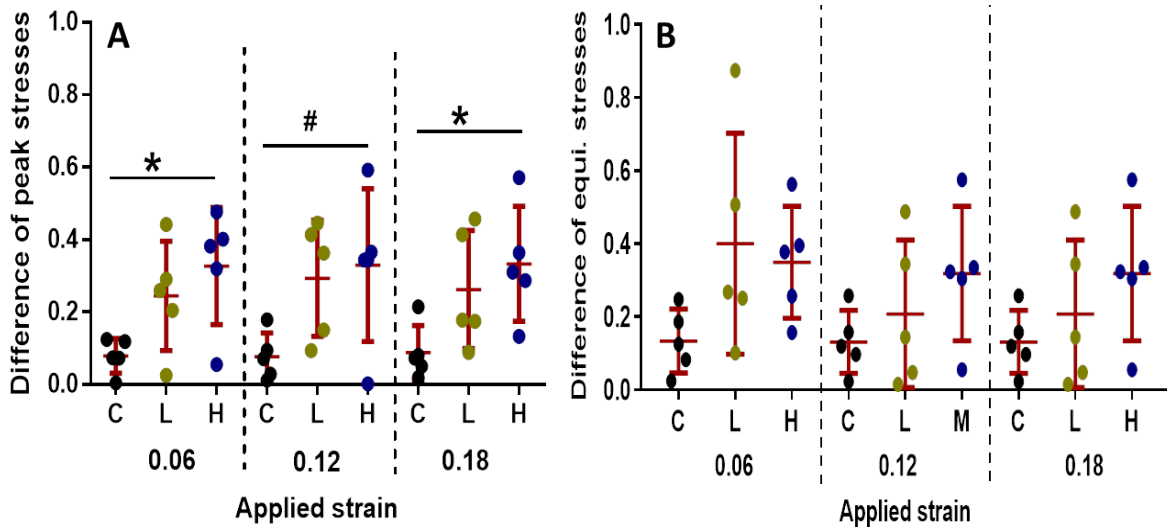


Fig. 6.11 Difference of peak (A) and equilibrium stresses (B) between left and right SSTs from control (C), low dose (L), and high dose (H) groups. 0.06, 0.12, and 0.18 are applied step strain; * for $p < 0.05$; # for $0.05 \leq p \leq 0.1$.

Peak stresses from different treated groups were correlated with tissue strain, which was calculated using camera images. Tissue strain was found to be $\sim 1/3$ of applied strain (Fig. 6.12). Consistent with our hypothesis, the slope of peak stress vs. tissue strain curve fits decreased in a dose-dependent way after BAPN treatment (control: 3.18, low dose: 2.65, high dose: 2.13), demonstrating that BAPN treatment did cause decrease SST mechanical strength. However, peak stresses of low dose and high dose groups were somewhat poorly correlated with tissue strain (i.e., low R^2 values). This could be attributed to high variability in peak stresses of BAPN treated tendons. Slopes of peak stress vs. tissue strain curve were greater than slopes of equilibrium stresses vs. tissue strain (Fig. 6.12& 6.13). Similarly, the slope of equilibrium stress vs. tissue strain curve decreased in a dose-dependent way after BAPN treatment (control: 1.72, low dose: 1.64, high dose: 1.26) (Fig. 6.14). Equilibrium stresses were also somewhat poorly correlated with tissue strains.

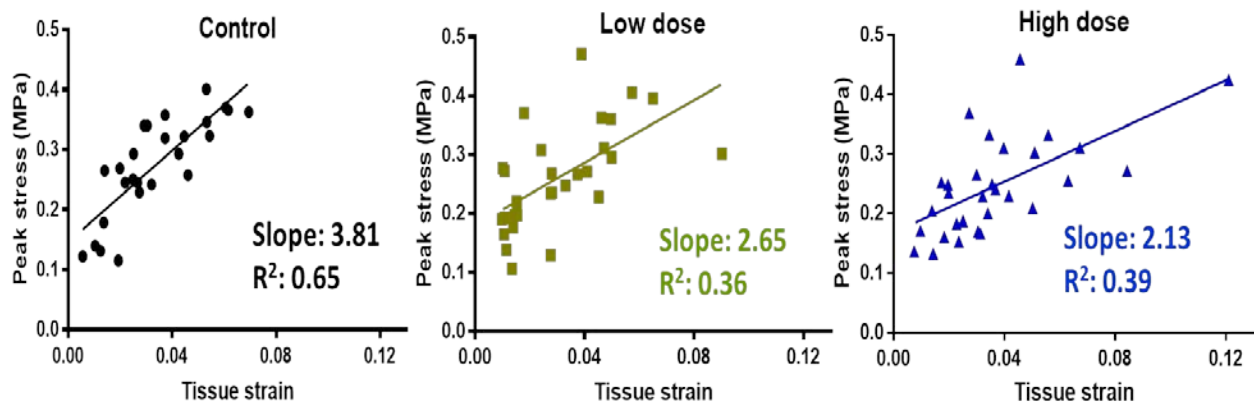


Fig. 6.12 Correlation plots between tissue strain and peak stresses of control, low dose, and high dose BAPN treated groups. Solid lines show best linear fit, with corresponding slope and R² values.

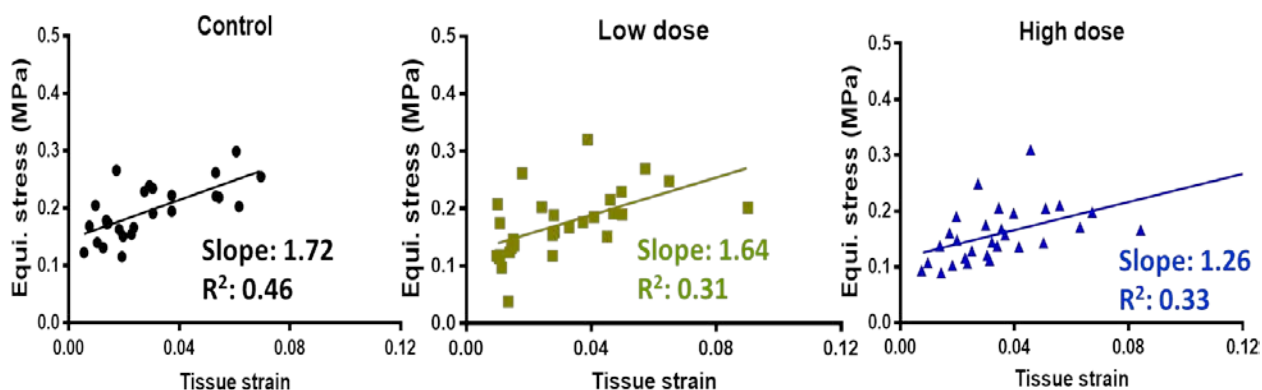


Fig. 6.13 Correlation plots between tissue strain and equilibrium stresses of control, low dose, and high dose BAPN treated groups. Solid lines show best linear fit, with corresponding slope and R² values.

Surprisingly, all three groups exhibited negative microscale tensile strain, demonstrating that collagen fibers on the microscale can experience compressive deformation even when tensile strain is applied on the tissue scale (Fig. 6.14). All these groups showed similar microscale tensile strain (E_{11}), which implied that BAPN treatment did not influence collagen fiber stretch on the microscale. Even under tensile loading, tendons from all three groups also exhibited non-zero microscale shear strains (E_{12}), which are attributed to collagen fiber sliding. Microscale shear strains were more variable and greater in BAPN treated groups than the control group, indicating that more sliding occurred between collagen fibers in BAPN treated groups. However, microscale tensile and shear strains were not significantly different among the three treated

groups. Our results showed that crosslink density was decreased significantly in SST treated with the highest dose of BAPN compared to control (Fig. 6.15). The group treated with the low dose of BAPN had smaller, but not significantly different HP than control. LP density was also dose-dependent, with smaller values in BAPN treated tendons compared to control, but no significant differences were detected among different groups.

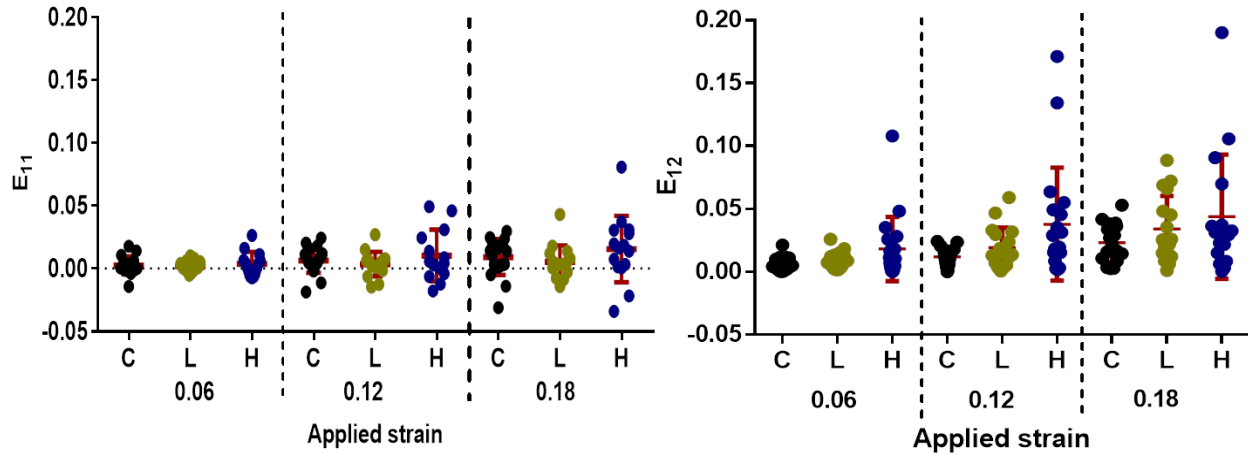


Fig. 6.14 Microscale tensile strain (A) and shear strain (B) of control, low dose, and high dose BAPN treated groups, calculated using microscopic images.

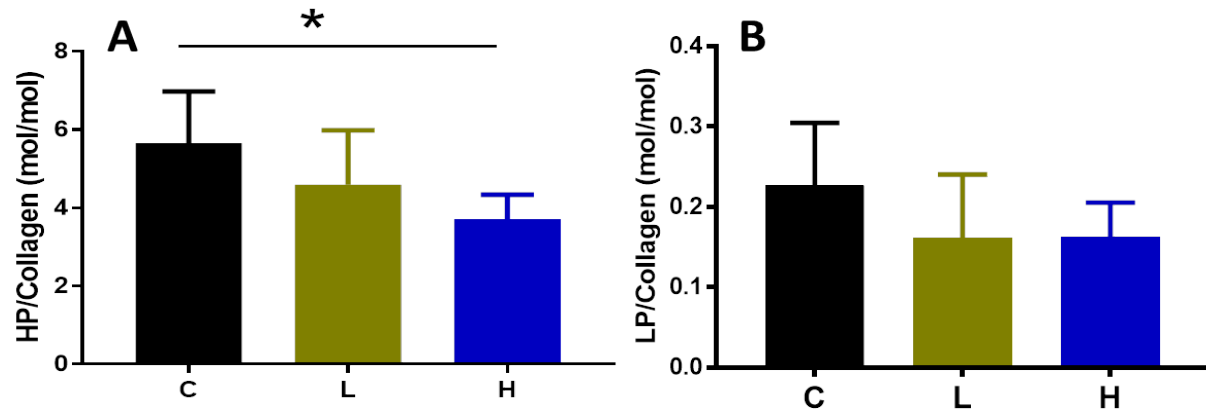


Fig. 6.15 Crosslink densities HP (A) and LP (B) of control, low dose, and high dose BAPN treated groups. * for $p < 0.05$.

6.4 Discussion

This study evaluated crosslink content in tendons after *in vivo* treatment and *in vitro* culture. *In vitro* culture with lyxyl oxidase appeared to tendon modulus, possibly due to increased crosslink density in cultured tendons. *In vivo* treatment with BAPN decreased tendon stresses compared to control during stress relaxation testing, although without significant differences among groups. Slopes of peak/equilibrium stresses vs. tissue strain curves were greater in BAPN treated SSTs and also showed BAPN-dose dependence. Our results demonstrate that *in vivo* treatment with BAPN successfully decreases collagen crosslinks in SST and leads to subtle changes in mechanical strength. Interestingly, *in vivo* treated SSTs had similar tensile strain on the microscale as control SSTs, but subtly greater shear strains. This result suggests that the bond between collagen/collagen fibrils formed by crosslinks could contribute to tendon viscoelasticity by reducing collagen fiber sliding.

Parameters such as peak and equilibrium stresses derived from stress relaxation testing enabled evaluation of tendon viscosity and elasticity. Smaller equilibrium stresses in BAPN treated SSTs could be due to collagen crosslinks between collagen molecules inhibiting intermolecular slip and increasing the tendon elastic response. However, this possibility contrasted with the finding that microscale tensile strain did not show differences between treated and control SSTs. Microscale tensile strain in treated SSTs were more variable than control, which may partially explain the lack of any obvious differences of tensile strain among treated groups. Surprisingly, even under tensile loading, both treated and control SSTs had compressive strain (negative tensile strain) on the microscale, which has also been found in ligament under tension [35, 36]. This result demonstrates that tendon exhibits heterogeneity on the micron/nano scale. Collagen fiber stretching, sliding, and even reorganization occur in

response to tensile loading. Treated SSTs showed greater and more variable microscale shear strain, implying that more sliding between collagen fibers occurred in treated SSTs. Taken together, results suggest that crosslinks could govern both tendon viscosity and elasticity and the location of crosslinks could determine the specific types of physical mechanism that regulates tendon deformation on the microscale.

Higher variability of mechanical parameters (i.e., peak and equilibrium stresses, microscale tensile and shear strain, difference of stresses between left and right SSTs) in BAPN treated SST groups could be caused by several factors. First, BAPN was injected subcutaneously, so efficient BAPN delivery to the tendon could not be guaranteed. Although not shown, growth plate of the humeral head was easily detached from rat humerus and also certain damaged spots were identified in cartilage in rats treated with high dose BAPN, raising possibility that BAPN might target tissues such as bone and cartilage. Previous studies also confirmed that BAPN injection in rats caused decreased collagen crosslinks in bone [37, 38]. Additionally, it is well accepted that BAPN binds to LOX and deactivates its catalysis to promote crosslink formation [3, 4]. Our real-time PCR analysis found LOXL2 was a primary homolog in tendon from 14-day-old mice. It is unknown whether rat tendon also primarily expresses LOXL2 and its homologs in a time-dependent way and whether BAPN can inhibit LOXL2, in addition to LOX, activity to further prevent crosslink formation. Mechanisms for how BAPN regulates crosslink formation should be further examined and confirmed by additional studies. Furthermore, greater differences between stresses from left and right SSTs from the same rats could be due to variable activity between left and right limbs. One study showed that rats injected with BAPN and subjected to treadmill running had similar modulus in bone compared to control animals, but larger modulus than

BAPN-treated rats without treadmill running [39]. Therefore, exercise could potentially counter the mechanical effect of BAPN treatment by increasing crosslink density.

Our study indicated that collagen crosslinks in tendon may help dictate tendon physical deformation on the microscale, influence mechanical signal transfer among different length scales, and contribute to tendon mechanical strength on the tissue scale. *In vivo* treatment of BAPN and *in vitro* culture showed the trend of decreasing and increasing crosslinks in tendon; additional data will confirm this analysis. Furthermore, the treatment/culture conditions (e.g., time, duration, dose/concentration) should be adjusted to optimize treating/culturing efficiency. By examining crosslink contribution to tendon multiscale mechanical properties, this study further explores the mechanisms that maintains the mechanical integrity of tendon and provides an approach to nondestructively evaluate and manipulate tissue strength for regenerative medicine applications.

6.5 References

1. Fang, F. and S.P. Lake, Experimental evaluation of multiscale tendon mechanics. *Journal of Orthopaedic Research*, 2017. 35(7): p. 1353-1365.
2. Hanada, M., et al., A biochemical study of the distribution of collagen and its crosslinks in knee ligaments and the patellar tendon. *Connective tissue research*, 2014. 55(5-6): p. 378-383.
3. Makris, E.A., et al., Developing functional musculoskeletal tissues through hypoxia and lysyl oxidase-induced collagen crosslinking. *Proceedings of the National Academy of Sciences*, 2014. 111(45): p. 4832-4841.
4. Marturano, J.E., et al., Lysyl oxidase-mediated collagen crosslinks may be assessed as markers of functional properties of tendon tissue formation. *Acta biomaterialia*, 2014. 10(3): p. 1370-1379.
5. Garnero, P., The contribution of collagen crosslinks to bone strength. *BoneKEy reports*, 2012. 182: p. 1-8.
6. Makris, E.A., et al., A copper sulfate and hydroxylysine treatment regimen for enhancing collagen crosslinking and biomechanical properties in engineered neocartilage. *The FASEB Journal*, 2013. 27(6): p. 2421-2430.

7. Reddy, G.K., Glucose-mediated in vitro glycation modulates biomechanical integrity of the soft tissues but not hard tissues. *Journal of orthopaedic research*, 2003. 21(4): p. 738-743.
8. Sajithlal, G., P. Chithra, and G. Chandrakasan, Advanced glycation end products induce crosslinking of collagen in vitro. *Biochimica et Biophysica Acta (BBA)-Molecular Basis of Disease*, 1998. 1407(3): p. 215-224.
9. Andreassen, T.T., H. Oxlund, and C.C. Danielsen, The influence of non-enzymatic glycosylation and formation of fluorescent reaction products on the mechanical properties of rat tail tendons. *Connective tissue research*, 1988. 17(1): p. 1-9.
10. Sung, H.W., et al., Crosslinking of biological tissues using genipin and/or carbodiimide. *Journal of Biomedical Materials Research Part A*, 2003. 64(3): p. 427-438.
11. Puxkandl, R., et al., Viscoelastic properties of collagen: synchrotron radiation investigations and structural model. *Philosophical Transactions of the Royal Society of London B: Biological Sciences*, 2002. 357(1418): p. 191-197.
12. Svensson, R.B., et al., Fracture mechanics of collagen fibrils: influence of natural crosslinks. *Biophysical journal*, 2013. 104(11): p. 2476-2484.
13. Haut, R., The effect of a lathyrictic diet on the sensitivity of tendon to strain rate. *Journal of biomechanical engineering*, 1985. 107(2): p. 166-174.
14. Willett, T.L., et al., Changes in collagen with aging maintain molecular stability after overload: evidence from an in vitro tendon model. *Journal of biomechanical engineering*, 2010. 132(3): p. 031002.
15. Suzuki, D., et al., Biochemical study of collagen and its crosslinks in the anterior cruciate ligament and the tissues used as a graft for reconstruction of the anterior cruciate ligament. *Connective tissue research*, 2008. 49(1): p. 42-47.
16. Thorpe, C., et al., Mechanical properties of the equine superficial digital flexor tendon relate to specific collagen cross-link levels. *Equine Veterinary Journal*, 2010. 42(s38): p. 538-543.
17. Coupe, C., et al., Mechanical properties and collagen crosslinking of the patellar tendon in old and young men. *Journal of applied physiology*, 2009. 107(3): p. 880-886.
18. Fang, F. and S.P. Lake, Modelling approaches for evaluating multiscale tendon mechanics. *Interface Focus*, 2016. 6(1): p. 20150044.
19. Eyre, D.R., M.A. Paz, and P.M. Gallop, Crosslinking in collagen and elastin. *Annual review of biochemistry*, 1984. 53(1): p. 717-748.
20. Yoshida, K., et al., Cervical collagen network remodeling in normal pregnancy and disrupted parturition in Antxr2 deficient mice. *Journal of biomechanical engineering*, 2014. 136(2): p. 021017.
21. Kindt, E., et al., Determination of hydroxyproline in plasma and tissue using electrospray mass spectrometry. *Journal of pharmaceutical and biomedical analysis*, 2003. 33(5): p. 1081-1092.
22. Codman, E.A., The shoulder rupture of the supraspinatus tendon and other lesions in or about the subacromial bursa. 2007.

23. Soslowsky, L., et al., Neer Award 1999: Overuse activity injures the supraspinatus tendon in an animal model: a histologic and biomechanical study. *Journal of Shoulder and Elbow Surgery*, 2000. 9(2): p. 79-84.
24. Lee, V.S., et al., Loss of function mutation in LOX causes thoracic aortic aneurysm and dissection in humans. *Proceedings of the National Academy of Sciences*, 2016. 113(31): p. 8759-8764.
25. Skelley, N.W., et al., Regional Variation in the Mechanical and Microstructural Properties of the Human Anterior Cruciate Ligament. *The American journal of sports medicine*, 2016. 44(11): p. 2892-2899.
26. Komatsu, K., et al., Effects of hydrocortisone and β -aminopropionitrile on stress-strain and stress-relaxation behaviors, and birefringent retardation of collagen fibers in the rat incisor periodontal ligament. *Connective tissue research*, 2002. 43(4): p. 581-588.
27. Zhang, G., et al., Development of tendon structure and function: regulation of collagen fibrillogenesis. *J Musculoskelet Neuronal Interact*, 2005. 5(1): p. 5-21.
28. Gineyts, E., et al., Quantification of immature and mature collagen crosslinks by liquid chromatography–electrospray ionization mass spectrometry in connective tissues. *Journal of Chromatography B*, 2010. 878(19): p. 1449-1454.
29. Saito, M., et al., Single-column high-performance liquid chromatographic–fluorescence detection of immature, mature, and senescent crosslinks of collagen. *Analytical biochemistry*, 1997. 253(1): p. 26-32.
30. Orth, M.W., et al., The presence of lysylpyridinoline in the hypertrophic cartilage of newly hatched chicks. *Biochimica et Biophysica Acta (BBA)-General Subjects*, 1993. 1157(2): p. 229-232.
31. Eleswarapu, S.V., D.J. Responde, and K.A. Athanasiou, Tensile properties, collagen content, and crosslinks in connective tissues of the immature knee joint. *PLoS one*, 2011. 6(10): p. e26178.
32. KNOTT, L., J.F. TARLTON, and A.J. BAILEY, Chemistry of collagen crosslinking: biochemical changes in collagen during the partial mineralization of turkey leg tendon. *Biochemical journal*, 1997. 322(2): p. 535-542.
33. Birch, H.L., et al., Age-related changes to the molecular and cellular components of equine flexor tendons. *Equine veterinary journal*, 1999. 31(5): p. 391-396.
34. Bank, R.A., et al., Lysylhydroxylation and non-reducible crosslinking of human supraspinatus tendon collagen: changes with age and in chronic rotator cuff tendinitis. *Annals of the Rheumatic Diseases*, 1999. 58(1): p. 35-41.
35. Moffat, K.L., et al., Characterization of the structure–function relationship at the ligament-to-bone interface. *Proceedings of the National Academy of Sciences*, 2008. 105(23): p. 7947-7952.
36. Fang, F. and S.P. Lake, Multiscale strain analysis of tendon subjected to shear and compression demonstrates strain attenuation, fiber sliding, and reorganization. *Journal of Orthopaedic Research*, 2015. 33(11): p. 1704-1712.

37. Paschalis, E., et al., Lathyrism-induced alterations in collagen crosslinks influence the mechanical properties of bone material without affecting the mineral. *Bone*, 2011. 49(6): p. 1232-1241.
38. Turecek, C., et al., Collagen crosslinking influences osteoblastic differentiation. *Calcified tissue international*, 2008. 82(5): p. 392-400.
39. McNerny, E.M., J.D. Gardinier, and D.H. Kohn, Exercise increases pyridinoline crosslinking and counters the mechanical effects of concurrent lathyrogenic treatment. *Bone*, 2015. 81: p. 327-337.

Chapter 7: Summary and Future Directions

7.1 Summary of findings

This work designed a custom biomechanical testing device that was combined with two-photon microscopy to evaluate mechanical properties of bovine flexor tendon in shear and compression and corresponding mechanical signal transfer. To further address tendon structure-composition-function relationship, we have successfully altered the amount of linking components (i.e., elastin, proteoglycans, collagen enzymatic crosslinks) in tendon by enzyme digestion, *in vivo* animal treatment, and *in vitro* tissue culture, and evaluated their contribution to tendon mechanical behavior at different length scales. These studies have probed deeply tendon composition/structure and provided insight regarding their contribution to the biomechanical response to load.

This work was the first to quantify location-dependent mechanical responses of energy storing tendons (i.e., DDFT) under non-tensile loading scenarios and simultaneously evaluate microscale deformation via two-photon microscopy. Results showed large differences in the elastic behavior between regions: distal region stresses were 4–5 times larger than proximal region stresses during compression and 2–3 times larger during shear. Surprisingly, the viscous (i.e., relaxation) behavior was not different between regions for either compression or shear. Strain transfer was attenuated from tissue to local matrix under both shear and compression. Nuclear aspect ratios exhibited smaller changes for distal samples, suggesting that cells were more shielded from deformation in the distal region. Collagen fiber sliding was observed to contribute significantly in response to shear, while uncrimping and fiber reorganization were the predominant mechanisms under compression. Histological analysis showed that collagen and

proteoglycan in the distal region distributed differently from the proximal region. Results demonstrate mechanical differences between two regions of DDFT under compression and shear loading, which are attributed to variations of composition and microstructural organization.

These results inspired us to further examine the mechanical influence of components present in small quantities, such as elastic fibers and GAGs, on the biomechanical response and microscale deformation of tendon. Contrary to highly inhomogeneous tensile properties of the supraspinatus tendon, we found that three distinct SST regions showed similar stresses and microscale deformation in shear. Collagen fiber reorganization and sliding were the physical mechanisms observed as the SST response to shear loading. Measures of microscale deformation were highly variable, likely due to a high degree of extracellular matrix heterogeneity. After elastase treatment, SST samples exhibited significantly decreased stresses under shear loading, particularly at low strains, but without significantly different microscale strain and cell movement. These results show that elastin contributes to tendon mechanics in shear, while the effect of elastin depletion on microscale deformation was possibly counteracted by the high level of heterogeneity of human SSTs, likely due to natural characteristics and/or unknown levels of tissue degeneration.

Consistent with previous work showing that GAG depletion did not deteriorate tendon strength [1-5], this study used ChABC treatment to digest GAGs in SST without disrupting collagen fibers. During shear stress relaxation, peak and equilibrium shear stresses decreased only slightly after ChABC treatment and were not significantly different from pretreatment values. Reduced stress ratios were computed and shown to be slightly greater after ChABC treatment compared to PBS incubation without enzyme, suggesting that these relatively small changes in stress values were not due strictly to tissue swelling. Microscale deformations were

not different after ChABC treatment. All these results demonstrate that GAGs possibly play a minor role in contributing to the mechanical behavior of SST in shear, but are not a key tissue constituent to regulate shear mechanics.

Enzymatic collagen crosslinks have been hypothesized to contribute to soft tissue mechanical integrity and strength, but previous results examining the mechanical function of collagen crosslinks in tendon were inconsistent. Our study showed that BAPN treated tendons, with decreased amounts of collagen crosslinks, had slightly decreased dose-dependent stresses during tensile stress relaxation. As hypothesized, tendons from control rats exhibited greater shear microscale strains, although not statistically different from BAPN treated tendons, but similar tensile microscale strains along collagen fibers. Even under tensile loading, collagen fiber stretching, sliding, and reorganization, demonstrated by the breaking and rigid rotation of photobleached grid lines, were shown to be microscale deformation modes in response to tensile loading. One interesting result was that BAPN treated rats exhibited more dramatic side-to-side differences of tendon stresses than control animals; this merits further exploration. Overall, these results suggest that collagen crosslinks could bond collagen microfibrils/fibrils together, resist relative motion inside tendon microstructure, and improve tendon integrity.

There are several factors which should be considered when interpreting these results. For tendon biomechanical testing, tendons were subjected to displacement-controlled testing to determine its strength under loading. It is not completely surprising, therefore, that there were only a few significant differences shown for microscale deformation between treated and control tendons, or among different tendon regions. Our studies show certain microscale structural responses to these loading conditions, for example, more cell movement in elastin-depleted tendons and greater shear strain in BAPN treated tendons. The human tendon samples evaluated

in these studies were observed to be very heterogeneous, with areas of both organized and disorganized collagen fibers and with areas of GAG-concentrated micro-domains. High levels of microscale inhomogeneity could neutralize distinct structural responses between different groups and account for similar observed microscale deformation. Additionally, tendons of various types or regions might have different types/amounts of collagen, elastic fibers, proteoglycans, and/or other tissue constituents. The relative percentages of mechanical function attributed to each of these different components have not been answered. The interconnected nature of tissue constituents complicates experimental evaluation since it is difficult to only modify one parameter at a time (i.e., component amount) in tendons. For example, enzymatic treatment was utilized in these studies to target and remove specific tissue components. To fully evaluate the effect of treatment, the efficiency of enzyme treatment on targeted components and the side effects on tendon structure and quantities of other constituents should be addressed further. Enzyme treatment may only partly deplete targeted components, which is a limitation of this type of experimental approach. Furthermore, *in vivo* treatment with BAPN to decrease crosslinks did not significantly cause reduced mechanical properties of tendons, which may be partly due to the efficiency of BAPN delivery and activity. Although tendons cultured *in vitro* to increase collagen crosslinks showed trends towards increased stresses, treatment duration, LOX concentration, and tendons from certain growth period should be also verified to optimize crosslink amount to be increased as desired.

Analysis of tendon mechanical behavior under shear loading and related mechanical signal transfer not only complements knowledge of tendon mechanics under multiaxial loading, but also has clinical significance concerning degeneration/injury of human tendon. Evaluation of the contribution of elastic fibers, proteoglycans, and collagen crosslinks provide insight into how

specific ECM components are distributed and how they function to support and transfer multiaxial forces. In summary, the knowledge obtained through this work is of great value by (1) defining structure-function relationships under physiologically-relevant non-tensile loading conditions, (2) quantifying the microscale deformations that cells experience to drive location-specific changes of ECM composition/organization, (3) providing insight into altered multiscale strain behavior that may occur following ECM changes that accompany tendon injury/degeneration, and (4) establishing criteria for rationally designed tendon replacements to meet requirements for proper function in complex *in vivo* loading environments.

7.2 Future directions

Based on the interesting and exciting findings in our studies, there are several future studies/topics which could be conducted to expand and deepen our understanding, Potential research topics include: (1) determining location-dependent distributions of collagen crosslinks, elastic fibers, and different types of proteoglycans in tendons with biochemical assays, immunostaining, or liquid chromatography-tandem mass spectrometry, and further exploring their correlation with mechanical properties of different locations; ; (2) developing a standard protocol to evaluate mechanical signal transfer in soft tissues from joint to nuclei levels under physiological loading environment and explore principles of mechanotransduction and cell fate; (3) addressing whether tendon heterogeneity, such as varying alignment of collagen fibers, governs mechanical signal transfer and different levels of strain attenuation across several length scales; (4) adopting transgenic animal models (i.e., elastin/LOX haploinsufficiency) to obtain modified tissues with desired composition, which could provide a complementary approach to eliminate the limitation induced by enzyme digestion, *in vivo* treatment, and *in vitro* culture (5) establishing computational models to determine the mechanical role of elastic fibers, collagen

crosslinks, proteoglycans, and their synergistic interactions. More details concerning each future investigation will be discussed.

7.2.1 Correlation of mechanical properties of tendon in multiaxial loading environment with tendon structure and composition

The reciprocity between components/structure and mechanical behavior has been well recognized, but still lack comprehensive understanding. Compared to the proximal region, that resembles a typical tendon, current research showed that greater density of aggrecan and collagen type VI in the distal region helps support compressive and frictional loads, acting almost as a fibrocartilage [6, 7]. Implementation of *in vivo* bend/twist load and *in vitro* cyclic compressive load enhanced synthesis of large proteoglycans and led toward fibrocartilage formation [8-10]. These reports have shown an experimental method to investigate tendon properties, but do not answer questions such as: (1) what relative expression of different types of proteoglycans, collagen, collagen crosslinks, and elastic fibers in various regions of bovine flexor tendon; (2) whether any component dominates tendon mechanical behavior in particular loading conditions (i.e., shear, compression, torsion); (3) what cellular events occur inside tendon in response to different types of loading.

Furthermore, the relationship of tendon mechanics and structure/composition has not been evaluated precisely in the same length scales. More specifically, tendon is commonly accepted to be heterogeneous on the nano- and micro- scales. For example, inter-fascicular matrix, which surrounds and encloses collagen-rich fascicles to form whole tendon, contains more proteins than within the fascicles themselves [11]. These proteins showed differential abundance between matrix phases and their turnover depended on age [11]. Most available data about tendon mechanical strength are force/stress responses of whole tendon/fascicle to loading on the tissue

scale. To successfully match the correlation between structure/composition and function on the length scales, techniques such as laser capture dissection, nano indentation, and atomic force microscopy could be used as experimental approaches to evaluate samples in microscale mechanical evaluation [11].

In many tendon physiological *in vivo* environments, tendons experience multiaxial loading during normal function. However, analysis of tendon mechanics has been conducted almost entirely under uniaxial loading. Undoubtedly, these simplified models could be beneficial to find underlying mechanism concerning tendon function, but combined testing protocols and platforms should be developed to mimic tendon physiological loading scenarios, through incorporating muscle-transmitted force and interactions caused by anatomical contact with neighboring tissues and bones.

7.2.2 Strain/stress transfer in soft tissues from joint to nuclei levels under physiological loading environment

To demonstrate the multiscale nature of tendon mechanics, applied strains were found in previous research to be attenuated from tissue to local matrix scale in both equine superficial digital flexor and common digital extensor tendons [12, 13]. Illustrative of tendon multiaxial mechanical properties, our work has shown that distinct regions of bovine DDFT exhibited different stresses under shear and compressive loading, and similar to tensile results, strain transfer was attenuated from the tissue to nuclei scales under non-tensile deformation [14]. The modification of composition and structural properties, which occurs across different length scales, certainly contributes to altered overall tendon mechanics and function [15-17]. Although evaluation of strain/force transfer inside connective tissue among different length scales is

challenging due to the involvement of different techniques, this knowledge is critical for interpreting tissue degeneration/disease.

Currently, few studies have fully addressed mechanical signal transfer from the tissue to nuclear levels, especially in determining relationships with mechanotransduction and cell fate. Based on recently advanced techniques, magnetic resonance image could be applied to measure intra tissue strain, which could be correlated with applied strain. Soft tissues could also be harvested from transgenic modified mice, whose cells are fluorescently marked to visualize cell fate (i.e., quiescence, senescence, apoptosis). AFM combined with deformation microscopy would be utilized to track force/strain transfer in soft tissues at different development stages under physiological loading. Specifically, extracellular strain/stress, pericellular strain/stress, cellular strain/stress, nuclei strain, and RNA synthesis of soft tissue from mice at different ages can be tested under physiological loading. The activity of senescence-associated elements and cell apoptosis can be examined by advanced techniques (e.g., in situ fluorescent staining, flow cytometry, western blotting, PCR, and immunohistochemistry [18, 19]).

Furthermore, research could try to identify the threshold of mechanical loading that govern cell (e.g., fibroblast, chondrocyte) fate. HA-PEG hydrogel systems can be modified to mimic the microenvironment of young fibroblasts/chondrocytes. Different durations of physiologically related loading could be applied to promote transition to different cell fates. The same techniques (i.e., flow cytometry, western blotting, PCR, immunohistochemistry) aforementioned could be performed to evaluate cell activity and transcriptional regulators, such as YAP/TAZ. This prospective study could facilitate understanding of age-related microenvironment changes due to repetitive physiological loading and address the regulation of extracellular matrix to cell fate from multiple length scales.

7.2.3 Examination of SST heterogeneity and its influence on cell fate

Whether soft tissue is determined to be homogeneous or heterogeneous heavily relies on the studied/assigned length scale of evaluation. On the macroscale, tendon has continuously aligned collagen fascicles/fibers, however disorganized collagen fibers with PG-rich regions have also been reported to broadly distribute inside tendon on the mesoscale or microscale [20, 21]. Similarly, PG-rich microdomains in annulus fibrosus, meniscus, and cartilage were proposed to have significance on minimizing strain transfer from tissue to cells, shielding cells from tissue-level strain, and altering mechanobiologic response through integrin receptors and calcium signaling [22]. These PG-rich microdomains was also found to locate within injured or degenerated tissue locations [23]. Strain attenuation of meniscus from tissue to nuclei scale has been compared among different ages (i.e., fetal, juvenile, adult) and correlated with the amount of PG-rich microdomains. Related to how microdomains modulate mechanosensing, cells residing in PG-rich domains of engineering scaffolds had lower frequency of spontaneous calcium oscillations than cells in extracellular matrix of aligned collagen fibers [24]. Microscopic images in our studies showed that some photobleached regions of human SSTs had microscale compressive strain even under tensile strain, which could be attributed to reorganization of short collagen fibers in PG-rich microdomains [20, 21, 25].

The existence of microdomains further complicates the interpretation of highly variable microscale strain in modified tendons, which were adopted to determine the mechanical role of elastic fibers, collagen crosslinks, and proteoglycans [20, 21]. Current studies have examined PG expression in these microdomains by histology and used nuclear aspect ratio to indicate microscale strain. It remains unanswered whether PG-rich domains have more or less quantities of other components (i.e., elastic fibers, crosslinks) and whether there is a gradient strain transfer

from the region adjacent to the microdomain. More work should be completed to elucidate microscale strain maps, calculated using image registration instead of marker tracking, of both regions of organized and disorganized collagen fibers. Strain magnitude based on localized structure (i.e., organized collagen region vs. PG-rich domains) should be separated to determine structured-based mechanical strain transfer. Due to the accessibility of tissue-engineered constructs with non-fibrous PG-rich microdomains, tendon stem/progenitor cells could be encapsulated inside this domain in order to determine whether these microdomains could also influence cell differentiation and fate (i.e., senescence, quiescence, apoptosis). Mechanotransduction mechanisms dictating how cells remodel the surrounding extracellular matrix could also be evaluated.

7.2.4 Transgenic mouse models to compensate the evaluation of elastic fibers and collagen crosslinks

To characterize tendon structure-function relationships, two dominant experimental approaches have been widely applied to modify tendon composition and structure. The first approach is to use chemicals/enzymes to *in vitro* or *in vivo* target certain components, such as the density of elastin, proteoglycans, and collagen crosslinks in tendon changed by *in vitro* or *in vivo* treatment with elastase, ChABC, BAPN, and LOX in our work. However, this approach could possibly also affect non-target proteins. For example, ChABC catalyzes the depletion of chondroitin sulfate A&C, dermatan sulfate, hyaluronan, but not keratin sulfate, heparin, or heparan sulfate. Since ChABC does not act on all proteoglycans and ChABC has limited penetration inside tendon, PGs cannot be completely eliminated from tendon. As another example, elastase breaks down elastin into small segments, but these fragments may persist in tendon and may still have a contribution to tendon mechanics. Additionally, BAPN is proposed to inhibit the activity of lysyl oxidase, but its influence on other LOX homologs, especially

LOXL2 as a predominant isoform in tendon, is unknown. In contrast, tissues from appropriate transgenic mouse models could have desired altered amounts of specific components. More significantly, the features of these models can better represent human disease.

Therefore, elastin haploinsufficient mouse models may be used to complement our work using a different approach. It was reported that elastin in artery from elastin hemizygous mice (ELN^{+/-}) was reduced to 50% of wildtype mice [26]. It is reasonable to expect that tendon from ELN^{+/-} mice could also express one half elastin of wildtype (ELN^{+/+}) mice. The mechanical role of elastin and its influence on mechanical signal transmission could be concluded by comparing mechanical behaviors of ELN^{+/-} and ELN^{+/+} tendons. Additionally, deteriorated mechanical properties and structural abnormality of human tendon at different ages in elastin and elastic fiber related defects, such as Marfan syndrome, Willians syndrome, and Menkes syndrome, can also be explored with the use of similar genetic mouse models [27].

LOX or LOX-like 1-4 inhaploinsufficient mouse model could potentially serve as another option to obtain tendons with decreased crosslinks, compared to normal tendons. Although only immature collagen crosslinks were examined and found to decrease in lungs of LOX and LOXL3 hemizygous mice [28, 29], mature collagen crosslinks in tissues from LOX and LOX homolog (i.e, LOXL 1-4) hemizygous mouse models should be quantified first to select the right model. It is possible that certain LOX homologs influence elastin synthesis and other LOX homologs primarily regulate crosslink formation. The adoption of mouse models with different modifications of LOX and LOX-like genes could isolate the mechanical contribution of collagen crosslinks from elastin. Another application of these mouse models is to investigate and compare whether inter-fibrillar and intra-fibrillar collagen crosslinks regulate tendon mechanical signal transfer by different physical mechanisms. As the names imply, intra-fibrillar collagen crosslinks

bundle collagen together into microfibrils/fibrils for resisting collagen fibrils stretching during loading, but inter-fibrillar crosslinks locate between microfibrils/fibrils to prevent sliding among collagen fibrils. One study showed that LOX and LOXL1 localized inside collagen fibers and might only promote inter-fibrillar crosslink formation [30]. Comparison of two animal models which have different amounts of collagen intra- and inter-fibrillar crosslinks could uncover mechanisms that determine how crosslinks govern tendon mechanical properties. Last, due to the availability of state-of-the-art genetic tools (i.e., tamoxifen-induced cre-loxP recombination), LOX/LOXL1-4 knockout phenotypes can be induced in a time-specific way so that the expression of collagen crosslinks at tendon development stages and the corresponding mechanical effect could be analyzed. Tendon aging/disease could also be assessed to promote/inhibit crosslink production. Meanwhile, drugs for treating the diseases pertinent to these gene mutations could also be evaluated to improve tendon function.

In conclusion, the employment of transgenic mouse models enables basic research of biological consequences and mechanical deterioration caused by tendon component remodeling, and also helps translate this knowledge to address important mechanisms of pathology.

7.2.5 Computational models to determine the mechanical role of elastic fibers and collagen crosslinks and their synergy

A number of recent studies have characterized the anisotropic, inhomogeneous, and viscoelastic properties of tendons in different species and in different anatomical locations. For example, rat patellar tendon exhibited less ultimate stress than rabbit patellar tendon, and human supraspinatus tendon had smaller elastic modulus than human patellar tendon [31-35]. Several other factors such as age, genetic modification, injury treatment, and especially *in vivo* mechanical environment, can also influence tendon mechanics [35]. However, it is time-

consuming and costly to experimentally evaluate different tendons under all types of conditions. Computational modeling offers an approach that can provide insight into tendon relationships, which are difficult to measure *in vivo*. In addition, models can be beneficial in handling large amounts of data and complicated loading situations, including interactions with neighboring anatomy. Appropriately defined models could be formulated for a specific tendon with its unique properties (e.g., multiaxial mechanical properties, location-specific microstructural organization, inhomogeneous distribution of non-fibrillar matrix, site-specific geometry, etc.) and, using a multiscale approach, could be constructed to enable mechanical evaluation across the full range of length scales relevant to the hierarchical organization of tendon. Importantly, well-validated models enable predictions of tissue behavior under different loading conditions, including those that are difficult to explore experimentally, and can be utilized to study the effects of disease, degeneration, and/or injury on functional mechanical properties. Particularly in our studies, one application of computational models is to validate and predict the mechanical role of different constituents of tendon composition.

A coupled fiber-matrix multiscale model in previous studies has been demonstrated to successfully (1) mimic collagen network as well as the noncollagenous matrix of native tissue (i.e., arterial wall, tendon), (2) predict microscale fiber behavior by using tissue response to uniaxial and biaxial loading conditions, (3) reproduce the large Poisson's ratio measured experimentally [36-38]. This multiscale model could be adopted and modified to evaluate the contribution of collagen crosslinks and elastic fibers to tendon mechanics on different length scales. It can also be used to predict the synergistic interaction between collagen and other noncollagenous matrix, which is challenging to examine by experimental approach. Additionally, tendon heterogeneity can also be included into this modeling to further evaluate whether/how

varying organization of collagen fiber influences microscale deformation and its related mechanisms (i.e., sliding, reorganization, uncrimping, stretching) under multiaxial loading conditions.

With experimental data from our studies availability, the modified coupled fiber-matrix multiscale model could be developed and verified to address the problems encountered in our previous experiments, especially like off-target effects of enzyme digestion and inefficient *in vivo/ex vitro* culture. It can also be extended to apply to other collagenous tissue (e.g, ligament, cartilage, meniscus) and examine mechanotransduction of fibroblasts, chondrocytes, and tenocytes to understand the mechanism of tissue remodeling or degeneration.

7.3 References

1. Fessel, G. and J.G. Snedeker, Evidence against proteoglycan mediated collagen fibril load transmission and dynamic viscoelasticity in tendon. *Matrix Biology*, 2009. 28(8): p. 503-510.
2. Fessel, G. and J.G. Snedeker, Equivalent stiffness after glycosaminoglycan depletion in tendon—an ultra-structural finite element model and corresponding experiments. *Journal of theoretical biology*, 2011. 268(1): p. 77-83.
3. Gordon, J., et al., Achilles tendons from decorin-and biglycan-null mouse models have inferior mechanical and structural properties predicted by an image-based empirical damage model. *Journal of biomechanics*, 2015. 48(10): p. 2110-2115.
4. Lujan, T.J., et al., Effect of dermatan sulfate glycosaminoglycans on the quasi-static material properties of the human medial collateral ligament. *Journal of orthopaedic research*, 2007. 25(7): p. 894-903.
5. Lujan, T.J., et al., Contribution of glycosaminoglycans to viscoelastic tensile behavior of human ligament. *Journal of Applied Physiology*, 2009. 106(2): p. 423-431.
6. Koob, T.J. and K.G. Vogel, Site-related variations in glycosaminoglycan content and swelling properties of bovine flexor tendon. *J Orthop Res*, 1987. 5(3): p. 414-424.
7. Vogel, K. and J. Peters, Histochemistry defines a proteoglycan-rich layer in bovine flexor tendon subjected to bending. *J Musculoskelet Neuronal Interact*, 2005. 5(1): p. 64-69.
8. Robbins, J.R., S.P. Evanko, and K.G. Vogel, Mechanical loading and TGF- β regulate proteoglycan synthesis in tendon. *Archives of biochemistry and biophysics*, 1997. 342(2): p. 203-211.

9. Vogel, K.G., The effect of compressive loading on proteoglycan turnover in cultured fetal tendon. *Connective tissue research*, 1996. 34(3): p. 227-237.
10. Vogel, K., What happens when tendons bend and twist? Proteoglycans. *Journal of Musculoskeletal and Neuronal Interactions*, 2004. 4(2): p. 202-203.
11. Thorpe, C.T., et al., Anatomical heterogeneity of tendon: Fascicular and interfascicular tendon compartments have distinct proteomic composition. *Scientific reports*, 2016. 6.
12. Thorpe, C.T., et al., Helical sub-structures in energy-storing tendons provide a possible mechanism for efficient energy storage and return. *Acta biomaterialia*, 2013. 9(8): p. 7948-7956.
13. Thorpe, C.T., et al., Capacity for sliding between tendon fascicles decreases with ageing in injury prone equine tendons: a possible mechanism for age-related tendinopathy? *Eur. Cells Mater.*, 2013. 25: p. 48-60.
14. Fang, F., A.S. Sawhney, and S.P. Lake, Different regions of bovine deep digital flexor tendon exhibit distinct elastic, but not viscous, mechanical properties under both compression and shear loading. *Journal of biomechanics*, 2014. 47(12): p. 2869-2877.
15. Ingber, D.E., Tensegrity-based mechanosensing from macro to micro. *Prog Biophys Mol Biol*, 2008. 97(2-3): p. 163-179.
16. Lavagnino, M. and S.P. Arnoczky, In vitro alterations in cytoskeletal tensional homeostasis control gene expression in tendon cells. *J Orthop Res*, 2005. 23(5): p. 1211-1218.
17. Marino, M. and G. Vairo, Stress and strain localization in stretched collagenous tissues via a multiscale modelling approach. *Computer methods in biomechanics and biomedical engineering*, 2014. 17(1): p. 11-30.
18. Jeon, O.H., et al., Local clearance of senescent cells attenuates the development of post-traumatic osteoarthritis and creates a pro-regenerative environment. *Nature Medicine*, 2017. 23(6): p. 775-781.
19. Kim, K.-W., et al., Senescence mechanisms of nucleus pulposus chondrocytes in human intervertebral discs. *The Spine Journal*, 2009. 9(8): p. 658-666.
20. Fang, F. and S.P. Lake, Multiscale mechanical evaluation of human supraspinatus tendon under shear loading after glycosaminoglycan reduction. *Journal of Biomechanical Engineering*, 2017. 139(7): p. 071013.
21. Fang, F. and S.P. Lake, Multiscale mechanical integrity of human supraspinatus tendon in shear after elastin depletion. *Journal of the Mechanical Behavior of Biomedical Materials*, 2016. 63: p. 443-455.
22. Han, W.M., et al., Macro- to microscale strain transfer in fibrous tissues is heterogeneous and tissue-specific. *Biophys J*, 2013. 105(3): p. 807-817.
23. Choi, R.K., et al., Chondroitin sulfate glycosaminoglycans contribute to widespread inferior biomechanics in tendon after focal injury. *Journal of Biomechanics*, 2016. 49(13): p. 2694-2701.

24. Han, W.M., et al., Microstructural heterogeneity directs micromechanics and mechanobiology in native and engineered fibrocartilage. *Nature materials*, 2016. 15(4): p. 477-484.
25. Fang, F. and S.P. Lake, Multiscale strain analysis of tendon subjected to shear and compression demonstrates strain attenuation, fiber sliding, and reorganization. *Journal of Orthopaedic Research*, 2015. 33(11): p. 1704-1712.
26. Li, D.Y., et al., Novel arterial pathology in mice and humans hemizygous for elastin. *Journal of Clinical Investigation*, 1998. 102(10): p. 1783-1787..
27. Vrhovski, B. and A.S. Weiss, Biochemistry of tropoelastin. *European Journal of Biochemistry*, 1998. 258(1): p. 1-18.
28. Hornstra, I.K., et al., Lysyl oxidase is required for vascular and diaphragmatic development in mice. *Journal of Biological Chemistry*, 2003. 278(16): p. 14387-14393.
29. Zhang, J., et al., Loss of lysyl oxidase-like 3 causes cleft palate and spinal deformity in mice. *Human molecular genetics*, 2015. 24(21): p. 6174-6185.
30. Wagenseil, J.E. and R.P. Mecham, New insights into elastic fiber assembly. *Birth Defects Research Part C: Embryo Today: Reviews*, 2007. 81(4): p. 229-240.
31. Butler, D.L., M.D. Kay, and D.C. Stouffer, Comparison of material properties in fascicle-bone units from human patellar tendon and knee ligaments. *J Biomech*, 1986. 19(6): p. 425-32.
32. Lake, S.P., et al., Tensile properties and fiber alignment of human supraspinatus tendon in the transverse direction demonstrate inhomogeneity, nonlinearity, and regional isotropy. *J Biomech*, 2010. 43(4): p. 727-732.
33. Andreassen, T.T., K. Seyer-Hansen, and A.J. Bailey, Thermal stability, mechanical properties and reducible crosslinks of rat tail tendon in experimental diabetes. *Biochim Biophys Acta*, 1981. 677(2): p. 313-317.
34. Chimich, D., et al., Water content alters viscoelastic behaviour of the normal adolescent rabbit medial collateral ligament. *J Biomech*, 1992. 25(8): p. 831-837.
35. LaCroix, A.S., et al., Relationship between tendon stiffness and failure: a metaanalysis. *Journal of Applied Physiology*, 2013. 115(1): p. 43-51.
36. Zhang, L., et al., A coupled fiber-matrix model demonstrates highly inhomogeneous microstructural interactions in soft tissues under tensile load. *Journal of biomechanical engineering*, 2013. 135(1): p. 011008.
37. Lake, S.P., et al., Mechanics of a fiber network within a non-fibrillar matrix: model and comparison with collagen-agarose co-gels. *Annals of biomedical engineering*, 2012. 40(10): p. 2111-2121.
38. Sander, E.A., et al., Image-based multiscale modeling predicts tissue-level and network-level fiber reorganization in stretched cell-compacted collagen gels. *Proceedings of the National Academy of Sciences*, 2009. 106(42): p. 17675-17680.